REMOTE SENSING STUDIES OF CHHOTA-SHIGRI GLACIER, HIMALAYAS

Ph. D. THESIS

by
REET KAMAL TIWARI

DEPARTMENT OF EARTH SCIENCES
INDIAN INSTITUTE OF TECHNOLOGY ROORKEE
ROORKEE-247 667 (INDIA)

JULY, 2014

REMOTE SENSING STUDIES OF CHHOTA-SHIGRI GLACIER, HIMALAYAS

A THESIS

Submitted in partial fulfilment of the requirements for the award of the degree of

DOCTOR OF PHILOSOPHY

in

EARTH SCIENCES

by

REET KAMAL TIWARI

DEPARTMENT OF EARTH SCIENCES
INDIAN INSTITUTE OF TECHNOLOGY ROORKEE
ROORKEE-247 667 (INDIA)

JULY, 2014

INDIAN INSTITUTE OF TECHNOLOGY ROORKEE
ROORKEE

CANDIDATE'S DECLARATION

I hereby certify that the work which is being presented in this thesis entitled **"REMOTE SENSING STUDIES OF CHHOTA-SHIGRI GLACIER, HIMALAYAS"** in partial fulfilment of the requirements for the award of the Degree of Doctor of Philosophy and submitted in the Department of Earth Sciences of the Indian Institute of Technology Roorkee, Roorkee is an authentic record of my own work carried out during the period from January, 2010 to July, 2014 under the supervision of Dr. R. P. Gupta, Professor, Department of Earth Sciences, Indian Institute of Technology Roorkee, Roorkee, and Dr. M. K. Arora, Professor, Department of Civil Engineering, Indian Institute of Technology Roorkee, Roorkee (on lien).

The matter presented in the thesis has not been submitted by me for the award of any other degree of this or any other Institute.

(REET KAMAL TIWARI)

This is to certify that the above statement made by the candidate is correct to the best of our knowledge.

(M. K. ARORA)
Supervisor

(R. P. GUPTA)
Supervisor

Date: July , 2014

The Ph.D. Viva-Voce Examination of **Mr. Reet Kamal Tiwari**, Research Scholar, has been held on _____.

Signature of Supervisor (s) Signature of Chairman, SRC Signature of External Examiner

Head of the Department/Chairman, ODC

Dedicated to Maa and Papa

"ऐ पर्वतराज हिमालय तू, निजमस्तक नित ऊँचा रखना;
बहती ही रहे नदियाँ, हिम-नदियाँ, इसके भी लिए तत्पर रहना ।
हम शपथ तुम्हारी लेते हैं, हिमकिरीट न तुम्हे खोने देंगे;
हम प्रहरी हैं एक-एक हिमकण के, अध्ययन से प्रतिरक्षण देंगे ॥0॥"

रचना - डॉ. राम कुमार तिवारी

"Oh! Majestic Himalayas! Always reign high in your grandeur;
May there be incessant flow of rivers and glaciers in you.
We are the sentinels to protect your splendour by our research,
And vow would never let you lose your snow crest."

By - Dr. Ram Kumar Tiwari

ABSTRACT

The Himalayas, designated as the third pole of our Earth, is the land of thousands of glaciers. These glacial snowfields store about 12,000 km^3 of freshwater, which is the supply source for perennial rivers such as the Indus, Ganga and Brahmaputra feeding most part of India. Studies have shown that glaciers are shrinking due to the effect of climatic change. The changes in the glaciers may lead to catastrophic events, *viz.* glacial lake outburst floods (GLOF). These changes need to be monitored periodically to assess the glacier health and prevent such events. Contemporaneously, it is observed that the knowledge about the glacial changes is very limited over the Himalayas. In India, the glaciological studies have been limited to primarily field based studies but it has been emphasized in several studies that the synoptic nature of remote sensing can play a major role in completing the inventorying of the glacier database. In today's world, large temporal database of remote sensing images are available, which can be used to monitor the past changes also.

In this research, using field data, satellite images and ancillary data (toposheets, previous glacier maps and Digital elevation models (DEMs)), several aspects of Chhota-Shigri glacier have been studied. Field data includes collection of GCPs, temperature information and photographs of different glacial features. Satellite images of varying spatial, spectral and temporal resolution from ASTER and WorldView-2 PAN sensors have been used to generate credible data about the glacial landforms, terrain cover, surface ice dynamics and recession of this glacier. DEMs of varying spatial resolutions (ASTER DEM and SRTM DEM) have been used to extract primary and secondary topographic parameters. Data management, processing and analysis have been done in the GIS platform.

Digital image processing techniques such as orthorectification, supervised classification, band transformation, edge enhancement and image correlation have been extensively used in this research for glacial terrain mapping and dynamics study.

A novel methodology has been proposed for the mapping of debris-covered glacier terrain classes and the results have been compared with the output of maximum likelihood classification (MLC). In the developed methodology, a new hybrid classification method has been proposed which integrates both MLC and knowledge based classification (KNC). Empirical formulae based on band transformations for contrast enhancement of ASTER bands have been proposed, which have increased the separability of various glacier cover classes, especially between cloud and snow. The classified image from the MLC and the transformed bands has been found to be very accurate with an overall accuracy of 89.75%. The user's and producer's accuracies of supraglacial debris have been found to be 91.40% and 92.10% respectively and for periglacial debris 91.25% and 92.23% respectively. Cloud has also been classified accurately using the transformed bands which justify the contrast enhancement performed to increase the separability between the glacial terrain classes.

An evaluation of MLC *vis-à-vis* hybrid classification has been done. Hybrid classification gives an overall accuracy of 86.65% which is above the acceptable values. The user's and producer's accuracies of supraglacial debris have been found to be 85.50% and 86.50% respectively and for periglacial debris 89.63% and 90.10% respectively. Though the individual accuracies for supraglacial debris and periglacial debris have decreased in comparison to MLC based classification, yet they are above the general acceptable values. This classification does not require post-processing of the output maps since the user knowledge about the classes are inherently taken care of during the classification. The proposed method however needs to be tested in other larger areas or with different debris-covered glaciers with diverse debris properties for establishing its utility in glacial mapping.

The effects of changing climate are well seen as markers on the glacier surface as well as in the valley walls which embrace them. Field based methods give insight to the change in the glacier surface but they are limited due to highly precarious terrain. The synoptic nature of remote sensing in conjunction with field data can help overcome these limitations. Considering this, a large scale glacial geomorphological map of the glacier has been prepared using satellite images and ancillary information. The DEM and DTM of the area along with the high spatial resolution WorldView-2 multispectral and panchromatic images have been found very elucidating particularly for the landform distribution.

The recessional trend has been studied for the Chhota-Shigri glacier. Past and recent recessions have been estimated using different satellite images, time series ASTER images and ancillary data (DEM and DEM derivatives). Paleo-morainic loops have been mapped in the inactive zone of the glacier, presence of which is the indicator of recessional history of the glacier. The textural differences seen on the high resolution WorldView-2 multispectral and panchromatic images in conjunction with the surface elevation profile and the DEM derivative like rate of change of slope have been used to map the exact position of these loops. Seven distinct loops have been mapped using this technique and their locations have been verified using the published map of loops, which were prepared using field surveys. A good correlation has been found between the two. The map prepared using field survey shows presence of only five distinct loops whereas using the proposed approach seven loops have been mapped. This clearly indicates the advantage of using remote sensing technique over the field based surveys in perilous terrain like Himalayas.

Surface ice velocity of this glacier has been derived using sub-pixel image correlation technique (COSI-Corr software) on the ASTER time series images (2003–2009). The remote sensing derived measurements have been found to match quite well with the field measurements. In general, the surface ice velocity varies from ~20 my^{-1} to ~40 my^{-1}. Velocity variations occur in different parts of the glacier and also from year to year. In time period considered for this glacier, the mid-ablation zone and the accumulation zone exhibit higher velocities whereas the zones near the snout and equilibrium line altitude have relatively lower velocities. Further, the velocities have been found to be relatively higher in the years 2005–2006 and 2007–2008 and lower in the years 2006–2007 and 2008–2009. These spatial and temporal variations in velocity, which may be related to the glacier morphology and hydro-metrological factors, need to be further studied.

The studies conducted in this research fairly demonstrate the synergy between field based and remote sensing based methods for mapping different aspects of glacier. All the results derived in this study have been validated using field data or the published maps based on field surveys. The high correlation between the field data and the remote sensing based derived results has been observed in this research. The large available database of the satellite image makes it an effective tool for filling the knowledge gap in the field of glaciology. The research reported in this thesis corroborates the use of remote sensing

techniques to map the glacial extent, changes in the landforms, glacial recession and for deriving long term surface ice velocity data with high accuracy.

ACKNOWLEDGMENT

A thesis is not a work of a single individual. It involves the hard work, criticism, advices, and endless discussions of many others. Today, I stand here at the verge of completing my Ph.D. Mere words could not describe their support and help but still I wish to acknowledge all those who helped me at different stages of this wonderful journey.

Without edict of the **Great Almighty**, the author of knowledge and wisdom, nothing is possible. Therefore, in this opportunity of thanksgiving I would like to start with Him. I will always be bound to Him for his countless love and strength that he has bestowed upon me throughout this journey.

I would like to express my profound gratitude to my supervisors, **Prof. R. P. Gupta** and **Prof. M. K. Arora** for their precious guidance and productive criticism during the tenure of my research work. Professional expertise, open discussions, endless advices and constant unflinching support rendered by them have shaped this thesis to its present form. I'm immensely thankful to them for their patience, motivation, enthusiasm, and immense knowledge. Their guidance helped me in all the time of research and writing of this thesis. To them, I remain, professionally and emotionally indebted. I could not have imagined having better advisors and mentors for my Ph.D. study.

I'm grateful to the committee members **Prof. G. J. Chakrapani, Prof. A. K. Sen** and **Dr. Sudhir Kumar** for sparing their valuable time in monitoring the work progress and providing useful tips, critical comments and precious suggestions from time to time. My heart-felt thanks to Prof. A. K. Sen for also kindly agreeing to be my caretaker supervisor. **Prof. A. K. Saraf** (Head, Department of Earth Sciences) is gratefully acknowledged for providing me the necessary research facilities to complete this work.

I express my special gratitude to **Prof. A. K. Gupta (Director, WIHG, Dehra Dun) and Dr. D. P. Dhobal (Scientist-F, CFG, WIHG, Dehra Dun)** for providing support and guidance time to time after my joining to **CFG**.

I'm thankful to **Prof. Al. Ramanathan (JNU, Delhi)** and his glaciological research group for providing me support during my field work.

I was blessed by a treasure of friends who were with me from the start and some joined later but became integral part of this work with time. **Rohan Kumar** has remained with me from my graduation days till today. I'm very lucky to have him as my friend. I would like to express special thanks to **Varinder Saini**. She joined our research group later on and became an integral part of it. She has helped in all the aspects of organization of this thesis. I hope my friends will always be with me through my journey of life and research.

I will always be obligated to my **parents, bhaiya** and **bhabhi** for their unconditional support during my research work. I am deeply thankful to my wife, **Nishi,** for her love, support, and sacrifices. Without her understanding and co-operation I would never have reached this mile-stone. Special thanks to **Gupta Madam** who was always present with her motherly affection and unforgettable delicious meals that I savored with my colleagues.

My sincere gratitude to some special individuals- **Prof. Anupma Prakash** and **Dr. Rudiger Gens** from **University of Alaska Fairbanks, Dr. Pitambar Pati, Madan** and **Laxamanan** from **IIT Roorkee** and **Rajeev Ahluwalia, Dr. Amit Walia** and **Dr. Rakesh Bhambhri** from **CFG** for their help during the thesis**.** Thanks for being there with me and for chipping in wherever and whenever required.

There's another person without whose help the journey to this thesis would have been very difficult. I specially thank **Nair Ji** for being always there and helping me with all the paperwork and other formalities during my Ph.D. work.

REET KAMAL TIWARI

CONTENT

LIST OF FIGURES

LIST OF TABLES

LIST OF PUBLICATIONS

RESEARCH PAPERS IN REFERRED JOURNALS

1. **Tiwari, R. K.,** Gupta, R. P. and Arora, M. K., "Estimation of surface ice velocity of Chhota-Shigri glacier using sub-pixel ASTER image correlation," *Current Science*,Vol.106 No.6, March 2014, PP. 853-859.
2. **Tiwari, R. K.,** Arora M.K. and Gupta, R. P., "Comparison of MLC and knowledge based classification for debris cover glacier mapping using aster optical-thermal image," (Communicated to Remote Sensing of Environment).
3. **Tiwari, R. K.,** Gupta, R. P. and Arora, M.K., "Landform of Chhota-Shigri Glacier watershed, Himachal Himalayas, India," (To be communicated)

PAPERS IN CONFERENCE/SYMPOSIA

1. **Tiwari, R, K.,** (2008), "Remote Sensing & GIS as a tool in Petroleum Explorations," In: National Conference on Water & Mineral Resource Informations and Environmental impacts analysis using High Resolution Satellite Imageries, 27th - 28th March 2008, Dept. of industries and Earth Sciences, The Tamil University Tanjavur, Tamil Nadu, India.
2. **Tiwari, R. K.** and Gupta, R. P., (2012), "Integrated use of multi-sensor images for investigations in Chhota-Shigri glacier, Himalayas," In: International Conference on Geospatial Technologies and Applications, 26th - 29th February 2012, IIT Bombay, Bombay, India (**Best Paper Award**).
3. **Tiwari, R. K.,** Gupta, R. P., Gens, R., Prakash, A., (2012), "Use of optical, thermal and microwave imagery for debris characterization in Bara-Shigri glacier, Himalayas, India," In: Proceedings of IEEE International Geosciences and Remote Sensing Symposium 2012, 22-27th July 2012, Munich, Germany. **(Full Length Paper)**
4. **Tiwari, R. K.,** Gupta, R. P. and Arora, M.K., "Changes in the Chhota-Shigri Glacier: A Benchmark Glacier in Himalayas," In: HOPE-2013, International

conference organized by Humboldt House ofUttarakhand, 12th-14th September 2013, Nainital, Uttarakhand.

5. **Tiwari, R. K.,** Gupta, R. P. and Arora, M.K., “Integrated use of remote sensing and field investigations to study changes in the Chhota-Shigri glacier, Himalayas,” In: National Conference on Earth Sciences in India: Challenges and Emerging Trends, November 7-9, 2013, IIT Roorkee, Roorkee, India.

CHAPTER 1

INTRODUCTION

1.1 General

Glaciers are the large flowing mass of ice. They are formed when snow is continuously deposited in an area over a period of time. The accumulated snow (ice pack) gradually gets metamorphosed under the action of temperature and pressure with time (Paterson, 1994; Goudie, 2004; Bennett and Glasser, 2009). Gradually, the pressure exerted by the weight of accumulated ice crosses the limit of strength of ice pack, and it starts to move. This outward or downward moving ice when confined to narrow space or valley is called glacier (Goudie, 2004; Bennett and Glasser, 2009; Singh *et al*., 2011).

Majestic glaciers, with their sheer splendour and vastness have always fascinated everyone with a scientific or aesthetic psyche. These are the most important parts of the cryosphere. They are also considered an indispensable constituent of the culture, landscape and environment in high mountain and Polar regions (UNEP, 2008). For the society, glaciers are the vital source of freshwater for agricultural, industrial and domestic use and also an important economic component of tourism and hydro-electric power production (IPCC, 2013). In Indian context also, the glaciers are the most important source of freshwater as millions of people depend on the perennial rivers which are fed by the Himalayan glaciers.

In 2007, the Intergovernmental Panel on Climate Change (IPCC) (Cruz *et al.*, 2007) reported that the Himalayan glaciers will disappear in very near future in response to the changing climate, arising many controversies and attracting more intense research

toward the dynamics of the glaciers. In their latest report in 2013, the IPCC have again said that the long lived component of the cryosphere (i.e. glaciers) is changing in response to the change in the climate. It is also reported that the changes in the high altitude glaciers are not only in response to the rising temperature as asserted earlier, but is also in response to the integrated change in the climatic factors (e.g., temperature and precipitation together). The detailed examination of the glacial changes leads to the conclusion that the current glacial extents are out of balance with current climatic conditions, indicating that the glaciers will continue to shrink in future even without further rise in the temperature. Further, the rapid changing glaciers are the source of some serious natural hazards such as glacier-outburst floods, snow and ice avalanches, glacial surges, (Haeberli *et al.*, 1998, 2001; Haeberli and Kääb, 2001; Kääb *et al.*, 2005; Kargel *et al.*, 2005; Quincey *et al.*, 2005; Bajracharya *et al.*, 2009; Dobhal *et al.*, 2013) etc.

In view of the above facts, it is very important that the glaciers, especially glaciers in high mountain regions such as in the Himalayas are monitored regularly. This can be done either through field surveys and/or by using remote sensing techniques. With the advancement in the satellite remote sensing data acquisition and processing techniques, their use in glacier monitoring has increased considerably. Remote sensing has been employed in various glaciological applications, such as estimation of area, depth, volume, velocity, albedo and mass balance, as these constitute vital input parameters for hydrological, climatological and hazard prediction models (Bishop *et al.*, 2000; Bahuguna *et al.*, 2004; Bishop *et al.*, 2004; Bahuguna *et al.*, 2007; Bajracharya *et al.*, 2008; Scherler *et al.* 2011a, b; Bolch *et al.*, 2012; Gardelle *et al.*, 2012; Kääb *et al.*, 2012; McNabb *et al.*, 2012; Yao *et al.*, 2012; Malenovsky *et al.*, 2012; Ahluwalia *et al.*, 2013; Cruz et al., 2007; Paul *et al.*, 2013).

In this research, Chhota-Shigri glacier in Himachal Himalayas has been studied using remote sensing techniques. The Chhota-Shigri glacier is situated in the Lahaul-Spiti valley in the State of Himachal Pradesh in India. It is relatively a small glacier with a length of around 9 km (Latitude 32.08˚ N to 32.29˚ N and Longitude 77.47˚ E to 77.55˚ E) located on the northern slopes of the Pir-Panjal range. Due to its climatic settings and other geological and geomorphological characteristics, since 2002 it has been chosen as a representative glacier in Himalayas for long term monitoring using field based techniques

by various groups of glaciologists (Ramanathan, *et al.*, 2011). The present research based on remote sensing attempts to fill the gap in the field collected data on various aspects of this glacier like ice dynamics (such as ice velocity and retreat) and mapping of glacial terrain.

1.2 Significance of Glaciers

Global environment and socio-economics are affected by glaciers in many ways. Glaciers are vital source of freshwater in the many parts of the world such as in the northern India. The glaciological studies in the past have suggested that the glaciers are melting (Kieffer *et al.*, 2000; Kulkarni and Alex, 2003; Kulkarni *et al.*, 2004; Kulkarni, 2007) and retreating all over the world except some cases in Karakoram region where glaciers are stable or advancing (Quincey *et al.*, 2011; Scherler *et al.*, 2011b; Bolch *et al.*, 2012; Gardelle *et al.*, 2012; Kääb *et al.*, 2012; Yao *et al.*, 2012; IPCC, 2013). This very dynamic nature of glaciers may trigger some key catastrophic events. Thus, a detailed study on monitoring of glaciers is justified and relevant in view of the following thematic applications.

1.2.1 Management and planning of water resources

The cryosphere is the collective term used for the components of the Earth system that contain a substantial fraction of frozen water (Table 1.1). Only 0.7% of the world's fresh water is contained in the glaciers outside Antarctica and Greenland (Williams and Hall, 1993). However, even this small amount is very precious as it is utilized for different purposes by vast population. In Indian sub-continent, the seasonal snow and glaciers of the Hindu-Kush and Himalayas provide a substantial amount of runoff to the lowland dry-season flows of the Indus, Ganges and Brahmaputra rivers and their vast distributory and irrigation networks (Haritashaya *et al.*, 2006). Singh *et al.* (1997) reported that the annual flows of a few Himalayan rivers receive substantial contribution from snow and glaciers melt-water runoff (Table 1.2). Snow and glacier melt ensures continuous availability of streamflow, which, in combination with mountainous topography, provides a huge potential for hydropower generation.

Table 1.1: Representative statistics for cryospheric components indicating their general significance (Source: IPCC, 2013).

Ice on Land	**Percent of Global Land Surface[a]**	**Sea Level Equivalent[b] (metres)**
Antarctic ice sheet[c]	8.3	58.3
Greenland ice sheet[d]	1.2	7.36
Glaciers[e]	0.5	0.41
Terrestrial permafrost[f]	9–12	0.02–0.10[g]
Seasonally frozen ground[h]	33	Not applicable
Seasonal snow cover (seasonally variable)[i]	1.3–30.6	0.001–0.01
Northern Hemisphere freshwater (lake and river)	1.1	Not applicable
Total[k]	**52.0–55.0%**	**~66.1**
Ice in the Ocean	**Percent of Global Ocean Area[a]**	**Volume[l] (103 km^3)**
Antarctic ice shelves	0.45[m]	~380
Antarctic sea ice, austral summer (spring)[n]	0.8 (5.2)	3.4 (11.1)
Arctic sea ice, boreal autumn (winter/spring)[n]	1.7 (3.9)	13.0 (16.5)
Sub-sea permafrost[o]	~0.8	Not available
Total[p]	**5.3–7.3**	

[a] Assuming a global land area of 147.6 Mkm^2 and ocean area of 362.5 Mkm^2.

[b] See Glossary. Assuming an ice density of 917 kg m^{-3}, a seawater density of 1028 kg m^{-3}, with seawater replacing ice currently below sea level.

[c] Area of grounded ice sheet not including ice shelves is 12.295 Mkm^2 (Fretwell *et al.*, 2013).

[d] Area of ice sheet and peripheral glaciers is 1.801 Mkm^2 (Kargel *et al.*, 2012). SLE (Bamber *et al.*, 2013).

[e] Calculated from glacier outlines (Arendt *et al.*, 2012), includes glaciers around Greenland and Antarctica. For sources of SLE see Table 1.3. (Source: IPCC 2013).

[f] Area of permafrost excluding permafrost beneath the ice sheets is 13.2 to 18.0 Mkm^2 (Gruber, 2012).

[g] Value indicates the full range of estimated excess water content of Northern Hemisphere permafrost (Zhang *et al.*, 1999).

[h] Long-term average maximum of seasonally frozen ground is 48.1 Mkm^2 (Zhang *et al.*, 2003); excludes Southern Hemisphere.

[i] Northern Hemisphere only (Lemke *et al.*, 2007).

[j] Areas and volume of freshwater (lake and river ice) were derived from modelled estimates of maximum seasonal extent (Brooks *et al.*, 2012).

[k] To allow for areas of permafrost and seasonally frozen ground that are also covered by seasonal snow, total area excludes seasonal snow cover.

[l] Antarctic austral autumn (spring) (Kurtz and Markus, 2012); and Arctic boreal autumn (winter) (Kwok *et al.*, 2009). For the Arctic, volume includes only sea ice in the Arctic Basin.

[m] Area is 1.617 Mkm^2 (Griggs and Bamber, 2011).

[n] Maximum and minimum areas taken from IPCC 2013 assessment.

[o] Few estimates of the area of sub-sea permafrost exist in the literature. The estimate shown, 2.8 Mkm^2, has significant uncertainty attached and was assembled from other publications by Gruber (2012).

[p] Summer and winter totals assessed separately.

Table 1.2: Snow and glacier melt contributions in some Himalayan rivers (Singh *et al.*, 1997).

Rivers	Catchment area (km^2)	Snow cover area (km^2)		Snow and glacier contribution in the annual flows (%)
		Maximum	Minimum	
Ganges (up to Deoprayag)	19700	9080 (40.9%)	3800 (19.3%)	29%
Chenab (up to Akhnoor)	22200	15590 (70.2%)	5400 (24.3%)	49%
Satluj (up to Bhakra Dam, Indian Part)	22305	14498 (65.0%)	4528 (20.3%)	60%

1.2.2 Global climatic changes

High sensitivity of glaciers for small changes in the local environment renders them as excellent indicators of prevailing global climatic changes. Earlier in view of less available data, glaciers were often called as 'natural thermometer' as they were believed to be retreating in view of rising global temperature (Sharma and Owen, 1996; Haeberli *et al.*, 1999; Orelemans, 2005; Khromova *et al.*, 2006; Paul *et al.*, 2007; Cruz et al., 2007; Kulkarni *et al.*, 2007). But with the growing understanding of the complexity of this response, it is increasingly clear that elements of the cryosphere should rather be considered as a 'natural climate-meter', responsive not only to temperature but also to other climate variables (e.g., precipitation) (IPCC, 2013). The impact of changing climate is manifested on the glaciers, different types of glaciers respond differently to the changing climate. Smaller mountain glaciers, with fairly constant slopes, adjust more quickly to the new climate by changing the size of their ablation area more rapidly. These changes may

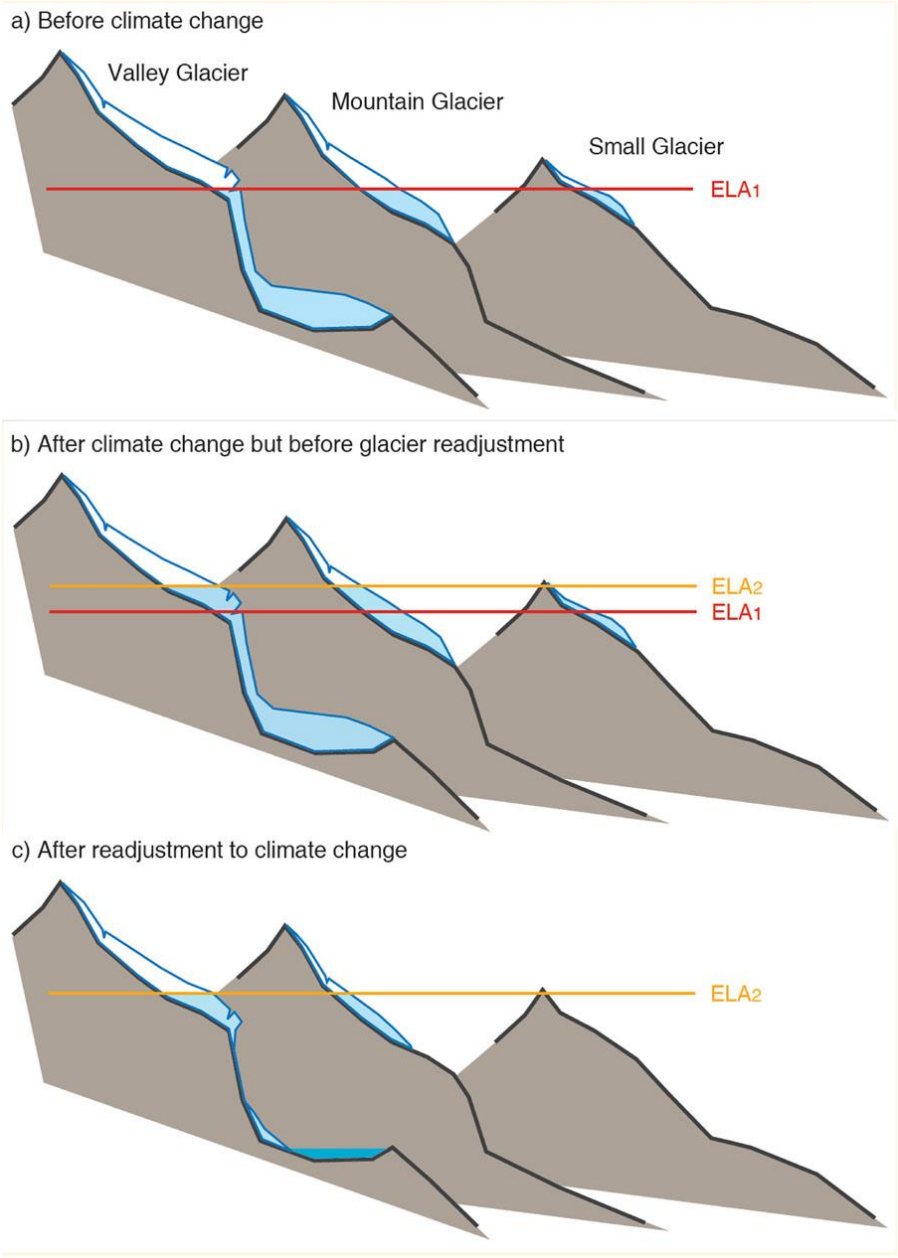

Figure 1.1: A schematic of three types of glaciers located at different elevations, and their response to an upward shift of the equilibrium line altitude (ELA). (a) For a given climate, the ELA has a specific altitude (ELA1), and all glaciers have a specific size. (b) Due to a temperature increase, the ELA shifts upwards to a new altitude (ELA2), initially resulting in reduced accumulation and larger ablation areas for all glaciers. (c) After glacier size has adjusted to the new ELA, the valley glacier (left) has lost its tongue and the small glacier (right) has disappeared entirely (Source: IPCC, 2013).

the size of their ablation area more rapidly. These changes may include change in the annual mass balance, length changes (retreat, measured by changing snout positions), changes in the areal extent (deglaciation) and volume changes (thinning). Figure 1.1 shows a schematic long-term response of prominent glacier types in response to the changing climate. However, the length and area changes comprise the clearest and directly comprehensible indicators of glacier recession.

1.2.3 Sea level rise

Mass loss from glaciers as a result of climate change eventually leads to an increase in the sea level. The knowledge about the glacier mass loss has increased in the last decade (IPCC, 2013). The use of satellite data for calculation of ice volume (ice thickness and depth) is being increasingly made. The latest advancement in the laser satellite altimetry is the main reason behind this. In the last decade, gravity observations from Gravity Recovery and Climate Experiment (GRACE) satellites have been used to measure mass change of the glaciers at global level. In the 20th century, global mean sea level rise has been mainly attributed to ocean thermal expansion and glacier melting (75% of the observed rise since 1971). The contribution of the Greenland and Antarctic ice sheets in mean sea level rise has increased since the early 1990s. It is predicted that the rate of global mean sea level rise during the 21st century will exceed the rate observed during 1971–2010 due to increases in ocean warming and loss of mass from glaciers and ice sheets (Wang and Swail, 2006; Mori *et al.,* 2010; Hellmer *et al.,* 2012; Fan *et al.,* 2013; Semedo *et al.,* 2013). A detailed analysis of sea level rise has been provided in IPCC 2013 report.

1.2.4 Glacier-related hazards

Glacier hazards pose threat to human lives, settlements, and infrastructure in high-mountain regions and the population downstream of the glacier fed rivers. The recent Kedarnath flood in Uttarakhand, India in the year 2013 has been one of the largest disasters associated with glaciers in the human history. Glacier disasters in high mountains include snow and ice avalanches and glacier lake outbursts floods (GLOFs). Furthermore, with the current and predicted scenario of global warming, it is expected that the frequency and magnitude of glacial hazards will increase. Thus, prevailing climatic changes together with

the extension of the human settlements and activities in high altitude regions make assessment and prediction of glacier disasters very important. In view of the recognized damage potential of glacial hazards, a number of assessment and mitigation studies have been carried out (Reynolds, 1998; Haeberli *et al.*, 1998, 2001; Haeberli and Kääb, 2001; Dhobal *et al.*, 2013; Sinha and Rasik, 2013).

1.2.5 Other socio-economic factors

Snow fields and glaciers are the main attraction of some of the most important tourist places in the world. Winter games are the source of income to the local residents and major contributor to the economy in many places around the world. But the decreasing snow and ice fields and their shifting to the higher reaches have direct implication to the tourism industry. Similarly, agriculture and many industries are also dependent on water supplied by the snow fed rivers. Therefore, if glaciers' area is reduced it will directly affect many socio-economic sectors.

1.3 Distribution of Glaciers

1.3.1 Global glacier distribution

The occurrence of glaciers is controlled chiefly by geographic and climatic conditions. The glaciers develop in areas where water precipitates in the form of snow, *i.e.* the temperatures are stably low and the rate of annual water precipitation in the form of snow significantly exceeds the rate of annual wastage. These conditions are usually found at higher latitudes and/or higher altitudes. In respect to the styles of glaciation in contrasting glaciological settings except that of Antarctic and Greenland, the glacier regions around the globe can be classified as:

(i) southern hemisphere temperate glaciers in Patagonia and New Zealand
(ii) northern hemisphere temperate glaciers in Alaska and Iceland
(iii) high-altitude glaciers in the Himalayas
(iv) tropical glaciers in the Cordillera Blanca, Peru
(v) polythermal glaciers in the Arctic.

In the IPCC 2013 report, a comprehensive analysis of glaciers around the world can be found. After many controversies arising out of the fourth report of IPCC in 2007 (Cruz *et al.*, 2007), the world glacier inventory (WGMS, 1989) was gradually extended by Cogley (2009) and Radić and Hock (2010). A new globally complete data set of glacier outlines- Randolph Glacier Inventory (RGI) has been compiled from a wide range of data sources from the 1950s to 2010 with varying levels of detail and quality (Arendt *et al.*, 2012). RGI has divided the world glaciers and the snow fields into 19 different regions (Table 1.3; Figure 1.2).

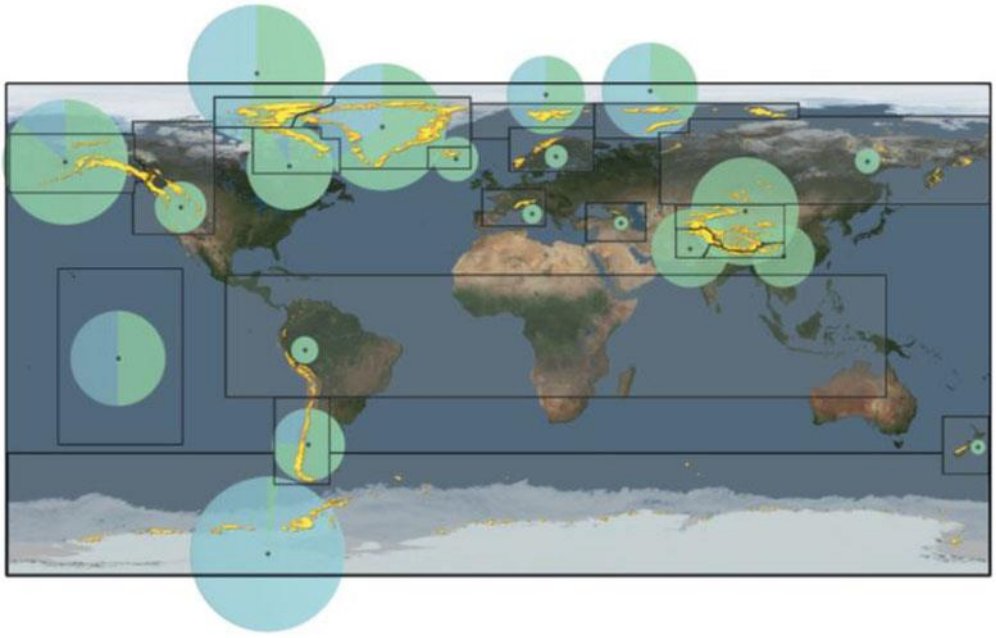

Figure 1.2: Global distribution of glaciers (yellow, area increased for visibility) and area covered (diameter of the circle), sub-divided into the 19 RGI regions (white number) referenced in Table 1.3. The area percentage covered by tidewater (TW) glaciers in each region is shown in blue. Data from Arendt *et al.* (2012) and Gardner *et al.* (2013) (Source: IPCC, 2013).

Arctic sea ice cover varies in different seasons, summer average ice extent is around 6 x 10^6 km^2, which in winter increases to 15 x 10^6 km^2 (Comiso and Nishio, 2008; Cavalieri and Parkinson, 2012; Meier *et al.*, 2012). The Antarctic sea ice cover is largely seasonal, with average extent varying from a minimum of about 3 × 106 km^2 in February to a maximum of about 18 × 106 km^2 in September (Zwally *et al.*, 2002; Comiso *et al.*,

2011). Most of the Antarctic ice is lost in the summer therefore mostly first-year ice is found in the Antarctic region. Thus, this ice cover is on an average thinner, warmer, more saline and more mobile than the Arctic ice (Wadhams and Comiso, 1992).

The two large ice sheets (Antarctica and Greenland) occupy about 96.5% of the total ice covered area of the globe. The current best estimate of total number of glaciers is around 170,000 covering a total area of about 730,000 km^2 (IPCC 2013). Nearly 80% of the glacier area is found in regions Antarctic and Subantarctic, Canadian Arctic, High Mountain Asia, Alaska, and Greenland (Table 1.3). The global glacier mass is estimated to be between 114,000 and 192,000 Gt (314 to 529 mm SLE). Glaciers of Asia cover an area of about 50% of all glaciers outside the polar region and a large part of them drain through the landmass of the Indian sub-continent (Sharp, 1988). Central Asia with an estimated total ice covered area of about 114,800 km^2, with Himalayas being its dominant mountain range are abode to most of the glaciers (33,050 km^2) in the region (UNEP, 2008). The other mountain ranges in the region (with their corresponding ice areas) are: Karakoram (16,600 km^2), Tien Shan (15,417 km^2), Kunlun Shah (12,260 km^2) and Pamir (12,260 km^2) (Dyurgerov and Meier, 2005).

IPCC 2013 have divided global glacier cover into 19 different regions (Table 1.3). The divisions of glaciers are mainly derived from the RGI 2.0 (Arendt *et al.*, 2012). It also gave an estimate of the tidewater fraction of snow/ice present in these glacierized regions based on the work of Gardner *et al.* (2013). In Table 1.3, the minimum and maximum values of glacier mass presented are the minimum and maximum of the estimates based on the studies of Huss and Farinotti (2012), Marzeion *et al.* (2012), Grinsted (2013) and Radić *et al.* (2013). Also, the mean sea level equivalent (SLE) of the mean glacier mass is the mean of estimates from the same studies, using an ocean area of 362.5 × 106 km^2 for conversion. All values were derived with globally consistent methods; deviations from more precise national data sets are thus possible. Ongoing improvements may lead to revisions of these (RGI 2.0) numbers in future releases of the RGI.

Table 1.3: The 19 glacier regions classified by IPCC, 2013 and their respective glacier numbers and area (absolute and in percent).

Region	Region Name	Number of Glaciers	Area (km^2)	Percent of total area	Tidewater fraction (%)	Mass (min.) (Gt)	Mass (max.) (Gt)	Mean SLE (mm)
1	Alaska	23,112	89,267	12.3	13.7	16,168	28,021	54.7
2	Western Canada and USA	15,073	14,503.5	2.0	0	906	1148	2.8
3	Arctic Canada North	3318	103,990.2	14.3	46.5	22,366	37,555	84.2
4	Arctic Canada South	7342	40,600.7	5.6	7.3	5510	8845	19.4
5	Greenland	13,880	87,125.9	12.0	34.9	10,005	17,146	38.9
6	Iceland	290	10,988.6	1.5	0	2390	4640	9.8
7	Svalbard	1615	33,672.9	4.6	43.8	4821	8700	19.1
8	Scandinavia	1799	2833.7	0.4	0	182	290	0.6
9	Russian Arctic	331	51,160.5	7.0	64.7	11,016	21,315	41.2
10	North Asia[a]	4403	3425.6	0.4	0	109	247	0.5
11	Central Europe	3920	2058.1	0.3	0	109	125	0.3
12	Caucasus	1339	1125.6	0.2	0	61	72	0.2
13	Central Asia	30,200	64,497	8.9	0	4531	8591	16.7
14	South Asia (West)	22,822	33,862	4.7	0	2900	3444	9.1
15	South Asia (East)	14,006	21,803.2	3.0	0	1196	1623	3.9
16	Low Latitudes[a]	2601	2554.7	0.6	0	109	218	0.5
17	Southern Andes[a]	15,994	29,361.2	4.5	23.8	4241	6018	13.5
18	New Zealand	3012	1160.5	0.2	0	71	109	0.2
19	Antarctic and Sub-Antarctic	3274	13,2267.4	18.2	97.8	27,224	43,772	96.3
Total		**168,331**	**726,258.3**		**38.5**	**113,915**	**191,879**	**412.0**

Notes: [a] For regions 10, 16 and 17 the number and area of glaciers are corrected to allow for over-inclusion of seasonal snow in the glacierized extent of RGI 2.0 and for improved outlines (region 10) compared to RGI 2.0 (updated from, Arendt *et al.*, 2012).

1.3.2 Glacier distribution in Indian Himalayas

The majestic Himalayas are the world's youngest mountain system. Developed in an arcuate shape they run for about 2500 km between Indus and Brahmaputra with an average width of 240 km separating the Indian subcontinent from the Tibetan plateau. True to their name, the massive Himalayas (the abode of snow) have the third largest snow and ice mass in the world after the two continental ice sheets (Antarctica and Greenland) and hence, are also some time referred to as the 'Third Pole' of the earth! The Indian Himalayan region lies between 21º57'-37º5' N latitudes and 72º40'-97º25' E longitudes occupying the strategic position of entire northern boundary (north-west to north-east) of the nation and includes as many as seven international borders of India. The Himalayan mountain range can be divided into three parallel longitudinal zones, namely, Higher or Greater Himalayas (elevation >6000 m), Lower or Lesser Himalayas (elevation 1500-5000 m) and the Outer Himalayas or Siwaliks (elevation 900-1200 m). World's 14 tallest peaks are located here at about 8000 m including the highest peak of the planet namely, Mt. Everest (8,848 m). Also, there are hundreds of peaks over 6000-7000 m above mean sea level (msl) (Bahadur, 2003).

Glaciers in Himalayas are distributed all across its length. In Indian part of the Himalayas, glaciers are mainly found within the latitude 27^{o} to 36^{o} N and longitude 72^{o} to 96^{o} E (Uttarakhand State of the Environment Report 2012). The Asian Monsoons together with Mid-Westerlies constitute the two independent and prime climatic regimes which are the chief source of moisture in this region (Böhner, 2006; Bookhagen and Burbank, 2010). Total numbers of glaciers in Himalayas are estimated to be around 22,829 (Bolch *et al.* 2012), out of which India has 9575 glaciers (Sangewar and Shukla, 2009). Bolch *et al.* (2012) reported the volume of the entire Himalayan glaciers from 1071 km^3 to 2431 km^3 based on different published data.

The latest Indian inventory of glaciers for Indian part of Himalayas has been prepared by the Geological Survey of India (Sangewar and Shukla, 2009) (Table 1.4; Figure 1.3 and Figure 1.4). The Indian states of Jammu and Kashmir, Himachal Pradesh, Uttarakhand, Sikkim and Arunachal Pradesh have glacier cover in the northern part. Total

area of the glaciers is around 27,000 km^2 with an approximate volume of 1300 km^3 (Table 1.4).

Table 1.4: Basin-wise inventory, areas and volumes of Indian glaciers.

Basin	No. of Glaciers	Area (km^2)	Volume (km^3)
Indus Basin			
Ravi	172	192.74	8.038
Chenab	1278	3058.99	206.15
Jhelum	133	94.18	3.3
Beas	277	599.06	36.94
Satluj	926	1250.86	60.99
Indus	1796	2165.86	104.6
Shyok	2658	7105.66	601.71
Kishanganga	222	174.28	5.93
Gilgit	535	8240	N.D.
Total	**7997**	**22881.23**	**1027.658**
Ganga Basin			
Yamuna	52	144.47	12.21
Bhagirathi	238	755.43	67.02
Alaknanda	407	854.59	90.72
Ghagra	271	729.42	43.77
Total	**968**	**2483.91**	**213.72**
Brahmaputra Basin			
Teesta	449	705.54	39.61
Arunachal	161	223.37	9.96
Total	**610**	**928.91**	**49.57**
Grand Total	**9575**	**26294.05**	**1290.95**

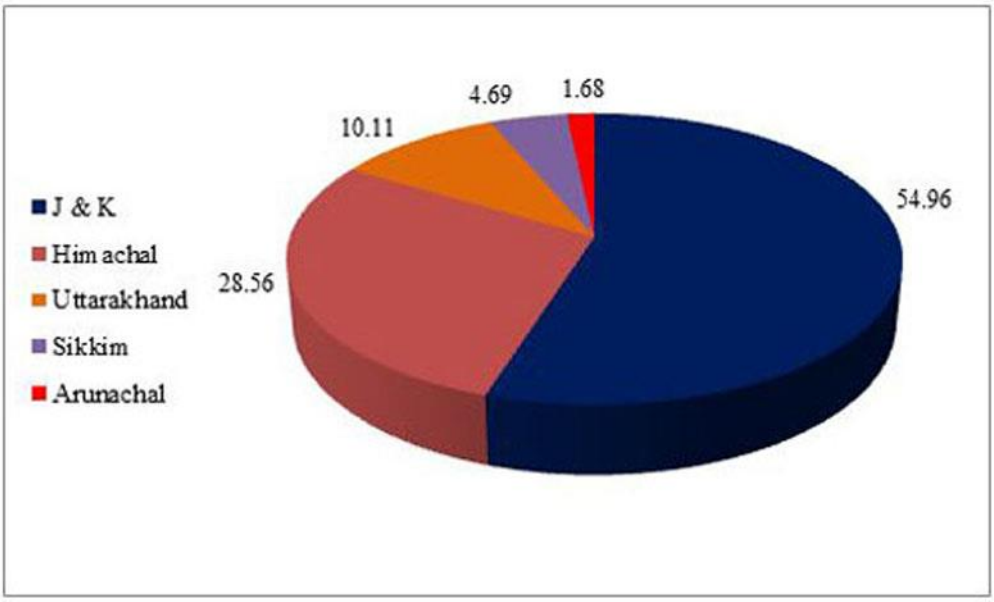

Figure 1.3: State wise distribution of Glaciers (percentage) in Indian Himalayas.

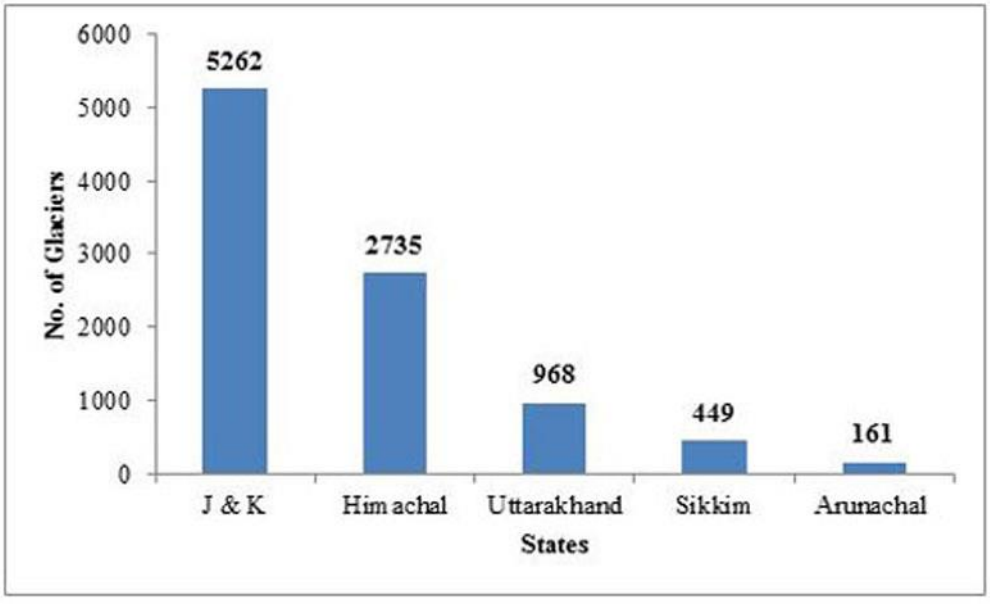

Figure 1.4: Distribution of glaciers (in numbers) in Indian Himalayas.

Distribution of glaciers along the Himalayan arc is uneven with the concentration of glaciers being higher in the NW than NE part of the Indian Himalayas. Glacier density across Himalayas varies, being highest in the Sutlej and Teesta river basins and moderate in Jhelum and Bhagirathi basins (Ahmad *et al.*, 2004). Arunanchal Pradesh basin has the

lowest glacier density. The variation in the glaciations characteristic across Himalayas can be attributed to the variations in terrain parameters, and regional climatic and geographic disposition. Some workers (Ahmad *et al.*, 2004) assert that these reasons have also led to the development of distinctive morphometric characteristics of glaciers across Himalayas.

It has been estimated that about 17% of the Himalayan mountain area is presently under permanent ice cover (Ahmad and Rais, 1998). Some of the major glaciers of Himalayas (with their respective estimated lengths) are: the Siachen Glacier (76 km), Hispar Glacier (62 km), Batura Glacier (58 km), and Baltoro Glacier (58 km) in Karakoram; Gangotri Glacier (30 km), and Milam Glacier (19 km) in Garhwal Himalaya; Zemu Glacier (26 km) and Kanchenjunga Glacier (16 km) in Sikkim Himalayas; Chhota-Shigri Glacier (9 km), Samudratapu Glacier (23 km) and Bara-Shigri Glacier (28 km) in Himachal Pradesh.

1.4 Remote Sensing Based Glaciological Studies

Aerial and satellite remote sensing technology has been used for glacier studies since its emergence. Though data from field based methods may be more accurate at small scale, these methods are often hard to apply in rugged mountain areas due to difficult access, complicated logistics, and political or cultural complexities. Use of remote sensing for glaciological studies has resulted in a multi-faceted improvement of studies. As glaciers are mostly located in inaccessible and high-mountain terrains, remote sensing becomes major and the most handy tool for both local and global retrieval of various snow and glacier characteristics (such as glacier area, length, volume, depth, elevation, velocity, albedo, surface flow fields, accumulation/ablation rates etc). The biggest advantage of remote sensing data is their repetitive and synoptic coverage of an area that permits near real time, year round and repetitive studies. Moreover, remote sensing data can be obtained at a range of spectral, spatial and temporal resolutions. Therefore, they have been widely utilized for varied glaciological applications, such as mass balance studies, glacier mapping, per and sub-pixel mapping of snow-cover and various supraglacial covers, snow cover depth estimation studies, glacier retreat and dynamics, snow and glacier-related hazard assessment etc. (Hall *et al.*, 1988; Sidjak and Wheate, 1999; König *et al.*, 2001; Vikhamar and Solberg, 2003; Berthier *et al.*, 2004; Kelly *et al.*, 2004; Salomonson and

Appel, 2004; Gupta *et al.*, 2005; Kääb, 2005; Kargel *et al.*, 2005; Quincey *et al.*, 2005; Kääb, 2007; Luckman *et al.*, 2007; Oerlemans, 2007; Bolch *et al.*, 2008a, b; Shukla *et al.*, 2010; Paul *et al.* 2013). A brief review of use of remote sensing for studying mountain glaciers is given below.

The increased availability of remote sensing data has led to the extension of measurements of glacier parameters over larger areas and longer time spans. In early 70s, airborne data were used for extracting glacier parameters. Later, medium spatial resolution (10-90 m of Landsat MSS, TM, ETM+; ASTER; SPOT; IRS LISS etc.) and high spatial resolution (0.5-1 m of IKONOS; Quickbird; GeoEye-1 etc.) data have become available (Racoviteanu *et al.,* 2008).

Precise estimation of glacier/snow cover area is one of the most important input parameter required in most glaciological studies such as the mass balance, volumetric estimation of cryospheric components, estimation of glacier fluctuations (length and area), meltwater runoff modelling, glacier hazard prediction modelling, climatological modelling etc. Mapping of ice and snow facies started in 1970s using Landsat MSS data (Ostrem, 1975; Rott 1976) and then in 1980s using TM data (Hall *et al.,* 1987; Williams *et al.,* 1991; Bayr *et al.,* 1994; Aniya *et al.,* 1996; Jacobs *et al.,* 1997; Philip and Ravindran, 1998). A number of authors have used a wide range of methods for mapping the glaciers. These include:

a) manual on-screen digitization (Rott and Markl, 1989; Williams *et al.,* 1997)

b) segmentation of ratio images (Hall *et al.,* 1988; Bronge and Bronge, 1999; Bayr *et al.,* 1994; Rott, 1994; Paul, 2000; Paul, 2002a, b)

c) various supervised and unsupervised algorithms (Aniya *et al.,* 1996; Bronge and Bronge, 1999; Sidjak and Wheate, 1999; Slater *et al.,* 1999; Shukla *et al.* 2010a, b)

d) spectral indices based techniques (Dozier, 1989; Hall *et al.,* 1995; Winther and Hall, 1999; Xiao *et al.,* 2001; Gupta *et al.,* 2005; Silvero and Jaquet, 2005; Shimamura *et al.,* 2006; Keshri *et al.,* 2009)

e) fractional snow-cover mapping techniques (Rosenthal and Dozier, 1996; Vikhamar and Solberg, 2003; Salomonson and Appel, 2004).

Several international endeavors with the aim of global glacier mapping and monitoring using field as well as remote sensing data have been launched, such as, the *World Glacier Monitoring Service* (WGMS), a service of the *International Association of the Cryospheric Sciences* of the *International Union of Geodesy and Geophysics* (IACS, IUGG) and the *Global Land Ice Measurements from Space* (GLIMS) (Haeberli *et al.*, 2002; Kargel *et al.*, 2005; Raup *et al.*, 2007). WGMS, in cooperation with the *US National Snow and Ice Data Centre* (NSIDC) and the GLIMS, is also the in-charge of the *Global Terrestrial Network for Glaciers* (GTN-G) within the *Global Climate/Terrestrial Observing System* (GCOS/GTOS) (GCOS/GTOS, 2004; UNEP, 2008).

However, mapping of glaciers solely on the basis of spectral properties of glaciers may lead to inaccuracies because of the presence of topographic shadows (Howarth and Ommanney, 1986). This effect may be eliminated by using DEM of the area as it compensates for the impact of solar elevation and azimuth in mapping glaciers in shaded areas (Parrot *et al.*, 1993). Cloud cover also poses a hindrance in mapping the glaciers using remote sensing Also, many of the valley glaciers in the mountainous terrain are fraught with debris. Mapping of the debris covered glaciers even by remote sensing has always been a challenge as can be seen from a number of studies (e.g., Paul, 2002a, b; Paul *et al.*, 2004; Ranzi *et al.*, 2004; Kargel *et al.* 2005; Bolch and Kamp, 2006; Buchroithner and Bolch, 2007; Bolch *et al.*, 2008a, b; Shukla *et al.*, 2010a, b; Paul *et al.* 2013). A comprehensive review of mapping debris covered glaciers has been presented in Chapter 5.

The presence of fog and similarity in spectral characteristics of snow and cloud also pose a problem in glacier mapping. To resolve this issue, microwave remote sensing data have been used by many workers. Nagler and Rott (1997) developed a methodology for mapping snow cover of glaciers from SAR images. But the biggest limitation of SAR data is their low spatial resolution, lesser geometric resolution and shadowing in images due to steep mountain slopes. Moreover, the identification potential of glaciological features on SAR images is affected by seasonality (Engeset and Weydahl, 1998).

In the earlier days, generally glacier mass balance studies were done through field based methods using stakes and pits on glacier surface (Mayo *et al.,* 1962; Ostrem and Brugman, 1991; Kaser *et al.,* 2002; Wagnon *et al.,* 2007; Azam *et al.,* 2012). It is, however, difficult to obtain sufficient data by such methods due to frequent loss of stakes. Moreover, the process is labor-intensive, expensive and, usually provides very limited spatial coverage. Thus, remote sensing data provides a practical approach for obtaining a statistically representative sample of mass balance estimates (Bamber and Rivera, 2007). Glacier mass balance may be estimated using satellite data by various methods such as, the budget approach (requiring ice thickness, surface and depth-average velocity etc.) (Bamber and Kwok, 2004); the volume-area scaling techniques (Bahr, 1997; Bahr and Dyurgerov, 1999; Oerlemans, 2007); the geodetic method (Berthier *et al.,* 2007; Racoviteanu *et al.,* 2007; Kääb, 2007); the Accumulation Area Ratio (AAR)/ Equilibrium Line Altitude (ELA) method (requiring glacier outlines and DEM) (Kulkarni, 1992); the template method (Dyurgerov, 1996); the ELA method (Rabatel *et al.*, 2008).

The motion of a glacier occurs in three dimension of space (Gao and Liu, 2001). Glacier surface ice velocity can be estimated from field based methods and also from multi-temporal satellite data using SAR interferometry, SAR image data intensity tracking (Goldstein *et al.*, 1993; Kwok and Fahnestock, 1996; Joughin *et al.,* 1998; Joughin et al., 2002; Strozzi *et al.,* 2002; Moll *et al.,* 2006; Bolon *et al.*, 2007; Luckman *et al.*, 2007; Kumar *et al.,* 2009), or feature tracking from optical data (Scambos *et al.*, 1992; Lucchitta *et al.*, 1993; Lefauconnier *et al.*, 1994; Evans, 2000; Kääb and Volmer, 2000; Berthier *et al.*, 2004; Kääb, 2005). Optical image correlation is another promising technique now used to deduce deformation or displacement of a moving object (Bindschadler *et al.,* 1996; Rolstad *et al.,* 1997; Rack *et al.,* 1999; Kääb, 2002; Berthier *et al.,* 2003; Skvarca *et al.,* 2003; Kaufman and Ladstädter, 2003; Leprince *et al.*, 2008; Scherler *et al.*, 2008; Copland *et al.,* 2009; Quincey and Glasser, 2009; Haug *et al.*, 2010; Scherler *et al.,* 2011a, b; Tiwari *et al.,* 2014). Estimation of glacier velocity can contribute to a significantly better understanding of glacier dynamics and may also help in monitoring various glacier related hazards (Kääb *et al.,* 2003).

Glacier-related hazards, mainly glacier floods and avalanches, threaten communities and commercial activities in many mountainous regions of the world. For

assessing damage posed by such hazards, fast data acquisition is a prerequisite, therefore remote sensing techniques offer the only practical approach for providing requisite repetitive information in a reasonable time frame for glacier disaster prediction and management (Huggel, 2004; Kääb, 2004; Kargel *et al.*, 2005; Quincey *et al.*, 2005).

Estimates on snow depth and snow cover are useful for evaluating regional and global climatic changes and basin scale water storage in mountainous areas. Remote sensing of snow depth or snow water equivalent (SWE) is possible using the detection of naturally upwelling microwave radiation from the earth's surface. Microwave remote sensing allows direct mapping of snow volume, as the microwave radiation can penetrate through the snow pack. Both active (SAR data) (Shi *et al.*, 1990; Guneriussen *et al.*, 2001) and passive microwave data (Chang *et al.*, 1987; Foster *et al.*, 1997) have been used for estimation of snow depth.

The foregoing discussion provides a broad overview of the present status, scope and problems in the use of remote sensing for glaciological studies.

1.5 Research Gaps

Extensive review of the literature on applications of remote sensing in glaciology in general, and on mapping of glacier and snow covered area in particular, reveals presence of various research problems and gaps and can be enumerated with special reference to Chhota-Shigri Glacier, as:

1. The type of landforms present and development in any glacier valley is the indicator of the health and the fate of the glacier. Also, the landforms can be used to derive the past changes that have happened in the area. The landform map prepared earlier needs updating with interpretation from high resolution remote sensing data sets.

2. Even as research with regard to mapping and monitoring of glaciers using remote sensing techniques is being extensively carried out throughout the world, in India even a complete inventory of Himalayan glaciers meeting global standards is lacking (Racoviteanu *et al*., 2008). Further, remote sensing data based mapping of glaciers in India is still widely used only for snout mapping (Bhambhri *et al.*, 2012).

3. Glaciers in most of the mountain ranges world over (Himalaya, Andes, Alaska, etc.) are covered with varying amounts of debris cover. Mapping of partially or wholly debris covered glacier boundaries has long been recognized as one of the major problems in accurate mapping of glaciers throughout the world. Though some attempts have been made using morphological and thermal satellite data, a dependable and standardized methodology/approach for accurate mapping of debris-covered glaciers is still lacking.

4. Further, to incorporate different ancillary information in classification process, only the binary classification method or the thresholding methods are used with Boolean logic. Potential of advanced methods like knowledge based method for incorporating such information in glacier mapping is still unexplored.

5. The importance of precise estimates of snow and glacier cover area in melt-water runoff modeling is well known. However, presently, nearly all runoff models till date consider the entire snow/ice/glacier basin as a homogenous body with the same potential of melt-water contribution. However, this is not true since glacier surface comprises of several water bearing zones such as snow, ice, ice mixed debris, and ice beneath supraglacial debris (SGD) (Gupta *et al.,* 2005). All these zones, having different hydrological behavior, need to be separately mapped and incorporated as individual entities which could be later incorporated in the snow/glacier meltwater runoff modeling.

6. In general, the understanding of microwave remote sensing for glaciology is very limited. The full potential of polarimetric and interferometric SAR techniques need to be intensively explored for mapping and monitoring of various snow and glacier parameters (such as area, velocity, depth and volume), particularly in the Himalayan region.

7. The optical image correlation has been widely tested for the study of deformation in the surface of earth and has been an established method. This method has also been used in the field of glaciology for studying the surface ice velocity. But the method has never been tested for its accuracy using the field data.

1.6 Chhota-Shigri – Site Selection

Chhota-Shigri (Figure 2.1) is considered as a model glacier in the Indian Himalayas. During the International Workshop jointly organized by International Commission on Snow and Ice (ICSI), UNESCO, Department of Science and Technology (DST), India, and Jawaharlal Nehru University (JNU), India, which emphasized the need of glacier mass balance measurements in the Himalayas, Chhota-Shigri glacier was proposed as a benchmark glacier in the Himalayan terrain. The ICSI has formulated certain guidelines for benchmark glaciers, *viz*.: glacier area neither too small nor too large, altitudinal range approximately 1000 m (to detect ELA variability), well defined catchment, simple geometry, easy accessibility, well defined accumulation area, single tongue, insignificant mechanical processes such as avalanches, relatively debris free and smooth surface, etc. It was generally agreed that the Chhota-Shigri glacier fulfilled most of the above requirements, and therefore it was chosen as a site for long term monitoring in the Indian Himalayas.

Following this, the glacier has quite continuously been monitored in the field from 2002 onwards on various aspects such as velocity, melt-water chemistry, snout fluctuation, etc. by various glaciologist groups. The review of previous works on this glacier (presented in detail in Chapter 2) indicates that the glacier has also been studied earlier (late 1980s) for landforms development and changes. Thus, a good amount of preliminary field collected data has been available for this glacier. In view of the above, the Chhota-Shigri glacier was chosen as the study site in this research programme.

On the other hand, due to the difficulty in collection of field data, the glacier landform map prepared earlier has never been updated. Also, the velocity data collected from the field based study has many absent years. The discharge from the glacier is directly related to the ice dynamics (mass balance, ice velocity, snow/ice cover and the debris cover), the absence of the map of the glacier terrain showing these aspect of glacier present problem in analysing the fate and health of this glacier. Therefore, in this research an attempt has been made to fill these gaps using various remote sensing techniques. The research also demonstrates the utility and accuracy of remote sensing method in glaciological studies.

1.7 Research Objectives

The main aim of the present research is to explore and demonstrate the potential of optical remote sensing data (particularly ASTER) for precise mapping of various supraglacial cover types (snow, ice, ice mixed debris, supraglacial debris, periglacial debris, valley rock, water and shadow) for the Chhota-Shigri glacier located in the Chenab basin of the Himachal Himalayas, north India. The above generalized goal has been realized by the application of routine, advanced and some novel techniques. Keeping in mind the existing lacunae within the domain of glacier and snow cover area mapping in India and otherwise, the specific research objectives may be enumerated as,

1. Detail geomorphological investigation and preparation of large scale (1:10000) geomorphological map of the Chhota-Shigri glacier.
2. Estimating retreat of the Chhota-Shigri glacier using multi-temporal remote sensing images and landform study.
3. Evaluating the advanced method like knowledge based method for incorporating information from various sources for improved glacier cover mapping.
4. Assessing the utility of combined optical and thermal data for glacier cover mapping.
5. Implementation and evaluation of COSI-Corr advanced technique of sub-pixel image correlation for glacier surface ice velocity estimation.

1.8 Thesis Outline

The thesis has been divided into nine chapters. Chapter 1 presents the importance of the glaciological studies in India and abroad along with the global and Indian distribution of glaciers. This chapter also presents a short review on the uses of remote sensing techniques for the glaciological mapping. The chapter also outlines the present research gaps and the objectives of this study. A review of all the work done in Chhota-Shigri glacier has been presented in the chapter 2.

In chapter 3, details of the data used for this study and their pre-processing have been presented. It also includes an overview of the broad methodology adopted in this research.

Chapter 4 presents the definition and characteristic of different terrain classes present in the studied glacier terrain. A comparison of the different techniques for glacier terrain mapping for the distribution of snow/ice, ice mixed debris and debris has been presented in chapter 5. The utility of the knowledge based classification has also been tested and presented for the debris cover mapping in this chapter. The focus of chapter 6 is on details of landforms present in this glacier mapped during two field works. The field collected data and the high resolution satellite image (WorldView-2) have been used to present an overview of the geomorphological features present in this glacier valley.

Chapter 7 presents the glacial recessional history derived using the presence of paleo-morainic loops in the inactive zone of the glacier mapped using the remote sensing technique. The recent recession of the glacier using time series ASTER images has been determined and presented in this chapter. The time series ASTER data has also been used to measure the surface ice velocity using an advanced image correlation method (COSI-Corr) and the results have been presented in chapter 8. Summary and conclusions of the thesis have been presented in chapter 9 along with the scopes of future work.

CHAPTER 2
STUDY AREA –THE CHHOTA-SHIGRI GLACIER

2.1 Introduction

This chapter describes the site of study, i.e. the Chhota-Shigri glacier. The chapter presents location, geographical aspects and geology of the study area. The geological description is limited to review in a broader–regional context only. A detailed description of the landforms-geomorphology has been presented separately later in chapter 6. This chapter also highlights a review of the glaciological work carried out by earlier workers in the Chhota-Shigri glacier.

2.2 The Study Area

2.2.1 Location and accessibility

The Chhota-Shigri glacier is situated in northern slopes of the Pir-Panjal range in the Lahaul-Spiti valley in the state of Himachal Pradesh, India. Chhota-Shigri is a small glacier with a length of around 9 km and an area of ~16 km^2 (Wagnon *et al.,* 2007). The glacier extends from Latitude 32.08˚ N to 32.29˚ N and Longitude 77.47˚ E to 77.55˚ E (Figure 2.1).

This glacier contributes its melt to the Chandra River, a major tributary of Chenab River. In its upper course through Lahaul valley, the river Chenab is known as the Chandra-Bhaga. It is formed by the confluence of rivers Chandra and Bhaga at Tandi and hence derives its name from there. These rivers are the main drainage lines of Lahaul. It is

in spate during the summer season when the snow on the mountains melts. Flash floods occur on regular basis in the early afternoon in summer and have been known to wash away hundreds of cattle each year. The river Chandra-Bhaga freezes occasionally during the winter season.

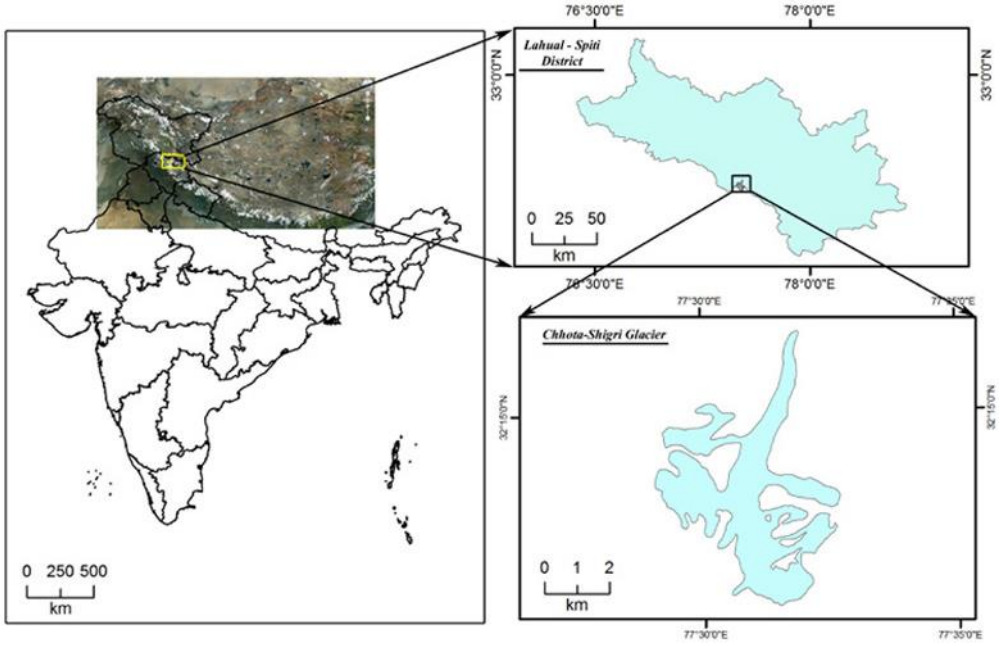

Figure 2.1: Location map showing Lahaul-Spiti valley and the study area Chhota-Shigri glacier.

This Lahaul-Spiti district is connected to Manali town (a famous tourist spot) through the Rohtang Pass (~ 3900 m altitude). Another route is through Kinnaur district for entry into Kaza in Spiti valley. Access from Manali is cut-off during winters due to the closure of Rohtang pass due to snowfall, but the route through Kinnaur remains open almost all round the year. Kunzum La or the Kunzum Pass (~ 4551 m altitude) is the entrance pass to the Spiti Valley from Lahaul. This road closes during winters for more than 9 months due to closure of Kunzam Pass owing to heavy snowfall. To the south, Spiti ends 24 km from Tabo, at the Sumdo where the road enters Kinnaur and joins with National Highway (NH) 22 (Kapadia, 1999).

The Chhota-Shigri glacier lies opposite to Chhota-Dara which can be reached *via* Gramphoo and Chattru, lying on the eastern bank of Chandra River. Near Chhota-Dara, a

rope bridge has been installed by the glaciology team of the Jawahar Lal University (JNU), Delhi, to cross the Chandra River. From this point on the western bank of Chandra River, a walking trek of around 2 km is used for reaching the base camp of the Chhota-Shigri.

2.2.2 Relief

The terrain presents a high relief area having steep mountain slopes. The river carries melt-waters from glaciers which lie on both sides of the valley at higher elevations. The relative relief map (Figure 2.2) prepared using ASTER GDEM clearly shows that the glaciated valley has low to moderate relief. Although, the entire river valley presents high relief, the Chhota-Shigri glacier presents low to moderate relief. The snout of Chhota-Shigri glacier lies at around 4100 m a.s.l, with the highest point in the glacier boundary at around 5250 m a.s.l.

2.2.3 Physiography

The region exhibits a wide variety of physical and geomorphic features. The detailed geomorphological interpretation and landform description has been provided later in Chapter 7. The terrain of Lahaul and Spiti presents a typical mountainous physiography. The area can be divided into high ridges, steep valley walls and deep cut valleys.

The Chhota-Shigri glacier is a valley type glacier, largely oriented south to north. The lower part of this glacier, near snout is fully covered with debris making it very difficult to extract the exact boundary of this glacier. The debris at the lower end is mainly brought by the tributary glacier in the eastern side near the snout. The debris brought by the main glacier gets restricted at the lower end by the already present debris at the snout. Because of this, three distinct ridges of debris rising from near the snout upstream can be seen. The glacier's ablation area is mainly covered with firn and snow with varying amount of mud or fine grained debris (called dirty snow in the present study (see Figure 4.3 in Chapter 4).

The accumulation area of Chhota-Shigri is segmented into two parts, A and B, located in the eastern side and the western side respectively (Wagnon *et al.*, 2007), along with other tributary glaciers. Both the glaciers are oriented largely south to north.

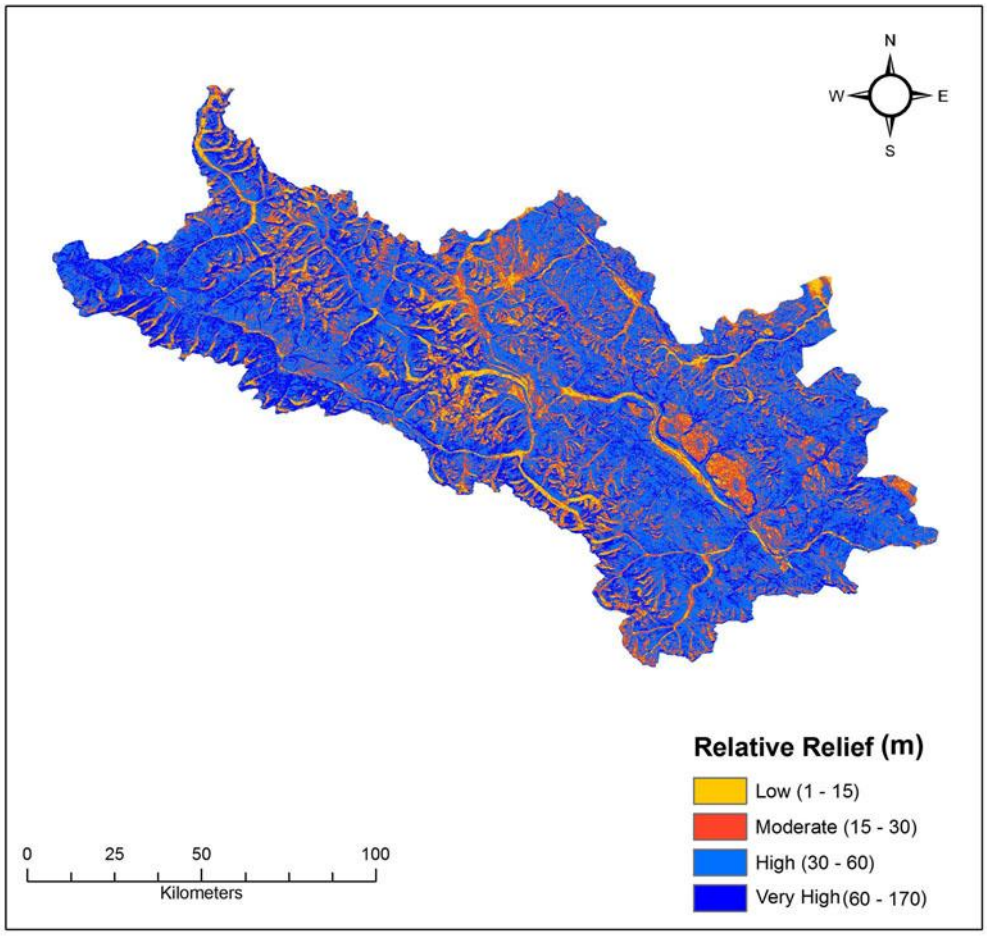

Figure 2.2: Relative relief map of Lahaul and Spiti prepared using ASTER DEM.

2.2.4 Climate

The area, in general, due to its high altitude experiences a very cold, alpine and glacial climate. Most of the precipitation is in the form of snowfall. Rainfall is very scarce and distributed in some lower altitudes of Lahaul-Spiti. Upper region is mostly devoid of rainfall, but winter is accompanied by heavy snowfall in almost all parts of the area. The temperature ranges from less than -20 ^{o}C during winters to around 15 ^{o}C during summers. In general, the areas above snowline experience moderate to low snowfall in evening during late ablation season i.e. September. Due to heavy snowfall during winter, the region is almost cut-off from rest of the country.

2.2.5 Flora and fauna

The harsh conditions of Lahaul permit only scattered tufts of hardy grasses and shrubs to grow, even below 4000 m. Glacier lines are usually found at 5000 m. Animals such as yaks and dzos roam across the wild Lingti plains. Over-hunting and decrease in food supplies have led to a large decrease in the population of the Tibetan antelope, argali, kiangs, musk deers, and snow leopards in these regions, reducing them to the status of endangered species. However, in the Lahaul valley, one can see ibex, brown bears, foxes and snow leopards during winter. The Shigri area is often tracked by shepherds for grazing sheep.

2.2.6 Geology

The Chhota-Shigri glacier lies in the Central Crystalline of the Pir-Panjal range of the Indian Himalayas. This crystalline axis is comprised mostly of meso- to keta-zonal metamorphites, migmatites and gneisses (Kumar *et al.*, 1987). In a few places, granitic rocks of different composition and younger age indicate geologic rejuvenation. The morainic deposits in the area consists of angular to sub-angular boulders, cobbles and pebbles of granite gneiss, mica-schist, augen gneiss and kyanite-schist of Rohtang gneissic complex with compact soil and sandy matrix. In Chhota-Shigri, Rohtang gneisses dominate throughout the glacier bed (Kumar *et al.*, 1987) while some sporadic occurrences of chalcopyrite have been reported upto a height of about 4700 m (Katoch, 1989).

The Precambrian rocks have wide distribution in different parts of the region. Some of the crystalline rocks constitute the oldest unit of rock formations in the Himalayas and correspond to the Archeans of the Peninsular India. The Vaikrita and parts of Haimanta Supergroups in Ladakh, Lahaul and Spiti regions are of Algonkian age.

The rocks belonging to the Cambrian System are exposed in parts of Lahaul and Spiti (Chhota-Shigri region). In Spiti, the Cambrian System is represented by greywackes, siltstones, black slates, quartzite and dolomites. These constitute part of the Upper Haimanta Supergroup and are mostly unfossiliferous (Gupta and Kumar, 1975).

2.3 The Chhota-Shigri Glacier: Review of Previous Studies

A number of studies have been carried out on the Chhota-Shigri glacier describing the landforms and morphology (Chaujar, 1987, 1992; Dhobal *et al.*, 1995); measuring the velocity, mass balance, ice thickness (Rawat *et al.*, 1989; Mundepi *et al.*, 1994; Wagnon *et al.*, 2007; Azam *et al.*, 2012 ; Azam *et al.*, 2014a, b); slope variation (Dhobal *et al.*, 1991); advances, retreat and fluctuation of snout (Chaujar, 1991; Kumar and Dhobal, 1994) Melt-water chemistry (Singh *et al.*, 2013 a, b) etc. As seen from the available literature that this glacier has been studied vastly in the late 80s to early 90s but for a decade this glacier has not been monitored and the literature generally remains silent. But after the increased awareness about the climate change and its relation to the glacier, this glacier has been again picked for continuous monitoring in the last few years. A brief review of some studies is given here to provide an insight into the extent and range of work that has already been done on this glacier.

2.3.1 Landforms and geomorphological studies

Chaujar (1987) was the first to carry out field investigations in the Chhota-Shigri glacier during 1984-85 and described the landforms of the area, particularly mentioning about the presence of cirques, crevasses, moraines, till, etc. A recession of 22 m in the snout position of the glacier over a period of one year was reported.

Survey of India (SOI) toposheets were used to examine the slope variation in the Chhota-Shigri glacier and its valley by Dhobal *et al.* (1991). The whole area was divided into three slope categories *viz*, gentle slope ($<15^{o}$), moderate slope (15^{o} to 40^{o}) and steep slope ($>45^{o}$). Taking the slope as a parameter, different geomorphic processes and the mechanism of debris flow were explained by them. It was concluded that due to slope morphology over the glacier and the glacier valley, most of the features developed due to mechanical weathering.

Chaujar (1991) again studied the advances and retreat of the Chhota-Shigri glacier based on the field observation of landforms. The presence of various loops of lateral and terminal moraines in the inactive zone of the glacier, i.e. below the snout was reported. Based on remnants of the loops, observations were made on the retreat history of the

glacier and five distinct loops of moraines were described. Based on the study of shape and size of the morainic loops, it was concluded that first three stages of glacial activity were quite stable and prominent compared to the last two stages with the energy of transport and deposition being highest in the first stage of glaciation. The presence of loops as the terminal ridges indicated that these were the push moraines, having been pushed from the south toward the north.

Later, Chaujar (1992) studied the streamlined landforms of the Chhota-Shigri glacier which were mostly concentrated between the end moraines and the second stage of glaciation. Some superimposed features were also reported from the proximity of the snout. The most prominent streamlined landform reported was flute, which were since characterized by low relief and a very elongated form like a cigar. A few rounded hummocks were also found to be close to the glacial margin on fine-grained tills resembling an inverted bowl of spoon, i.e. semi-elliptical form. It was suggested that the flute landforms would have formed in the earlier stages of glaciation followed by small hummocks in the later stages. All landforms were composed of pebbles and cobbles of the surrounding rock, i.e. Rohtang gneissic complex, forming an unconsolidated stony flow till.

Morphology of Chhota-Shigri glacier was studied in detail using field based surveys (1987-89) and SOI toposheets by Dhobal *et al.* (1995). A large scale (1:10,000) geomorphological map depicting all the glacier landforms of the Chhota-Shigri glacier was prepared.

2.3.2 Glacier dynamics

Nagar and Bahuguna (1989) studied and monitored the dynamics of Chhota-Shigri glacier on the basis of geodetic and geophysical surveys and various other observations and measurements in 1987 and 1988. The study concluded that:

a) the movement of glacier was very little

b) the retreating trend of the glacier was rapidly increasing

c) the glacier had a normal rate of melting

d) the ice thickness in the glacier gradually increased with surface heights from the north towards south

e) the change in ice thickness was rapid in the snout zone, gradual in the ablation zone and gentle in the accumulation zone

f) the bedrock topography along the east and west margins and the central strip was in agreement with the surface topography as regards to its shape and gradient

g) glacier bed in the snout zone and the ablation zone appeared to be relatively deeper along the central strip than at the margins

h) glacier bed in the lower and middle parts of the accumulation zone though varied gradually along its length, maintained uniformity in its level across the width of the glacier

i) a large concentration of high value contours in the accumulation zone probably indicated concentration of some magnetic material.

Rawat *et al.* (1989) carried out studies to measure the velocity of Chhota-Shigri glacier with stake network and to find the mass balance of the glacier. The study was carried out during August-September of years 1987 and 1988. The observations of network of 32 stakes (1987) and 86 stakes (1988) were taken to calculate the velocity and flux pattern. It was interpreted that in 1987 the largest horizontal velocity at surface was 41.12 my^{-1} and in 1988 it was 60.24 my^{-1}. Overall the mean horizontal surface velocity had considerably decreased since 1985-86. They also concluded that the glacier front varied little since 1984. The mass flux pointed to a negative mass balance. Also the submergence velocity in accumulation area was higher than the rise surface and emergent velocity was lower than that of negative net balance.

Kumar and Dobhal (1994) studied the fluctuation of snout for the period 1962-1989. A total recession of about 195 m was observed in these 26 years and an advancement of glacier by 17.5 m in the year 1987 was also reported. The reported advancement was based on the field work spanning over a period from 1986 to 1989. Traces of six old terminal moraines were also found which were interpreted as different stages of glacial recession.

Mundepi *et al.* (1994) studied glacier ice thickness and velocity using geophysical method, i.e. the gravimetric technique. Surface velocity was measured using stakes installed during 1988. The Bouguer anomaly was analyzed to calculate the ice thickness

and also applied the terrain correction. The ice velocity due to deformation, basal sliding, surface velocity and ice discharge was determined in several cross sections. It was observed that the velocity was mainly due to the basal sliding of ice in the ablation zone, though ice deformation also contributed to the velocity field in some cases. Velocity fluctuation was also reported during the years 1988-1989.

Using field surveys during 1987-89, mass balance thickness variation and ice velocity were studied and a negative mass balance was reported by Dhobal *et al.* (1995). Ice velocity was calculated to be around 12.6-14.2 cm day^{-1} near equilibrium line, and 8.8 cm/day over the ablation zone. Gravimetric technique was used to study the ice thickness and a map showing ice thickness was prepared which indicated variation in ice thickness from 15 m to 130 m from the snout to the accumulation zone. It was reported that during this period the ice thickness decreased at the rate of -4 my^{-1} in the snout, -3 my^{-1} in the ablation zone and increased at 1.5 my^{-1} in the accumulation zone. Five different depressions in the bed rock topography were observed which were responsible for the higher ice thickness at those points. They also concluded that due to westward convexing of the equilibrium line in the ablation zone, the western side is more deeply eroded than the eastern side of the glacier. Thus, the data on variations in ice thickness can lead to the determination of bed rock topography.

Kumar and Dobhal (1997) reported that Chhota-Shigri glacier showed thinning in the middle part by 3 m during 1987 and 1988. A gravity survey was conducted based on which it was reported that the glacier was relatively thicker on the western side than in the middle part. Also, high flow rate in the ablation zone indicated that basal sliding was the main movement mechanism of the glacier.

Wagnon *et al.* (2007) carried out similar study over a period of 4 years (2002 - 2006). It was reported that the glacier moved faster in the upper area of the ablation zone. The annual specific mass balance over the four-year period was found to be mostly negative varying from a minimum value of –1.4 m.w.e. in 2002/03 and 2005/06 (equilibrium-line altitude (ELA) 5180 m a.s.l.) to a maximum value of +0.1 m.w.e. in 2004/05 (ELA 4855 m a.s.l.). The Chhota-Shigri glacier was classified as a mid-latitude glacier, with an ablation

season limited to the summer months and a mean vertical gradient of mass balance in the ablation zone (debris-free part) of 0.7 m.w.e. similar to those reported in the Alps.

Pithan (2011) investigated the energy and mass balance of this glacier in the monsoon-arid transition zone of Western Himalayas using regional climate model PRECIS of Kumar *et al.* (2006). A correlation coefficient of 0.97 was noted between model derived mass balance and the observed mass balance from three years on 50 m altitude intervals across the glacier. They found that the monsoon precipitation was quarter to a third of total accumulation. Results also confirmed radiation as the main energy source for melt. Latent heat flux acted as an important energy sink in the pre-monsoon season. Mass balance was found to be most sensitive to changes in atmospheric humidity and temperature.

Later, Azam *et al.* (2012) revised and updated the work of Wagnon *et al.* (2007) on mass-balance and dynamic behavior of Chhota-Shigri glacier. The results for the period between 2002 - 2010 were presented and were compared with mass balance record of 1987 - 1989. A field based method for collecting the data as well as some inputs from remote sensing formed the basis of the study. It was found that during the period 2002 - 2010, the glacier experienced a negative glacier-wide mass balance of -0.67 ± 0.40 m.w.e. yr^{-1}. The surface ice velocity and elevation change between the years 2003 and 2010 were calculated using field based measurements and it was found that velocity was slowly decreasing in the ablation area leading to a 24% to 37% reduction in ice fluxes. Based on these observations, it was concluded that over the next years the glacier is further expected to continue retreat and thinning. Further, a small velocity change between 1987/1989 and 2003/2004 and the small terminus change between 1988 and 2010 suggests that the glacier has experienced a period of near zero or slightly positive mass balance in the 1990s, before shifting to a large imbalance in the 21st century.

ELA is the most useful parameter for studying the effect of climate change on glaciers. Multi-sensor remote sensing images (from 1980 to 2007) were used to study the ELA of 19 glaciers from the Chandra-Bhaga basin in a study conducted by Pandey *et al.* (2012). The Snowline Altitude (SLA) of Chhota-Shigri glacier was observed to be varying from 4672 to 5083 over the 27 years of study period. A negative mass balance during the

years 2000s was reported which was attributed to the increasing SLA due to increase in temperature and a decrease in winter snowfall over the years.

Singh *et al.* (2012) used Ground Penetrating Radar (GPR) survey to estimate the ice thickness of Chhota-Shigri glacier in 2010. The survey was done in discrete mode at 16 MHz frequency with 4 m antenna gap (transmitter and receiver) at 50 cm data-acquisition intervals along the glacier length at bare ice of the ablation zone. From the bed rock reflection, an ice thickness of about 110 to 150 m with approximately 0.049 km^3 water equivalent for the surveyed area was reported. An average depth of 130 m of the surveyed ablation area showed a volume of 0.0572 km^3 (water equivalent 0.049 km^3). The existence of subsurface features like point reflector and a linear non-bed reflection within the ablation ice zone was also reported.

Vincent *et al.* (2013) estimated the volume change and mass balance of the Chhota-Shigri glacier between 1988 and 2010 using *in-situ* geodetic measurements (Dobhal,1992; Nijampurkar and Rao, 1992; Dobhal *et al.*, 1995; Kumar, 1999) and field measurements carried out in 2010. The study indicated that this glacier experienced only a slight mass loss between 1988 and 2010 (–3.8 ± 2.0 m.w.e. y^{-1} corresponding to –0.17 pm 0.09 m.w.e. y^{-1}). A negative mass balance between years 1999 and 2010 (–4.8±1.8 m.w.e. using DEM based calculation, corresponding to –0.44±0.16 m.w.e. y^{-1}) was also seen. Thus, during the period between 1988 and 1999, a slightly positive or near-zero mass balance between 1988 and 1999 (+1.0±2.7 m.w.e. corresponding to +0.09±0.24 m w.e. y^{-1}) was found. Furthermore, based on DEM difference, the mass balance of the Chhota-Shigri glacier (–0.39 pm 0.15 m.w.e. y^{-1}) was reported slightly less negative than the mass balance of a 2110 km^2 glaciarized area in the Lahaul and Spiti region (–0.44 ± 0.09 m.w.e. y^{-1}) during 1999–2011. Finally, the study concluded that the ice wastage has been probably moderate in this region over the last 22 years, with near equilibrium conditions during the nineties, and an ice mass loss after, confirming more negative balances since the beginning of the 21^{st} century.

Azam *et al.* (2014a) reconstructed the mass balance of Chhota-Shigri glacier, and discussed the regional climatic drivers responsible for its evolution since 1969. A temperature-index and an accumulation model was used with inputs on daily air

temperature and precipitation records from the nearest meteorological station, at Bhuntar Observatory to reconstruct mass balance. The model was calibrated against 10 years of annual altitudinal mass balance measurements between 2002 and 2012 and decadal cumulative mass balances between 1988 and 2010. Three distinct mass balance periods were studied. Periods I (1969–85) and III (2001–12) showed significant mass loss at mass balance rates of –0.360.36 and –0.570.36 m.w.e. y^{-1} respectively, whereas period II (1986–2000) exhibited steady-state conditions with average mass balances of –0.010.36 m.w.e. y^{-1}. The comparison among these three periods suggest that winter precipitation and summer temperature are almost equally important drivers controlling the mass balance pattern of Chhota-Shigri glacier at decadal scale.

2.3.3 Melt-water chemistry

An isotopic study was also carried out on the Chhota-Shigri glacier (Nijampurkar and Rao, 1992). The study was based on the natural and artificial radio – isotopes (^{32}Si, ^{137}Cs), stable isotope ($\delta^{18}O$) and total β activity and focused on the ice dynamics, melt-water composition and identification of the possible deposition of the Chernobyl fall-out. The snout ice was dated to be ~250 years old based on which the past average surface ice flow rate was estimated to be ~28 my^{-1}. Based on $\delta^{18}O$ variation in a shallow ice core, the accumulation rate of the ice was estimated at ~520 kg $m^{-2}y^{-1}$. The ^{32}Si measurement of snout ice and the englacial melt-water indicated that 45% of the glacial melt in the month of August 1987 came from the old ice, and 55% from the snow melt. The deposition of the artificial radionuclide (^{137}Cs) and a very high β activity in the snow samples indicated the Chernobyl fall-out deposition even over the Himalayas.

Sharma *et al.* (2013) studied the hydro-geochemical processes and the solute sources of the melt-waters of the Chhota-Shigri glacier from 2003 to 2007. The melt-water was found to be almost neutral to slightly alkaline in nature with bicarbonate and sulphate as the dominant anions and calcium and magnesium as the dominant cations. The chemical weathering of rocks followed by precipitation were the main controlling factors which influenced the melt-water chemistry of this region. Using diurnal observations, the discharge was found to be lower in the morning and increased in the afternoon due to the

change in temperature, which has a great influence on snow- and ice-melt at the glacier surface.

Singh *et al.* (2013 a, b) carried out studies on dissolved ion chemistry and suspended sediment concentration of melt-water draining from Chhota-Shigri glacier. Singh *et al.* (2013a) compared the hydrochemistry of August 2008 with previous study carried out in 1987. Comparison between the two data sets showed that cations like Ca^{2+} increased nearly 6 times, Mg^{2+} 87 times, Na^{+} 10 times and K^{+} 19 times, while anions like Cl^{-} increased nearly 12 times, HCO_3^{-} 85 times and SO_4^{2-} 49 times between 1987 and 2008. This was attributed to increased weathering rates due to climate warming, atmospheric deposition or a combination of both. It was also pointed out that annual specific mass balance of this glacier was often sharply negative during 2002 – 2010, pointing to glacier recession. Singh *et al.* (2013b) studied major ions such as Mg^{2+}, Ca^{2+}, Na^{+}, K^{+}, HCO_3^{-}, SO_4^{2-} and Cl^{-} of melt-water during 2008 and 2009. The findings indicated that chemical characteristics of Chhota-Shigri glacier melt-water were mostly controlled by carbonate weathering followed by silicate weathering. Also, the ratio showed that dissolution and dissociation of atmospheric CO_2 is the major proton producer in this glacier melt-water. Marked seasonal and diurnal variations in the total dissolved solid (TDS) and suspended sediment concentration of glacier melt-water was observed during 2008 and 2009. High TDS was observed during October (low discharge) and low TDS during August (high discharge) in both years, implying that TDS is inversely correlated with discharge. On the other hand, higher suspended sediment concentration was observed during August (high flow regime) and low during October (low flow regime) in the sampling periods, following the discharge pattern of the glacier.

This brief review suggests that the Chhota-Shigri glacier has been studied earlier with a focus on glacier geomorphology, mass balance, ELA variation, ice thickness, ice velocity etc. The melt-water chemistry and mass balance have been studied in greater detail. However, the Chhota-Shigri still has to be mapped to show distribution of various terrain classes such as snow/ice, ice-mixed debris (IMD), and debris, and distribution of supraglacial and periglacial debris. This aspect has been focussed in the present investigation. Some studies have reported data on velocity and thickness of the glacier for limited period of time. In this study, velocity data for the past decade has been generated

without a gap year using sub-pixel image correlation to provide a more comprehensive picture of the overall glacier velocity.

The above review of literature suggests that the Chhota-Shigri glacier has been studied earlier (late 80s to early 90s) in great details. After that, no further studies have been carried out in this glacier. In recent years, studies on the melt-water chemistry and mass balance have been reported but other aspects of glacier showing distribution of various terrain classes such as snow/ice, IMD, and debris, and distribution of supraglacial and periglacial debris have not been studied. Further, the velocity and thickness of the glacier have been studied but at long time intervals. The main reason behind this may be attributed to the fact that earlier the velocity data were collected in the field and due to harsh climatic conditions in the glacier valley it is very difficult to collect data every year. In this study, focus has been placed on both mapping of the distribution of glacier terrain classes as well as estimation of velocity using remote sensing due to the availability of this data on continuous basis. An updated geomorphology map of the area has also been attempted depicting realistic mapping of the features based on remote sensing data.

CHAPTER 3

DATA USED AND METHODOLOGY

This chapter presents description of the data used in this study. It also provides an overview of the methodology employed and the pre-processing steps involved in data processing. The data used in this study can be divided in three categories namely (i) remote sensing data, (ii) ancillary data, and (iii) field data (Table 3.1). Details of all types of data and their pre-processing are presented in this chapter. Although, remote sensing data are available at different processing levels from various agencies, these still need to be pre-processed for some applications. The data can then become more readily usable with higher order of interpretation and analysis.

3.1 Remote Sensing Data

Remote sensing data from several satellite sensors have been used in this study. A list of these data is provided in Table 3.1. Images from ASTER, WorldView-2 and TerraSAR-X (TSX) have been used in the present case. A brief introduction of various data types and their uses in this study are discussed in the following paragraphs.

Terra-ASTER images have moderate spatial resolution with three radiometers VNIR, SWIR and TIR having fourteen bands in different spectral regions and one backward looking NIR band (3B). In visible and near-infrared range (VNIR), ASTER acquires data in four bands- green (B1), red (B2) and NIR (3N & 3B) with 15 m spatial resolution. NIR band provides the stereo viewing for DEM generation. SWIR radiometer has six bands

with 30 m spatial resolution. TIR has 90 m spatial resolution and has five bands. Specifications of ASTER data are given in Table 3.2.

ASTER image has been used as base image for glacier mapping in this study. It has been used to map the glacial outline and in classification of the glacial terrain. The ASTER images have also been converted into radiation images so as to estimate the ground reflectance of various glacial classes and the surface temperature of debris cover. ASTER time series data from 2003-2009 have also been used to calculate the surface ice velocity of this glacier using COSI-Corr software.

WorldView-2 image is high spatial resolution data with 8 multispectral bands. The panchromatic band of WorldView-2 image has been used for large scale mapping of the glacier terrain and geomorphic features. The multispectral data with high quantization of the WorldView-2 image has also been used for the discrimination of snow, debris, water bodies and other small features in the glacier terrain. Due to the higher spatial resolution of the image, it may also help in the mapping of extent and location of crevasses, snout and the paleo-lateral moraines. The specifications of WorldView-2 data are given in Table 3.3.

TSX data has also been procured for this study. The TSX is microwave data in the X-band with multiple polarizations. Single polarization mode data in ScanSAR mode with processing level Single Look Slant Range Complex (SSC) has been procured. This data is ideal for interferometric (surface movement and DEM generation) application and for the analysis of land cover mapping. It was initially proposed to integrate TSX images with optical and thermal image data sets, but unfortunately after preprocessing, these data showed high layover and shadows in the Chhota-Shigri glacier region due to steep depression angle, as can be seen from Figure 3.1. Due to this reason, the TSX data over this glacier was discarded for any investigation in this study.

3.2 Ancillary Data

Along with the remote sensing data, ancillary data in the form of ASTER DEM, SRTM DEM and SOI toposheets have also been used during processing and interpretations. ASTER GDEM (spatial resolution: 30 m) and SRTM 3 DEM (spatial resolution: 90 m) have been used for the study of topographic features in the study area.

Table 3.1: List of data used in this study with their applications.

Category of data	Sensor/Data specification	Bands used/No./Type	No. of scenes/Date	Applications
1. Remote sensing	(i) ASTER	VNIR, SWIR, TIR	18 scenes (04 Mar 2002, 28 Sep 2002, 30 Oct 2002, 08 Oct 2003, 24 Oct 2003, 17 Sep 2004, 07 Nov 2005, 30 Sep 2006, 16 Oct 2006, 17 Nov 2006, 10 Apr 2007, 21 May 2007, 20 Nov 2007, 15 Dec 2007, 01 Dec 2008, 15 Sep 2009, 01 Oct 2009, 30 Oct 2011)	Classification of glacier terrain and mapping glacier features
	(ii) WorldView-2	8 band data (VNIR)	1 (13 Oct 2010)	Mapping glacier features; paleo-morainic loops mapping; accuracy assessment
	(iii) TerraSAR-X	X band 3cm (Polarization HH)	2 Ascending (28 Aug 2011 & 30 Sep 2011), 2 Descending (18 Sep 2011 & 29 Sep 2011)	Not used because of shadowing and layover effect
2. Ancillary	ASTER GDEM	DEM	Released 2009	Paleo-morainic loops mapping; DTM generation; orthorectification
	SRTM3	DEM	Released 2000	Paleo-morainic loops mapping; DTM generation; orthorectification
	SOI toposheet	52 H/11 & 52 H/12	Published 1966 (surveyed using aerial photograph of 1961	Base map preparation.
3. Field	Photographs	----	Collected during field visit in 2011 and 2012	Glacier feature identification; field verification
	GPS points	----	Collected during field visit in 2011 and 2012	Field verification
	Temperature data		Collected during field visit in 2011 and 2012	Field verification of temperature data generated using remote sensing data

Table 3.2: ASTER data specifications.

Radiometer	Band Numbers	Spectral Range (μm)	Quantization Levels (bits)	Spatial Resolution (m)
VNIR	1	0.52-0.60	8	15
	2	0.63-0.69	8	
	3N	0.78-0.86	8	
	3B	0.78-0.86	8	
SWIR	4	1.60-1.70	8	30
	5	2.145-2.185	8	
	6	2.185-2.225	8	
	7	2.235-2.285	8	
	8	2.295-2.365	8	
	9	2.360-2.430	8	
TIR	10	8.125-8.475	12	90
	11	8.475-8.825	12	
	12	8.925-9.275	12	
	13	10.25-10.95	12	
	14	10.95-11.65	12	

Table 3.3: WorldView-2 data specifications.

Sensor band	Band Name	Spectral Range (μm)	Quantization Level	Spatial Resolution
Panchromatic	Panchromatic	0.45 - 0.80	11 bits	46 cm - 52 cm
Multispectral (8)	Coastal	0.40 - 0.45		1.85 m - 2.07 m
	Blue	0.45 - 0.51		
	Green	0.51 - 0.58		
	Yellow	0.58 - 0.62		
	Red	0.63 - 0.69		
	Red Edge	0.70 - 0.74		
	Near-IR1	0.77 - 0.89		
	Near-IR2	0.86 – 1.04		

Figure 3.1: An example of TSX image of Chhota-Shigri glacier showing high geometric distortions.

The accuracy of height/elevation from these DEMs is almost similar and therefore both can be used as a substitute for each other (Wang *et al.,* 2012). However, considering the high spatial resolution of ASTER DEM, it has been used as a main source of elevation data for orthorectification and DTM generation for the glacier boundary delineation. The DEM and its derivatives like, slope, aspect, etc. have also assisted in the mapping of paleo-terminal moraines considering the topographic breaks present due to successive morainic deposits.

SOI toposheets (numbers 52 H/11 and 52 H/12) at 1:50000 scale have also been used to map the glacier extent in the year 1963 (pre-satellite data). The toposheets have been scanned and then georeferenced using ArcGIS (GIS package). The georeferenced toposheets have been used to map the glacier extent by onscreen digitization and then comparing it with the glacier boundary mapped using high resolution WorldView-2 image.

3.3 Field Data

Two field expeditions, first of 10 days duration in September 2011 and the second of 15 days duration in September 2012 were carried out jointly with the scientific team of JNU, Delhi. The purpose of the field work was to collect the ground truth, temperature data and ground control points (GCPs). Several GCPs have been identified over the glacier surface. Temperature profiles of the glacier surface from accumulation zone to the snout have also been generated. The field data have been used for interpretation of glacier features and classification of glacier surface cover. Additional details on field data collected, their usage and analysis have been provided in later chapters.

3.4 Software Used

The following GIS and digital image processing software have been used for this study.

i. ArcGIS 9.3

ESRI's ArcGIS is a geographic information system (GIS) for working with maps and geographic information. The software has been used extensively in this research for:

i) creating and using maps

ii) compiling geographic data

iii) analyzing mapped information

iv) sharing and discovering geographic information

v) using maps and geographic information

vi) managing geographic information in a database.

ii. ERDAS Imagine 2011

ERDAS IMAGINE 2011 has also been extensively used in this study for various image processing and analysis tasks. This software aims primarily at geospatial raster data processing and allows the user to prepare, display and enhance digital images for use in

geographic information system (GIS) or in computer-aided design (CADD) software. It is a toolbox allowing the user to perform numerous operations on an image and generate an answer to specific geographical questions.

The software has been used for:

i) co-registration and other processing of the remote sensing images

ii) classification of the ASTER data for glacial terrain mapping

iii) creating various DEM derivatives like slope and aspect

iv) estimating rate of change of slope

iii. ENVI 4.7

Exelis Visual Information Solutions (Exelis VIS), a wholly owned subsidiary of ITT Exelis, provides a software for the analysis and visualization of scientific data and imagery. This software has been used here to apply various types of corrections to the acquired images and also for image interpretations.

All the pre-processing of ASTER images has been done using this software. The ASTER image has been first imported in the software from ***.hdf*** format and then processed and the output has been taken in ***.tiff*** format because it is supported in all other software. TIR data has also been pre-processed in this software. Then this pre-processed TIR data has been used to derive the land surface temperature of the glacier terrain which is one of the major inputs in the classification.

iv. SARscape 4.2 and MapReady

SARscape is a commercial software suite consisting of different modules covering SAR data processing, SAR and ScanSAR focusing and Interferometry, differential SAR Interferometry, Persistent Scatterers and SBAS, Polarimetry and Polarimetric Interferometry, running as an extension of ENVI under Windows and Linux.

The MapReady Remote Sensing Tool Kit accepts level 1 detected SAR data, single look complex SAR data from Alaska Satellite Facility and some other facilities. It can

terrain correct, geocode, apply polarimetric decompositions to multi-pol SAR data, and save to several common imagery formats including GeoTIFF. These two software have been used for SAR data processing and visualization.

v. COSI-Corr

COSI-Corr is a software module developed by Leprince *et al.* (2007) and has been integrated as a tool in ENVI. It provides processes to accurately orthorectify, co-register, and correlate optical remotely sensed images (aerial and pushbroom satellite images) with the ultimate objective of retrieving ground surface deformation from time series images (Leprince *et al.*, 2008; Scherler *et al.*, 2008 and Ayoub *et al.*, 2009). COSI-Corr has been used in this study to create a time series (2003-2009) of velocity of the study area. To derive the velocity or deformation, it uses the phase difference algorithm in the Fourier domain and does not transform the images back to the spatial domain. This method obtains better match than other available algorithms in areas with little contrast and is also generally a very robust method for glaciological applications (Heid and Kääb, 2012).

3.5 Overview of Methodology

In this research, it is proposed to study the detail geomorphology of the area, estimation of glacial retreat, glacial surface cover mapping with a focus on debris cover area and estimation of glacial dynamics of the Chhota-Shigri glacier. To fulfill these tasks, several specific methodologies have been envisaged, which have been presented in the later chapters. Here, a broad conceptual framework and methodology, as shown in Figure 3.2, has been presented. Based upon this, the work elements may be enumerated as:

1. Detailed review of relevant scientific literature on glacier terrain mapping, glacier ice dynamics and geomorphological mapping using remote sensing techniques for identification of the research gaps and subsequent formulation of the objectives has been carried out.
2. Field investigations in September 2011 (10 days) and September 2012 (15 days) have been carried out to collect the ground truth, temperature data and GCPs. Several GCPs have been identified and their data used for interpretation and validation of the results.

3. The remote sensing data (ASTER, WorldView-2 etc.) have been procured and image data pre-processing (radiometric, atmospheric and orthorectification) and their conversion to radiation data (surface reflectance for optical data, brightness temperature for thermal data and dB for microwave data) has been carried out for subsequent data analysis.
4. Various existing remote sensing techniques for classification (ratio based, MLC and knowledge based) have been implemented for glacier cover mapping followed by analysis and inter-comparison of the resulting glacier cover maps.
5. Glacial valley delineation has been carried out using remote sensing data (DTM) which provides information on orientation of the valley slopes and thus enables correct delineation of the watershed.
6. The geomorphological features have been identified and mapped in detail.
7. Time series ASTER images have been used to derive the surface ice velocity. The nadir viewing NIR band of the ASTER data have been first orthorectified, co-registered and then correlated to give displacement of surface ice using COSI-Corr software.

3.6 Data Pre-processing

Satellite images contain information about the earth objects but before this information could be extracted, the data must be brought in synchronization with the physical parameters. This is done through sequential processing steps called pre-processing. According to Mather (1999), the term pre-processing is defined as the correction of geometric and radiometric deficiencies and the removal of data errors. Before interpreting the data, it is generally required to remove the errors contained in it. The selection of methods to do so need to be properly defined and may be purpose dependent. It is required to define processing precisely based on the data and task.

It has been found that the data which are subsequently pre-processed produces more accurate outputs than those produced from the uncorrected data. Shukla, (2009) found in the study that if the data is atmospherically corrected and properly pre-processed, the classification accuracy increases. Also, the positional errors cause uncertainties in feature area calculation in land use/land cover mapping and change detection that can

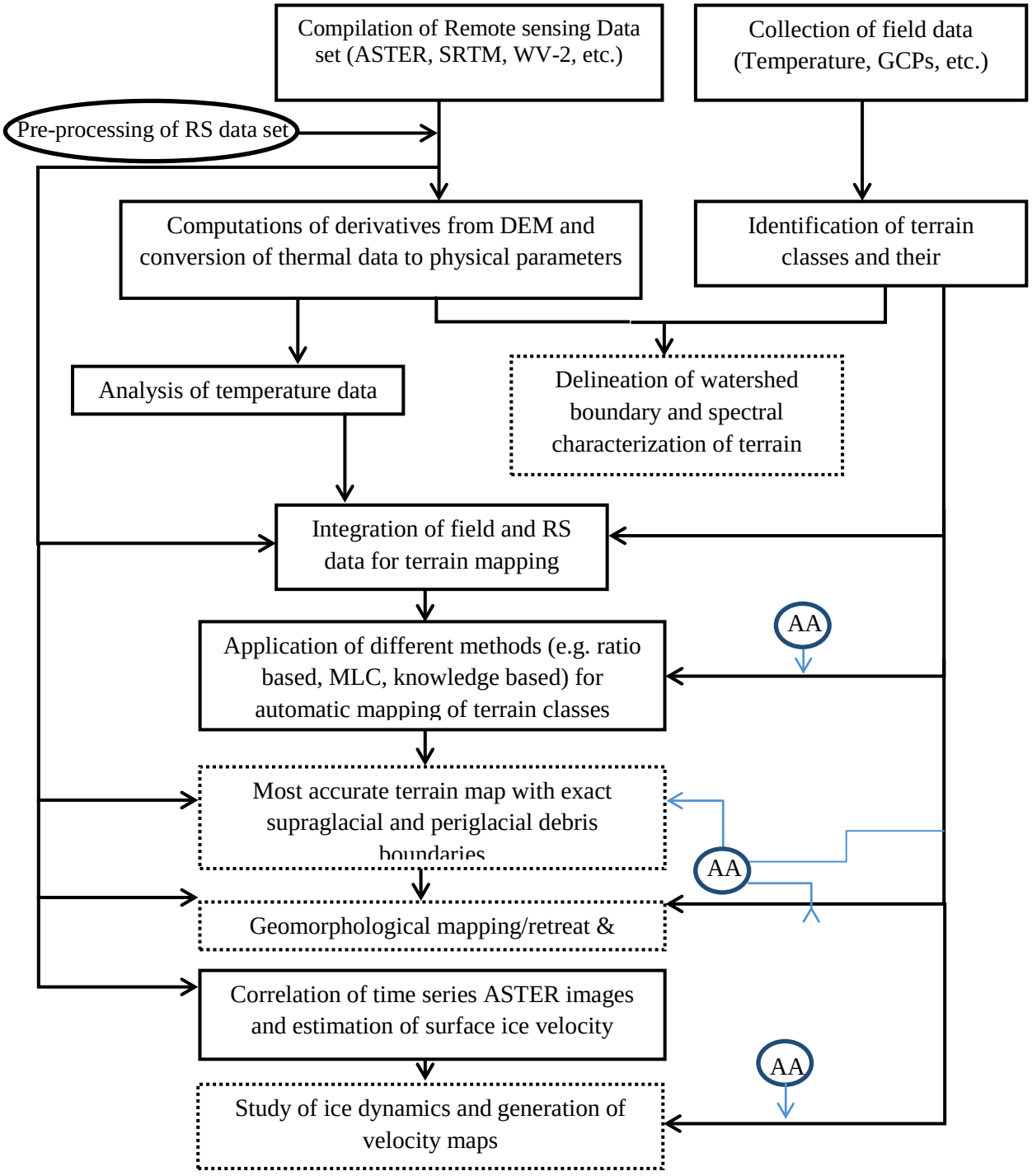

Figure 3.2: Flowchart showing conceptual framework of methodology adopted.

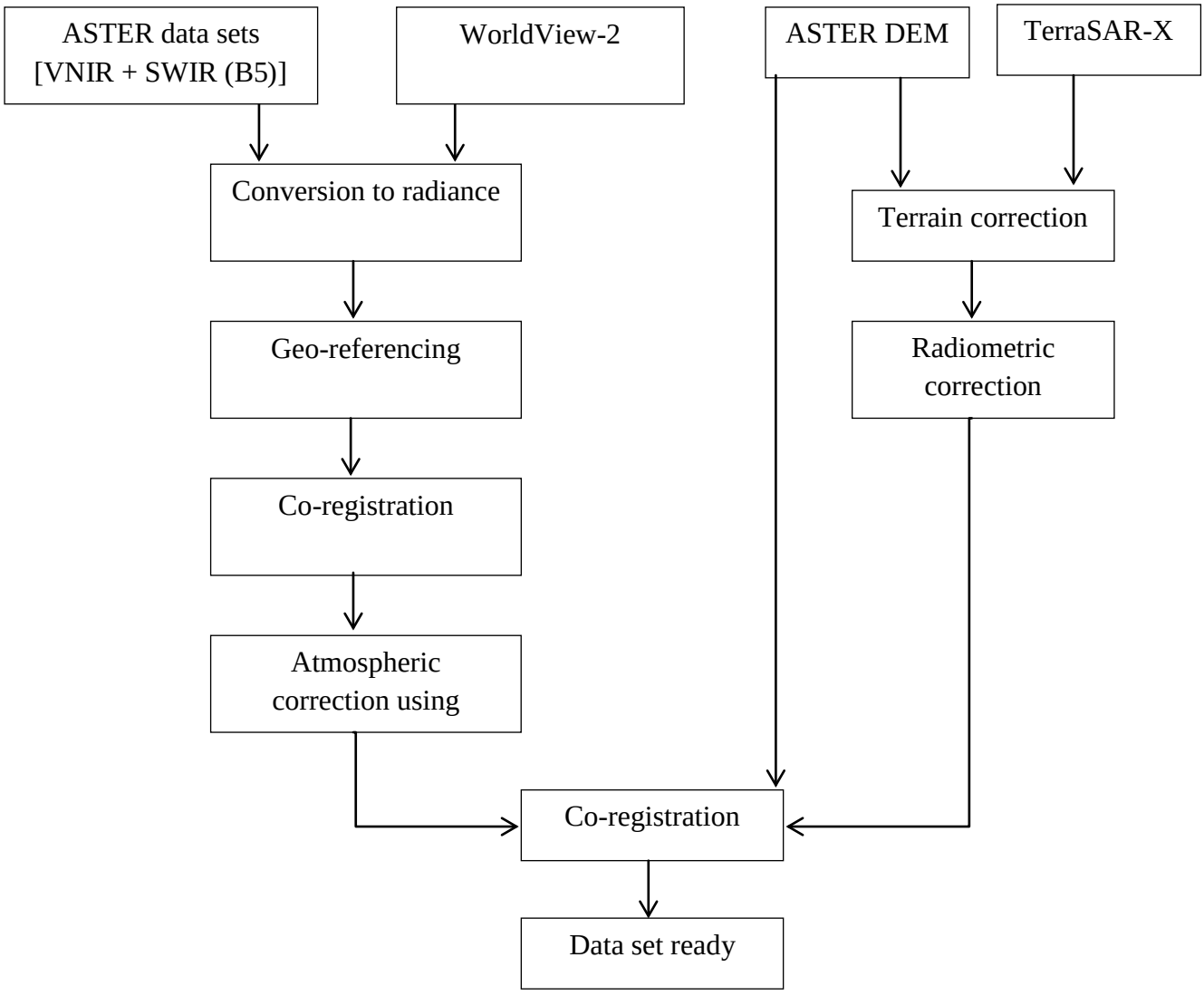

Figure 3.3: Flowchart showing overall pre-processing methodology.

have serious implications on the final results (Hunter and Goodchild, 1995, Ellis *et al.*, 2000; Davis and Wang 2003 and Wang and Ellis, 2007). Co-registration and orthorectification can improve the positional accuracy of the image and thus the results (Toutin, 2001; Kayitakire *et al.*, 2002; Davis and Wang, 2003; Toutin, 2004; Wang and Ellis, 2007). Therefore, in this study several pre-processing steps have been implemented to pre-process the data. The sensor wise pre-processing steps implemented in this study (Figure 3.3) are discussed in the following sections.

3.6.1 ASTER image pre-processing

i. Conversion of DN to radiance and Georeferencing: ASTER L1A data has been acquired for this study. The benefit of using L1A data is that the data corrections can be controlled. This in turn increases the accuracy and compatibility of the remote sensing data. Level 1A data is the raw DN values which are recorded by the satellite sensors. These data are converted to radiance values in ENVI software.

To convert from DN to radiance-at-sensor, the unit conversion coefficients (UCCs, defined as radiance per 1 DN) are used. Radiance (spectral radiance) is expressed in unit of $W\ m^{-2}\ sr^{-1}\ \mu m^{-1}$. The relation between DN values and radiances is given as,

(i) DN value of zero is allocated to dummy pixels
(ii) DN value of 1 is allocated to zero radiance
(iii) DN value of 254 is allocated to the maximum radiance for VNIR and SWIR bands
(iv) DN value of 4094 is allocated to the maximum radiance for TIR bands
(v) DN value of 255 is allocated to saturated pixels for VNIR and SWIR bands
(vi) DN value of 4095 is allocated to saturated pixels for TIR bands

The maximum radiances depend on both the spectral bands and the gain settings. The radiance can be obtained from DN values as,

Radiance = (DN value – 1) × Unit conversion coefficient

ii. Georeferencing: All the remote sensing images are georeferenced using well-distributed and carefully selected GCPs. However, finding good quality control points in high-altitude rugged and glacierized terrain such as Himalayas, where roads and other man-made features (usually used as control points) has been a very difficult task. Moreover, the spatial variation of snow and ice cover from one scene to the other creates further complications. The images have been studied very carefully in order to find good quality, well-distributed and sufficient number of GCPs. Features such as confluence of tributary glaciers, river tributaries, ridges etc. have been located and used as GCPs.

In case of each image (ASTER images of the multitemporal dataset), more than 30 GCPs have been selected and applied using a second-degree polynomial transformation,

resulting in a root mean square error (RMSE) of less than half a pixel. Finally, the georeferenced images have been resampled using the Nearest Neighbor (NN) resampling method. Georeferencing with reference to the SOI topographic maps of the area has been followed by the co-registration of the images.

iii. Co-registration: ASTER provides data in three different wavelength regions, i.e. VNIR, SWIR and TIR. The data acquired in VNIR has a spatial resolution of 15 m, SWIR has a resolution of 30 m and TIR has a resolution of 90 m. Image to image registration of different radiometer images as well as multitemporal data set has been done with 2^{nd} order polynomial transformation as the geometric model and NN as the resampling method. NN has been chosen as it does not alter the original pixel values during resampling. The co-registration has also been performed at an accuracy of half a pixel for all the images. The registration quality has also been checked visually by overlaying the master and the slave images and swiping over some selected ground features. The registered images have been processed to extract the image area equivalent to the watershed area of the glacier by using a watershed boundary mask of the glacier prepared from SOI toposheet.

iv. Orthorectification: Due to the high relief in mountainous terrain, the remote sensing images show high amount of relief displacement. Relief displacement alters the geometry of the object imaged. The effect gets more pronounced when multi-temporal data are used. Data acquired on different dates are imaged in different look angles. Therefore, the orientation of the imaged object is also different. Hence, orthorectification is important and is performed to create an orthophoto product.

v. Atmospheric correction of ASTER optical data: For quantitative retrieval and analysis of surface reflectance, removal of the influence of the atmosphere is a critical pre-processing step. The measured radiance-at-sensor is controlled by the transmission of solar EMR through the atmosphere. Atmospheric conditions can vary significantly both spatially and temporally, as a result of molecular scattering and absorption in the atmosphere. The main effects of the atmospheric scattering on remotely sensed data are upwelling atmospheric radiance or path radiance and atmospheric absorption (Slater, 1980).

Generally, in visible to infrared bands (as in ASTER bands), the main atmospheric effects are air molecules and aerosol particle scattering (respectively following Rayleigh and Mie scattering patterns), which are additive and create image haze. In the visible bands, the multiplicative component of atmospheric absorption caused by water vapors or other gases is very weak and can be safely ignored. Therefore, the impact on short wavelengths is mainly from the additive atmospheric scattering. However, in the NIR and SWIR wavelengths, the influence of atmospheric scattering is negligible (Misra, 2008).

In this study, FLAASH tool in ENVI software has been used to compensate for atmospheric effects. FLAASH is a first-principles atmospheric correction tool that corrects wavelengths in the visible through NIR and SWIR region, up to 3 µm wavelength. FLAASH incorporates the MODTRAN4 radiation transfer code to correct the images for atmospheric effects.

vi. Atmospheric correction of ASTER TIR data: As in the case of data in VNIR-SWIR range (ASTER data, seen in previous sections), the data in TIR spectral window is also affected by the atmospheric interference. The effect in this case is primarily due to multiplicative absorption, and the contribution due to atmospheric scattering is rather negligible. Atmospheric water is the main constituent which attenuates the radiances sensed remotely in the TIR region. The purpose of atmospheric correction of ASTER TIR at-sensor radiance data is to account for these influences and to retrieve surface radiances which are to be used in estimating the brightness temperature.

The atmospheric correction of the ASTER TIR recalibrated at-sensor radiance data has been performed using an algorithm similar to the In-Scene Atmospheric Compensation (ISAC) algorithm (Johnson and Young, 1998; Hernandez-Baquero, 2000; Gorin *et al.*, 2002) as implemented in the ENVI software package, described briefly as follows.

This algorithm assumes that the atmosphere is uniform over the data scene and that there is an occurrence of a near-blackbody surface within the scene. The location of the blackbody surface is not required. A single layer approximation of the atmosphere is used and it is assumed that there is no reflected downwelling radiance. The algorithm first determines the wavelength that most often exhibits the maximum brightness temperature. This wavelength is then used as the reference wavelength. Only spectra that have their

brightest temperature at this wavelength are used to calculate the atmospheric compensation. At this point, for each wavelength, the reference blackbody radiance values are plotted against the measured radiances. A line is fitted to the highest points in these plotted data and the fit is weighted to assign more weight to regions with denser sampling. The compensation for this band is then applied as the slope and offset are derived from the linear regression of these data with their computed blackbody radiances at the reference wavelength (ENVI User's Guide, 2008).

Upwelling atmospheric radiance and atmospheric transmission are approximated using the following method: first, the surface temperature of every pixel is estimated from the data and used to estimate the brightness temperature using the Planck's function and assuming an emissivity of 1; next, a line is fitted, using one of two methods - Top-of-Bins or Normalized Regression to a scatter plot of radiance vs. brightness temperature. The atmospheric upwelling and transmission are then derived from the slope and offset of this line. Figure 3.4 shows the initial at-sensor radiance and the surface radiance spectra of a pixel obtained after the atmospheric correction using the above-mentioned procedure. An improvement in the original radiance values after the application of atmospheric correction can be clearly observed.

vii. Computation of the brightness temperature: The radiation emitted from a surface in the TIR wavelengths is a function of both the surface temperature and emissivity. The emissivity relates to the composition of the surface and is often used for surface constituent mapping. In this study, temperature has been calculated in ENVI software. ENVI uses different techniques like Reference Channel Emissivity, Emissivity Normalization and Alpha Residuals to separate the emissivity and temperature information in radiance data measured with TIR sensors. Both the Reference Channel Emissivity and Emissivity Normalization techniques assume a fixed emissivity value and produce emissivity and temperature outputs. The Alpha Residuals technique does not provide temperature information.

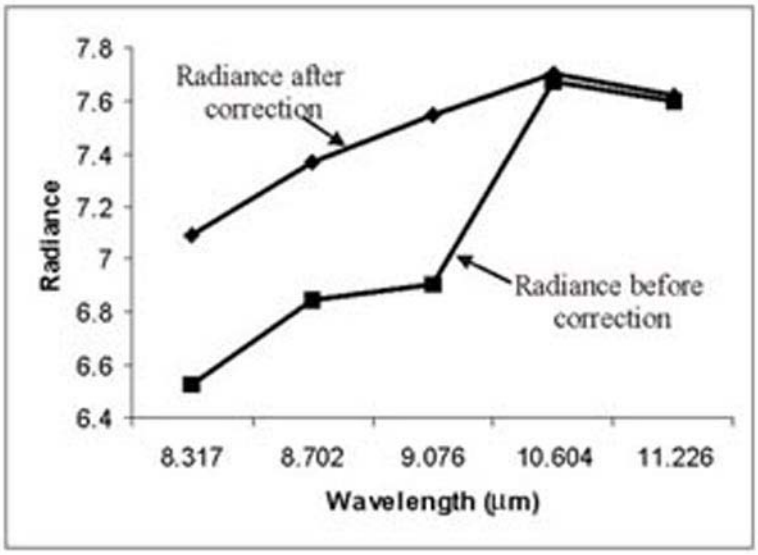

Figure 3.4: Comparison between the original at-sensor radiance and radiance after application of atmospheric correction of ASTER TIR image. An improvement in the radiance values after the correction can be clearly observed. Radiance values are in W m^{-2} sr^{-1} μm^{-1}.

In this study, Reference Channel Emissivity has been used to calculate emissivity and temperature values from ASTER TIR images. This technique assumes that all the pixels in one band of the TIR data have constant emissivity. Using this constant emissivity, a temperature image has been calculated and is used to calculate the emissivity values in all the other bands using the Planck's function.

3.6.2 WorldView-2 image pre-processing

One WorldView-2 image of the Chhota-Shigri area has been acquired (date of acquisition 10th Oct. 2010). The image has been georeferenced, co-registered and corrected for other generic errors. The image procured is in 8 small sub-scenes which are combined later to form single image of the study area. The image has also been converted to radiance image in ENVI using the information provided in the header file (metadata) of the data. This image is then co-registered with ASTER and other multi-temporal data sets.

3.6.3 TerraSAR-X image pre-processing

Four (4) TSX data have been acquired in ScanSAR mode - two ascending (28 Aug. and 30 Sep. 2011) and two descending (18 Sep. and 29 Sep. 2011) from DLR, Germany.

Ascending mode data have been processed for terrain errors and radiometric errors. Slant looking geometry of SAR system induces a high amount of geometric and radiometric error in the images. Due to the steep slope of the terrain, the data show effects like layover, shadow and foreshortening. TSX data has first been ingested and then terrain corrected using ASTER GDEM in MapReady software. DEM has been used to refine the geolocation of the SAR data, and to perform terrain correction. Terrain correction necessarily involves geolocation refinement as well. The terrain correction process alters the data in the SAR image, attempting to correct for the side-looking geometry of SAR.

Radiometric correction of terrain corrected TSX has been done to compensate for backscatter variation due to different viewing geometry and to convert DN values to dBs. This correction is important to retrieve information from the layover area and to normalize the brightness over the different slope aspects. TSX data has been first ingested and then terrain corrected using ASTER GDEM in MapReady software. Radiometric correction of terrain corrected TSX has been done to compensate for backscatter variations due to different viewing geometries and to convert the DN values to dBs.

In this chapter, characteristics of various types of data (remote sensing, ancillary and field data) used in the study have been described. ASTER and WorldView-2 data constitute the primary remote sensing data used for terrain mapping and geomorphological and ice dynamics studies. The ancillary data comprises of topographical maps, DEMs (ASTER GDEM and SRTM) and their derivatives. Description of the data characteristics was followed by a brief overview of the methodology adopted for the glacier terrain mapping. This paved the way for a discussion on the pre-processing techniques used for rectification of the data for geometric and radiometric effects. The ASTER VNIR and SWIR data were converted to radiance and then georeferenced and orthorectified. The orthorectified products were then co-registered and stacked together and later corrected for atmospheric path radiance and converted to surface reflectance. Similarly, ASTER TIR data was also first converted to radiance data using the sensor calibration parameters with subsequent corrections applied for atmospheric effects using ISAC and then converted to brightness temperature by Planck’s function.

CHAPTER 4
MAJOR GLACIER TERRAIN CLASSES AND THEIR CHARACTERISTICS

4.1 Introduction

One of the objectives of this study is to map glacier terrain classes in the Chhota-Shigri glacier using remote sensing techniques. It is therefore necessary to first understand different glacier classes present in this area, which can be identified in the field as well as on the remote sensing images. The aim of this chapter is to clearly define these classes and to understand how these can be characterised on remote sensing images. This understanding shall assist in extracting these classes through digital image classification of WorldView-2 and ASTER images of the Chhota-Shigri glacier.

Field work in the Chhota-Shigri glacier was carried in two seasons (Sep 2011 and Sep 2012) for about 15 days each to collect the ground data on glacier terrain classes and their distribution.

4.2 Major Glacier Terrain Classes

Six major glacier terrain classes have been identified in the Chhota-Shigri glacier. The description of these is given in the following sections.

4.2.1 Snow/Ice

Snow (density 0.01-0.3 g/cc) is a porous, permeable aggregate of ice crystals. The ice crystals are formed in the clouds at temperatures below 0°C by condensation of water vapours upon the condensation nuclei (dust particles, pollen grains, salt particles or small

frozen cloud droplets). Thus, the individual ice crystals nucleate, grow and begin their descent to earth as snowfall (Mellor, 1977). Freshly fallen snow is a mixture of ice crystals and air.

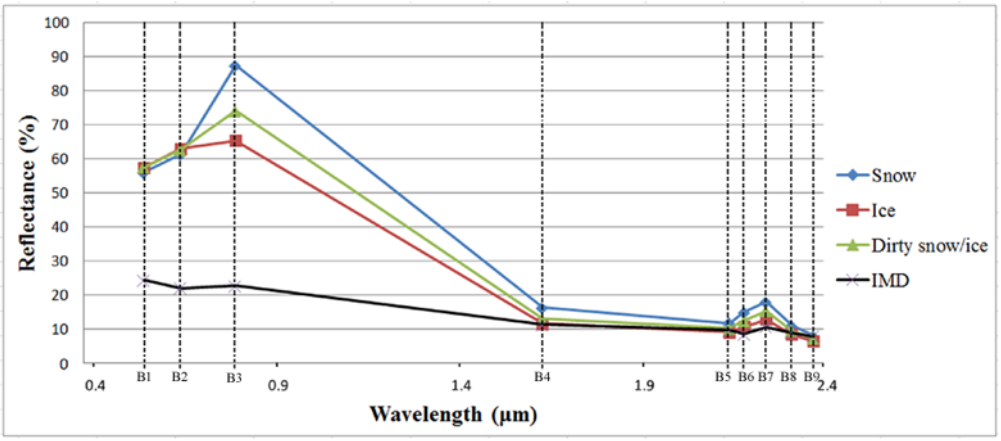

Figure 4.1: Spectral reflectance curves for snow, ice, dirty snow/ice and ice-mixed-debris, as derived from ASTER data.

Snow reflectance is very high in the visible region and shows a characteristic wide absorption trough in the short-wave-infrared (SWIR) region of the electromagnetic spectrum (Figure 4.1). Snow reflectance depends on various factors such as grain size, contamination, solar zenith angle, cloud cover, metamorphism and age factor, and liquid water content (Hall and Martinec, 1985; Dozier, 1989). On the ASTER FCC (R=4, G=3 and B=2) (Figure 4.2b), snow gives a typical white-cyan hue and is found to occupy mainly the high altitude regions of the accumulation zone. Snow and ice in the lower accumulation zone and the upper ablation zone are found to be mixed with minor debris (silt and clay) (Figure 4.3) which are unevenly distributed and sometimes found in patches. The presence of impurities in the snow/ice affects the reflectance of the snow/ice. This class may be referred to as dirty snow/ice.

As snow gradually starts to metamorphose, it gets compacted, pushing out the air from the spaces and turns into glacial ice (0.85-0.90 g/cc), which is composed of ice crystals and water molecules in a much dense arrangement. Like snow, ice also shows a similar higher reflectance, however, much lower as compared to snow in the visible region of the electromagnetic radiation (EMR) and a widespread absorption in the SWIR region.

Due to comparatively lower reflectance in the visible wavelengths, as compared to that of snow, ice appears in darker shades of blue on the satellite image and characterizes some part of the ablation zone of the glacier (Figure 4.4).

Spectral reflectance curves of the snow, ice and dirty snow/ice as derived from the ASTER image show the reflectance characteristics of these classes for this glacier (Figure 4.1). It may be seen that there is a very minor difference between the spectral characteristics of these classes in the VNIR region. The snow has very high reflectance in band 3 whereas ice has lower reflectance in this band. The reflectance of dirty snow/ice is the lowest in this band due to the presence of silt and clay. In the SWIR region of the ASTER image, the reflectance of all of these classes is similar with high absorption.

Snow, ice and dirty snow in this particular case have almost similar reflectance properties in the moderate resolution ASTER image. Thus it may be very dificult to distinguish these classes based only on multispectral classification. Also, the distribution of these classes is segregated in the upper part of the glacier. Therefore, these classes have been treated as a single class in the classification process i.e. Snow/ice.

4.2.2 Ice-Mixed Debris

In the ablation zone, towards the glacier terminus, as ice starts giving way to debris, there forms a mixture of the two classes which is called ice mixed debris (IMD). This mixed class covers a region between the ice covered area in the mid of the ablation zone and all-debris covered area in the lower reaches of the ablation zone, i.e. the glacier snout. The reflectance curve of IMD appears almost flat in the SWIR region with high absorption (Figure 4.1). In the visible region of the wavelength, it shows some peaks but has much lower reflectance as compared to the snow/ice due to the presence of debris. The drop of reflectance in the visible regions of EMR can also be attributed to the presence of high moisture in this class. As a result of its spectral characteristics, IMD appears in shades of dark bluish-greyish on the ASTER FCC (R=4, G=3 and B=2) (Figure 4.5b).

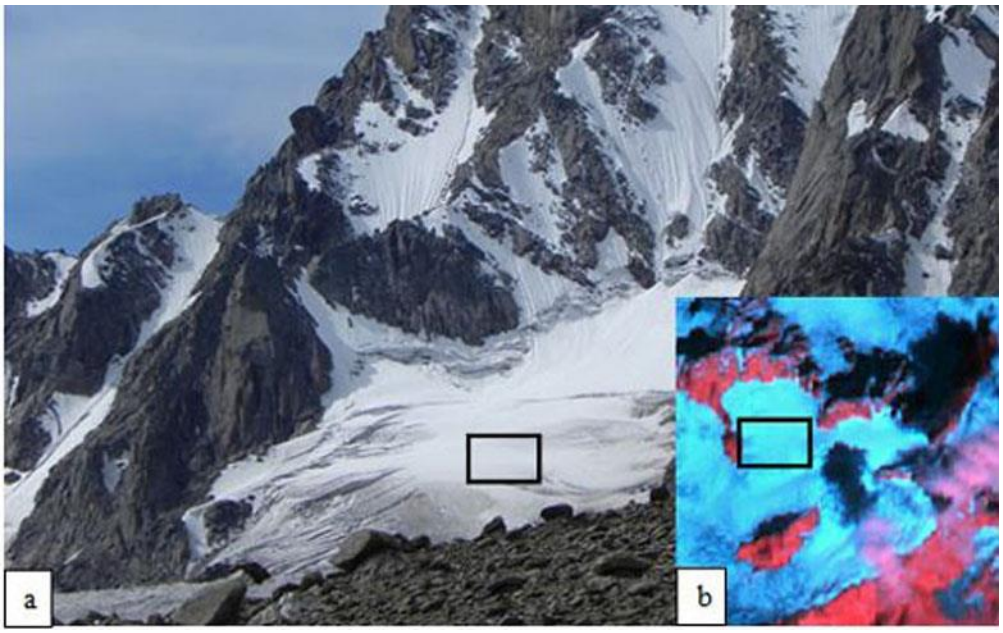

Figure 4.2: Snow in the accumulation zone (a) Field photograph; (b) Inset: ASTER FCC (R=4, G=3 and B=2).

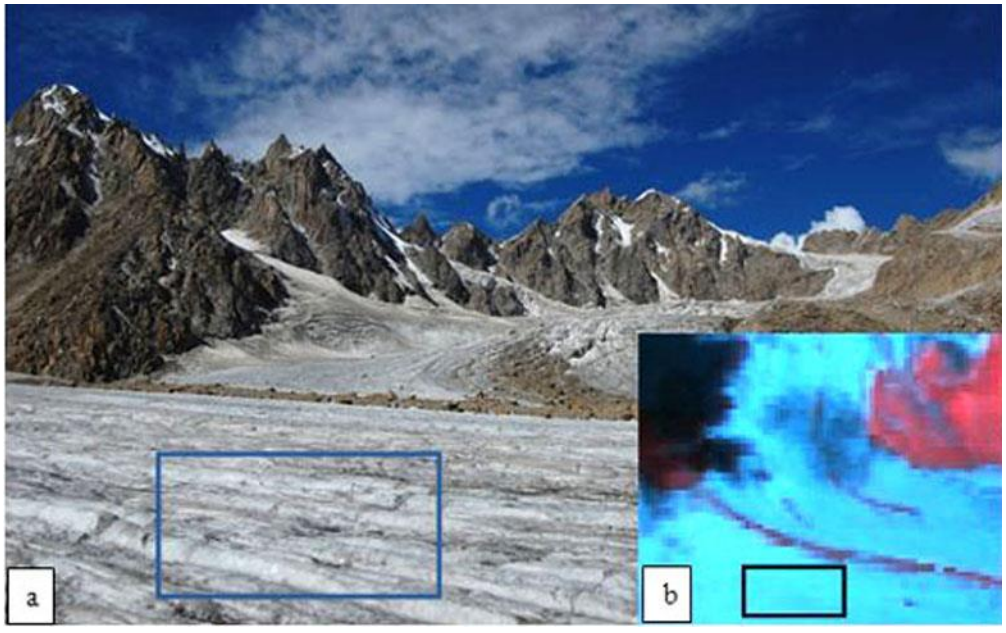

Figure 4.3: Dirty snow in the upper ablation zone (a) Field photograph; (b) Inset: ASTER FCC (R=4, G=3 and B=2).

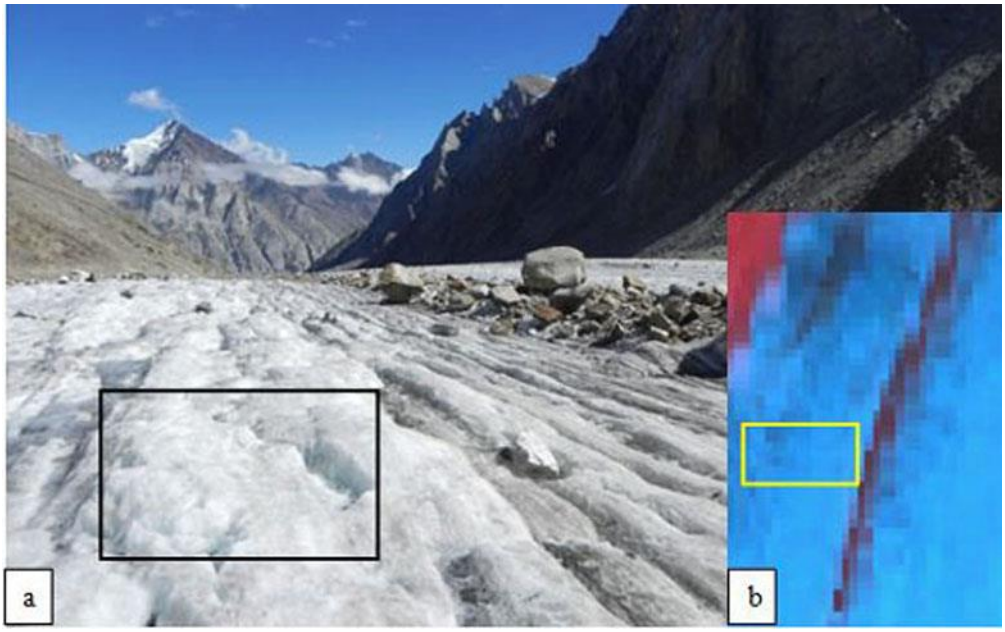

Figure 4.4: Ice in the upper ablation zone (a) Field photograph; (b) Inset: ASTER FCC (R=4, G=3 and B=2).

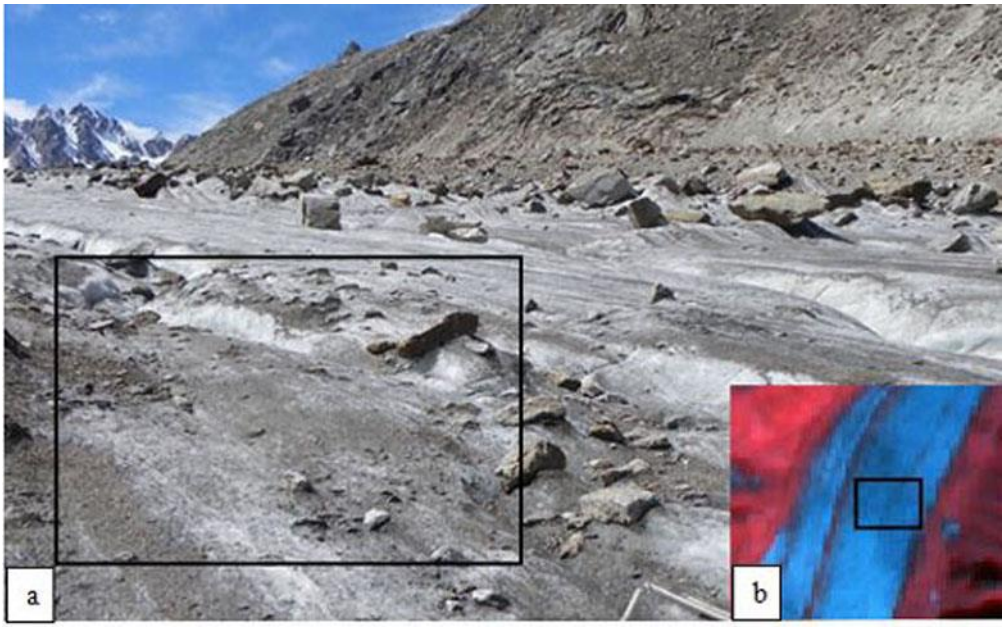

Figure 4.5: IMD in the lower ablation zone (a) Field photograph; (b) Inset: ASTER FCC (R=4, G=3 and B=2).

4.2.3 Debris

Debris is one of the most important classes in this glacier. The lower and lateral portion of the glacier is completely covered with rocks and boulders of different sizes. The debris is very important class because its distribution in the glacier affects the melting and dynamics of the glacier. Therefore, any change in the areal extent of the debris may affect the health and fate of the glacier (Bolch *et al.*, 2013). Figure 4.6 shows the spectral reflectance curves as derived from the ASTER image for the different types of the debris cover (SGD and PGD). These appear to have almost similar spectral trend but PGD has higher reflectance than SGD. Two types of debris have been identified and classified in this glacial terrain.

i. Supraglacial debris: In the ablation zone of the glacier, moving towards the glacier snout, the degree of glacier melting goes on increasing. As the ice melts away, the amount of debris covering the glacier surface also increases. Debris cover, in general, is derived from the weathering and erosion of the glacier bed and side valley rocks.

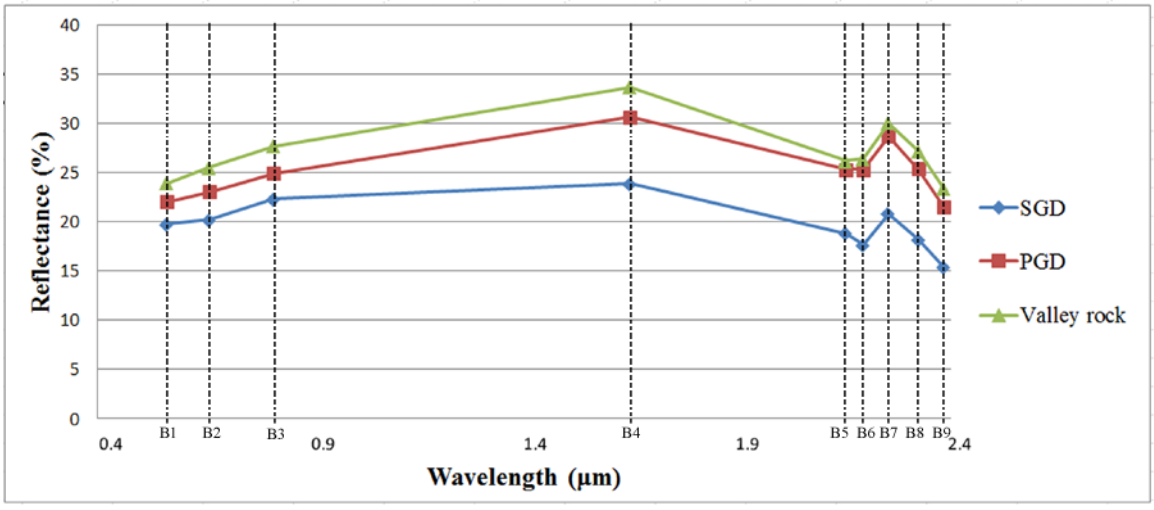

Figure 4.6. Spectral reflectance curves for SGD, PGD and valley rock, as derived from ASTER data.

In this study, a positional (with reference to the glacier) rather than genetic (medial, lateral moraine etc.) classification of debris cover has been followed. According to the positional classification of debris cover, debris lying on the glacier is called as SGD

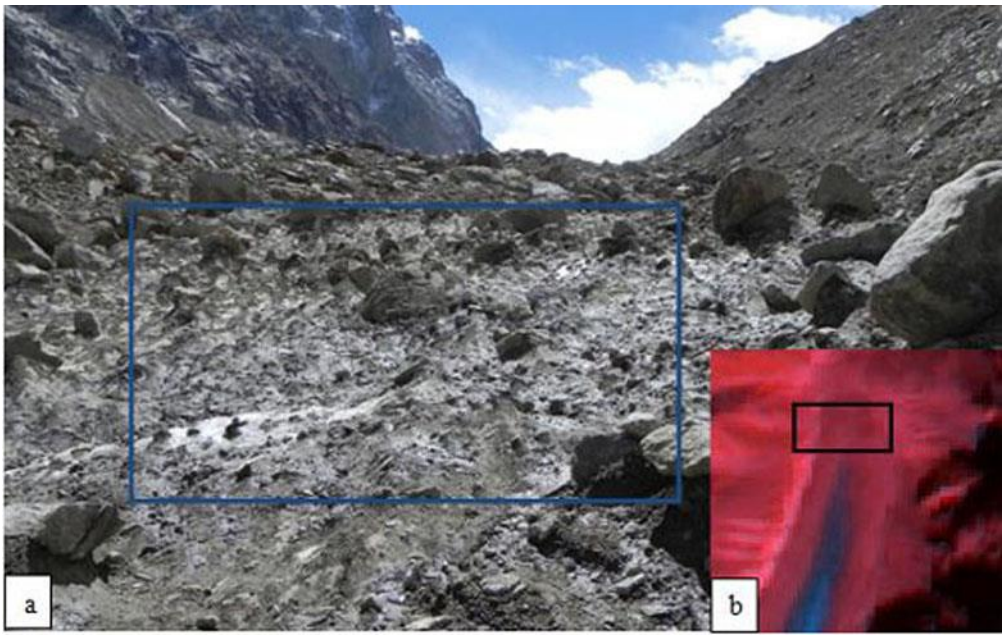

Figure 4.7: SGD near snout (a) Field photograph; (b) Inset: ASTER FCC (R=4, G=3 and B=2).

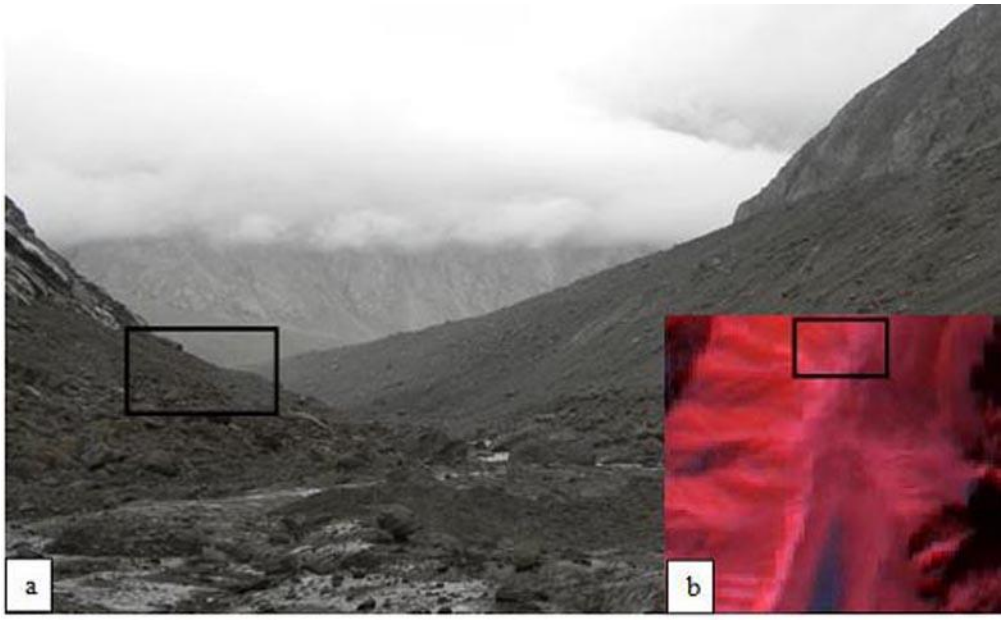

Figure 4.8: PGD below snout (a) Field photograph; (b) Inset: ASTER FCC (R=4, G=3 and B=2).

(Figure 4.7). Some of the factors affecting the reflectance of debris cover are moisture content, parent rock, type and degree of weathering, soil texture (proportion of sand, silt and clay), surface roughness, presence of iron oxide, and organic matter content. The spectral reflectance of SGD generally increases in the near-infrared (NIR; Band 3) and SWIR (Band 4) region (Figure 4.6) and hence it appears in shades of red/deep red on the ASTER FCC (R=4, G=3 and B=2) (Figure 4.7 b).

ii. Periglacial debris: According to the positional terminology of debris, the debris lying outside, yet along or near to the glacier margin, is referred to as PGD. As discussed above, debris of any kind (SGD or PGD) is derived from the valley rock and will have the same material composition. The only difference is possibly in their moisture content. PGD being drier (Figure 4.8a) shows higher values of reflectance throughout (Figure 4.6) and appears brighter than SGD in ASTER FCC (R=4, G=3 and B=2) (Figure 4.8b). Therefore, differentiation between PGD and SGD is very difficult in the visible and infrared regions of EMR. However, differentiation between the two can be made on the basis of temperature data in the thermal infrared region (Table 5.2 and 5.3).

4.2.4 Valley rock

This class includes the rocks constituting the side wall of the glacial trough or valley (Figure 4.9). The valley rock shows an increase in the reflectance from visible to NIR and SWIR regions of the EMR (Figure 4.6). It has a higher reflectance than the debris due to its consolidated and sometime sharp surface and perhaps due to its low water content also. A higher reflectance value in the SWIR region makes valley rocks appear in shades of bright red on the ASTER FCC (R=4, G=3 and B=2) (Figure 4.9b). Composition or type of bedrock and valley rocks in the region may differ spatially; however, as this study focuses on mapping and differentiation of glacier-related land cover types, all the differing lithologies have been treated as a single class.

4.2.5 Shadow

Shadows are mainly concentrated on the eastern side of the Chhota-Shigri valley as the sun is on the south-east in most of the remote sensing images. The shadows are quite

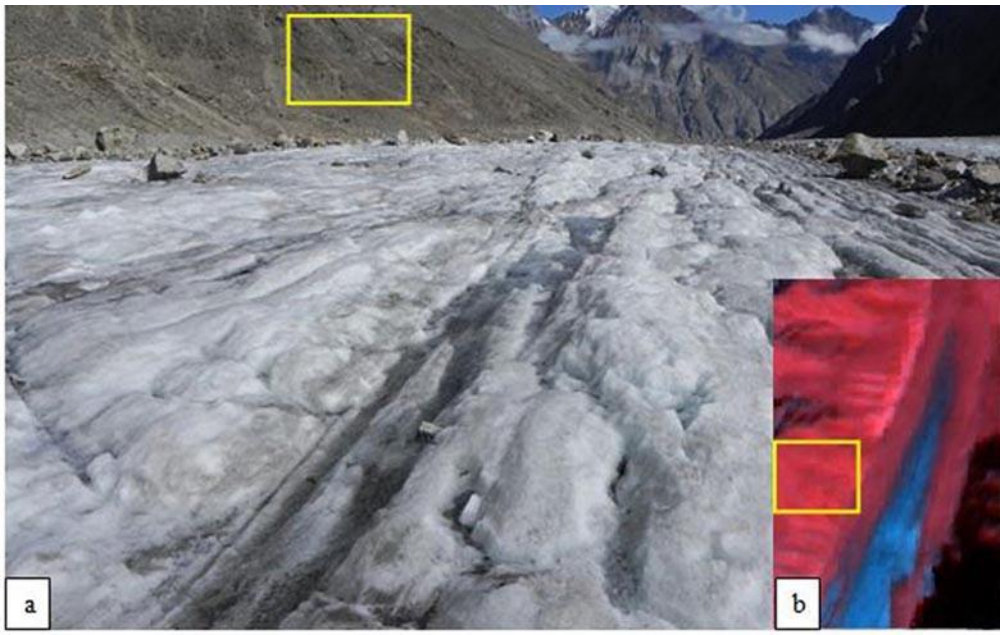

Figure 4.9: Exposed valley rocks in the western side (a) Field photograph; (b) Inset: ASTER FCC (R=4, G=3 and B=2).

Figure 4.10: Shadow in the eastern side of the valley (a) Field photograph; (b) Inset: ASTER FCC (R=4, G=3 and B=2).

deep and appear in shades of black to dark grey (Figure 4.10). It is difficult to identify what is beneath deeper shadows but it can be classified using multispectral classification. Therefore, during the classification shadow has been taken as one of the class.

Based on the spectral characteristics of different materials on the glacier surface in ASTER image, six terrain classes have been selected for classification (details in chapter 5). These are snow/ice, IMD, SGD, PGD, valley rock and shadow. Due to very similar spectral property, snow, ice and dirty snow/ice classes in the ASTER image, these have been merged as a single class i.e. snow/ice. Apart from the above classes observed in the field, some of the images were covered with clouds. Therefore, cloud may be considered as separate class in remote sensing data classification of those images. River channel (water) is not considered as a separate class during classification as the width of the water channel is quite small and could not be clearly seen in the moderate resolution ASTER images.

CHAPTER 5
DEBRIS COVER GLACIER MAPPING

5.1 Introduction

Himalayan glacial snowfields store about 12,000 km^3 of freshwater and are the major source of water for perennial rivers such as the Indus, Ganga and Brahmaputra (Cruz *et al.*, 2007) for most part of the central Asia. Millions of people in the countries, namely, India, Pakistan, Nepal, Bhutan, China and Bangladesh depend on these river waters for their daily needs. The glaciers are, however, shrinking due to the effect of climatic change (Haeberli *et al.*, 1999; Oerlemans, 2005; Paul *et al.*, 2007; Cruz *et al.*, 2007; Shukla *et al.*, 2010; Pandey *et al.*, 2012). It is also learnt that in most parts of the world, including the Himalayas, detailed inventory of glaciers has been lacking (Cruz *et al.*, 2007; Racoviteanu *et al.*, 2008; Racoviteanu *et al.*, 2010; Shukla, *et al.*, 2010; Paul *et al.* 2013). This may partly be due to the remoteness and vastness of mountainous glaciers making them inaccessible for continuous monitoring.

Remote sensing is perhaps the only effective tool for repeated mapping of mountainous glaciers in a comprehensive and cost effective manner. The increased use of remote sensing data for a number of glacier cover studies, as evident from the recent works (e.g., Ranzi *et al.*, 2004; Racoviteanu *et al.*, 2008; Racoviteanu *et al.*, 2010; Shukla *et al.*, 2010; Pandey *et al.*, 2012; Paul *et al.*, 2013), clearly demonstrates their utility. However, many glaciers are fraught with debris cover. Mapping of the debris covered glaciers even by remote sensing has always been a challenge, as can be seen from a number of studies (e.g., Paul, 2002a, b; Paul *et al.*, 2004; Ranzi *et al.*, 2004; Kargel *et al.* 2005; Bolch and Kamp, 2006; Buchroithner and Bolch, 2007; Bolch *et al.*, 2008 a, b; Shukla *et al.*, 2010; Paul *et al.* 2013).

The terminuses of the glaciers have shown continuous increase in the debris cover due to the recent retreat (Bolch and Kamp, 2006; Kulkarni *et al.* 2007; Paul *et al.* 2013). Several remote sensing based automated and semi-automated techniques may be found for mapping of the debris covered glaciers. Some of these techniques use geo-morphometric data (Bishop *et al.*, 2000, 2001; Paul *et al.*, 2004; Bolch and Kamp, 2006) while others use a combination of geo-morphometric and temperature data (Buchroithner and Bolch, 2007; Bolch *et al.*, 2008a, b). Recently, multispectral classification of combined optical-thermal data has been used effectively to map debris covered glaciers (Shukla *et al.* 2010; Karimi *et al.*, 2012).

The multispectral classification using combined optical and thermal data, as developed by Shukla *et al.* (2010) and subsequently examined by Karimi *et al.* (2012) is an automated method for mapping the debris covered glaciers. The method utilizes the existing temperature difference between the supraglacial debris (SGD) (on the glacier) and adjacent periglacial debris (PGD) (outside the glacier) to map the debris covered glacier boundary. Though the method developed by Shukla *et al.* (2010) presents the glacier terrain map with an overall accuracy of more than 85%, it has some limitations, as identified below,

(a) In this method, extent and effect of cloud cover, which is a major problem in the high mountain glacier mapping using optical data, has not be discussed.

(b) The glacier has been segmented in two parts- shaded and illuminated based on the aspect angle image and the solar azimuth angle of the optical image. It is found out that the area in the shaded region is relatively cooler than the area in the illuminated region. But this generalization may not always be true.

(c) The multi-spectral classification using maximum likelihood classifier (MLC) may fail when classifying data acquired at low radiometric resolution (e.g., ASTER sensor).

Chhota-Shigri glacier is one of the glaciers in Himachal Himalayas with lower part fully covered with debris making it very difficult to extract the exact boundary of the glacier. The thickness of the debris cover varies from few centimeters to meters. The size of the debris particles varies from fine grained dust and soil particles to very large boulders (Figure 5.1a, b). As discovered during the field work, the glacier's ablation area is mainly covered with firn and ice with varying amount of mud, fine grained debris and boulders

(this has been referred to as ice mixed debris (IMD) here, see Figure 5.1a, b). The debris cover at the bottom is mainly brought by the tributary glaciers in the eastern valley side (Figure 5.1c). The recurrent rock-fall in the eastern side of the valley (Figure 5.1d) is also one of the principal sources of heavy debris cover over this glacier.

In this chapter, the mapping of Chhota-Shigri glacier using the ASTER optical and thermal images has been discussed. The methodology is broadly based on the work of Shukla *et al.* (2010). Few adaptations in the methodology have been made to improve the accuracy of the classification results. Also, to improve the classification accuracy of cloud cover some contrast enhancement of ASTER image has been suggested.

Kääb *et al.* (2002) evaluated the utility of ASTER data in glaciology by concluding that this sensor is highly suitable for worldwide glacier monitoring from space. Subsequently, the ASTER images have been used for almost all type of glaciological mapping including velocity estimation, snow/ice cover mapping, mass balance, ELA fluctuation and thickness variation. Therefore, the optical and thermal images of ASTER sensor and the morphometric data derived from ASTER DEM are the major source of data used here. The multi-spectral classification has been performed using the most widely adopted MLC. Additionally, to accommodate data from different sources, a knowledge based classifier (KNC) has been proposed and its efficacy has been tested in generating an accurate debris cover glacier map of the region.

5.2 Mapping Debris Covered Valley Glaciers Using Geomorphometric and Temperature Difference Data – A Review

Bishop *et al.* (2001) investigated the utility of object-oriented data modeling and topographic analysis of Raikot glacier in Nanga Parbat, North Pakistan. They used a DEM derived from SPOT panchromatic stereo-pairs using the cross-correlation technique and *in situ* terrain information such as SGD load, ice velocities, ice thickness, and morphological character of the glacier surface for studying glacier features, namely, ice cliffs, debris mounds, moraines etc. and delineating the debris-covered glacier boundary. The DEM has a horizontal grid spacing of 20 m and a height accuracy of ± 8-12 m. They computed four DEM derivatives - slope angle, slope aspect, profile curvature and tangential curvature. Using these parameters they divided the terrain into several small segments called terrain form objects (TFOs) representing a local morphometrically contiguous portion of the landscape.

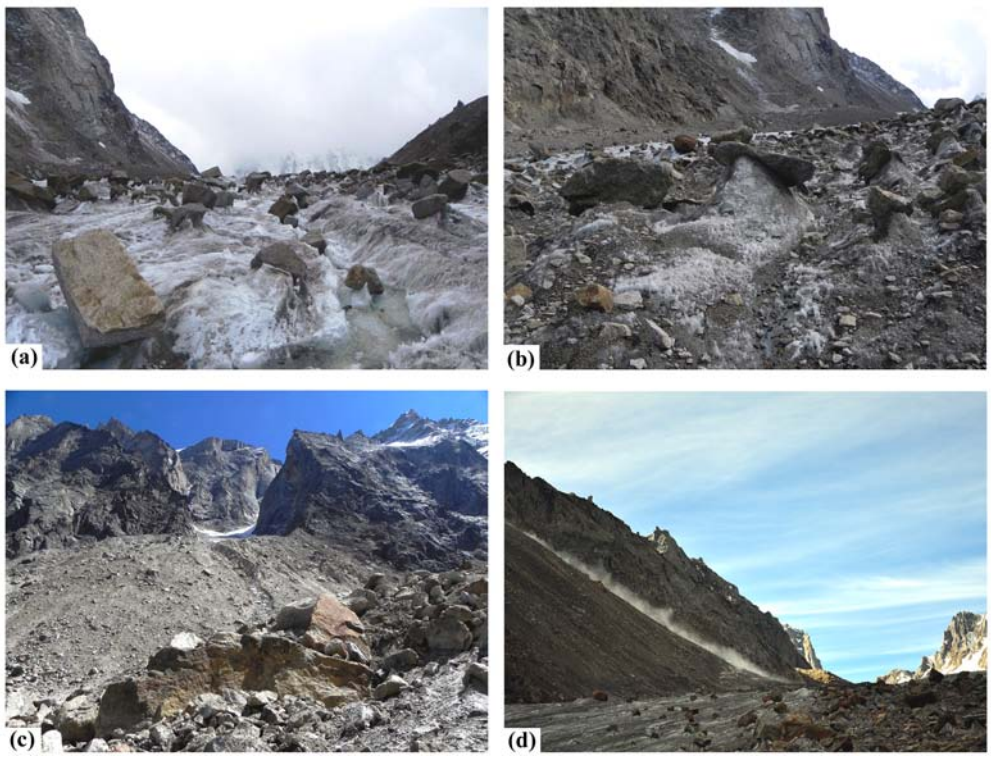

Figure 5.1: Field photographs (a) boulders in ablation zone; (b) boulders and fine grained debris in the ablation zone of the glacier which is referred as ice mixed debris (IMD); (c) debris brought by a tributary glacier in the lower eastern side of the main glacier valley; and (d) a rockfall in the eastern side of the valley.

These TFOs were used to identify the boundary of the glacier. Although, they did not present any quantitative assessment of the results but they concluded that using the morphometric parameters it was possible to identify the glacial boundary. In the study, Bishop *et al.* (2001) used a high resolution DEM for calculating the morphometric parameters and therefore this approach of mapping still needs to be tested with different freely available DEMs for global application in the field of glaciology.

A semi-automatic method for delineation of debris covered glacier was devised by Paul *et al.* (2004). The study involved the use of a DEM from the Swiss Federal Office of Topography (Swisstopo, 2001) with high spatial resolution (25 m) at improved elevation accuracy (a few meters). The test site selected was the Oberaletsch gletscher (23 km^2 in area), Swiss Alps. They used sequential steps to determine the glacier boundary. Firstly, TM4/TM5 ratio image was used to differentiate between glacier and non-glacier areas; then hue component of IHS transformation was used to map vegetated and non-vegetated areas, and the slope image (< 24°) was used to map the debris covered part of the glacier.

Afterwards, a neighborhood analysis was used to exclude all the areas that were not connected to glacier ice. Change detection was used to detach flat and vegetation-free glacier fore fields. Thus, by using multisource data they delineated the glacier boundary and correlated their results with a vector dataset from 1993, created by the Swiss Federal Office of Topography. No quantitative assessment was presented but they found a good correspondence between the two, with some deviations where: (a) slope $>24^0$, and (b) glacier recession since 1993 did occur. Later, artificial neural network with two hidden layers was used for debris classification. They found that the results from the ANN based classification of debris cover based on spectral properties alone were not satisfactory. However, they suggested that integration of slope data in ANN classification might improve results. Since DEM with high resolution and elevation accuracy are not available for all the glaciers, therefore ASTER DEM was also tested for delineating debris cover glacier boundary. It was reported that the ASTER derived DEMs could only be used for gently sloping glaciers and not the steep sloping glaciers because of the errors contained in the ASTER DEM and also due to its low resolution. This work signifies the use of morphometric parameters in the mapping of debris covered glaciers.

By using only the morphometric parameters of the glacier features, it is possible to delineate the glacial boundary (Bishop *et al.*, 2001 and Paul *et al.*, 2004). The high resolution DEM was found satisfactory to derive the morphometric parameters. However, high resolution DEM is not available at global scale. Therefore, many alternatives to this method have been developed recently. One of them is utilizing the thermal signature of the debris covered part.

The idea of using the temperature difference for mapping of debris covered glacier was first put forth by Lougeay (1974) after the analysis of some field collected temperature data. He suggested that the SGD are cooler than the PGD. Using this idea, Taschner and Ranzi (2002) and Ranzi *et al.* (2004) attempted to map the Belvedere and Calderone Glacier in the Italian Alps. They found the presence of temperature difference between the SGD and PGD using the *in situ* data. Further, they analyzed the thermal data from ASTER and Landsat-TM sensors and found similar pattern. Using this principle, they subjectively created a threshold of thermal data for separating the ice cored debris from the non-ice cored debris. This work signifies the use of the thermal data in debris covered glacier mapping and specifically to distinguish the SGD from the PGD.

Further, Shukla *et al.* (2010) developed a synergistic approach for mapping debris cover glacier utilizing multispectral classification of integrated AWiFS optical and ASTER thermal data. They used this technique for the mapping of Samudra Tapu glacier of Chandra basin in Himachal Himalayas and reported that the area in shaded and the illuminated parts of the glacier have different thermal signatures. The shaded and the illuminated areas were segmented based on the aspect angle image (derived from the DEM) and the solar azimuth angle of the image (derived from the image header information). They reported that the areas under the shaded region were relatively cooler than the areas under the illuminated region. Then the multispectral classification method (MLC) was performed to classify the glacier terrain into various classes such as SGD, PGD, valley rock, snow, ice, mixed ice and debris, water and shadow. Thermal information derived from the thermal bands was used to distinguish between the SGD and PGD. This technique was further tested by Karimi *et al.* (2012) for mapping of Alamkouh Glaciers, Iran. The results were satisfying in both the studies with a high accuracy (> 85 %) in delineating the debris covered glacier boundary.

Thermal information along with morphometric parameters were used by Bolch *et al.* (2007); Buchroithner and Bolch (2007); Bolch *et al.* (2008a,b) and Bhambri *et al.* (2011a, b) to map debris covered glaciers. They first computed the morphometric parameters like slope gradient, altitude and curvature from ASTER DEM. These data, in combination with optical and thermal IR data, were used for mapping the debris covered glacier extent. The delineation of glacial boundary was done out in a sequential manner by thresholding different parameters. Thermal data was used to separate the SGD and PGD by simple thresholding. The glacier boundary was delineated with ± 2-6 percent deviation from the manually identified glacier boundary. However, they faced problems at the distal and a few lateral parts of the debris covered glaciers, mainly because of the moderate resolution of DEM and non-existence of clear morphometric patterns.

The literature review suggests that perhaps there is only one method (i.e. method developed by Shukla *et al.* (2010), which describes a complete automatic approach for mapping the debris covered glacier. However, when this method was applied on ASTER data, the mapping accuracy reduced due to many misclassified patches found in the shadow-snow-IMD junction and the cloud-IMD-snow junction. This may be due to the low radiometric resolution of the ASTER data in comparison to the AWiFS data used by Shukla *et al.* (2010). Further, the error may be because of the similar spectral response of

snow and cloud in the visible region. The other possibility of this error may be due to the presence of mixed pixels at the boundaries of shadow/IMD-snow and cloud/IMD classes. In this study, simple contrast enhancement technique (addition and subtraction of different bands) has been suggested for resolving these issues.

The literature review also suggests that the semi-automated method i.e. sequential classification of glacier using both morphometric parameters and the thermal information has a great potential in mapping the debris covered glaciers. However, it requires a lot of time and it is required to sequentially proceed to get the final output map. To automate this procedure, a combination of MLC and KNC has been used (Hybrid classification). KNC is a new and advanced classification method in which various data sources can be integrated by forming simple production rules. A comparative study between MLC and the Hybrid classification has also been carried out.

5.3 Data Sources

The remote sensing data from ASTER for the post-ablation period (date of acquisition 3rd October, 2003) have been selected for the study. The literature review suggests that the VNIR bands of ASTER are very useful for mapping glacier classes and cover optimum spectral resolution for the mapping of clean glacier, whereas SWIR bands are helpful in identification of IMD and rocks or debris (Shukla *et al.,* 2010; Keshri *et al.,* 2009). Therefore, in this study, all the ASTER VNIR bands have been used along with one of its SWIR bands. The thermal information about different types of debris has been derived from the TIR band of the ASTER data. The data has a patchy cloud cover near the accumulation zone, which has been considered as one of the classes during classification. A very high resolution WorldView-2 panchromatic image has also been used for visual inspection of the final glacial boundary.

The ancillary data in the form of Survey of India (SOI) toposheet (at 1:50,000 scale, surveyed in 1961) has also been used to deduce the glacier boundary for the accuracy assessment and change detection. The details about the glacier and non-glacier classes present in the watershed have been collected during the two field campaigns carried out in September 2011 and September 2012. Snow/ice, IMD, SGD, PGD, valley rocks and shadow are the prominent classes found in this watershed. Snow/ice has a higher reflectance in the visible range and low reflectance in the SWIR region (Figure 5.2). In contrast, rocks have the opposite behavior; they have higher reflectance in the SWIR and

low reflectance in the visible region (Figure 5.2). IMD on the other hand has reduced reflectance than snow/ice in the visible range due to the mixing of the rocks with ice (Figure 5.2). The details of the data used in this study are given in the Table 5.1.

5.4 Methodology

A synergistic approach for mapping the debris covered glacier was first proposed by Shukla *et al.* (2010). As described earlier, in this method, the region was first divided into shaded and illuminated areas using the aspect angle image and the solar azimuth angle of the image. The training data was selected from each region separately and then classification is performed. They found that the regions in shaded portion were cooler than the illuminated region. The same concept was intended to be used here. However, on analyzing the thermal data for the debris cover in the shaded and illuminated areas of the glacier, it was observed that the distribution of the temperature did not follow such pattern (for details see section 5.4.2; Table 5.2 and Table 5.3). Thus, a new approach based on combination of MLC and knowledge based concept has been envisaged here. The KNC incorporates both temperature and morphometric data using a set of simple production rules based on the knowledge of the area.

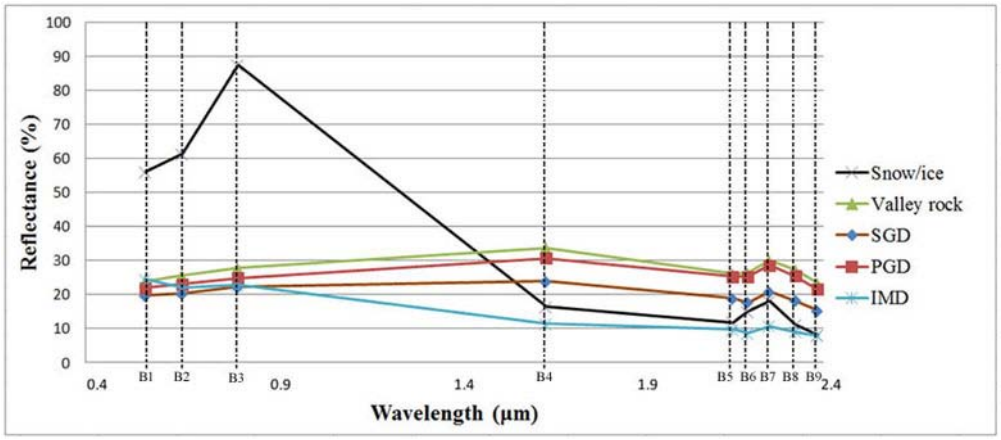

Figure 5.2: Spectral plots derived from ASTER image of 3rd October, 2003. Color lines show spectra of major terrain classes of Chhota-Shigri glacier i.e. snow/ice, valley rocks, SGD, PGD and IMD. Note: B1 to B9 represents different bands of ASTER image.

Table 5.1: Specifications of the data used in this study.

Data type	Satellite	Data Details					Purpose
Remote Sensing data	Terra ASTER	Subsystem / Radiometer	Band No.	Spectral Range (μm)	Spatial Resolution (m)	Radiometric Resolution (bits)	Classification of glacier terrain
		VNIR	1	0.52-0.60	15	8	
			2	0.63-0.69			
			3N	0.78-0.86			
			3B	0.78-0.86			
		SWIR	4	1.60-1.70	30	8	
		TIR	10	8.125-8.475	90	12	
			11	8.475-8.825			
			12	8.925-9.275			
			13	10.25-10.95			
			14	10.95-11.65			
	WorldView-2	Panchromatic	--	0.45 – 0.80	0.46	11	Visual interpretation of glacial boundary
Field data		Ground Control Points (GCPs, Field Photographs and Information on debris cover extent					Identification of glacier terrain classes and validation of results
Toposheet		SOI toposheet (surveyed in 1961)					Extraction of old glacier boundary and validation of results

The overall methodology is based on following sequential steps:

i) Dataset generation (pre-processing, contrast enhancement and generation of DEM derivatives)
ii) Analysis of the temperature differences between the SGD, PGD and valley rocks
iii) Supervised image classification (MLC and Hybrid classification)
iv) Accuracy assessment
v) Post-processing of the classified image
vi) Delineation of debris covered glacier boundaries.

Figure 5.3 shows the basic flow of steps as described now.

5.4.1 Dataset generation

5.4.1.1 Pre-processing of remote sensing data

The ASTER level AST14DMO has been used in this study. It is pre-geocoded and orthorectified data and comes in ***.tiff*** format. The VNIR (bands 1, 2, 3N) and SWIR (band 4) bands have been selected based on the analysis of spectral characteristics of the classes selected here. ASTER TIR bands (bands 10-14) have been used to compute the surface temperature of the watershed.

Firstly, the data have been converted to radiance. The unit conversion coefficient according to the gain settings has been taken from ASTER user's handbook version 2 (Abrams *et al.*, 2004). The radiance values are converted to reflectance by applying atmospheric correction using ENVI FLAASH software tool. Similarly, the TIR band data has also been corrected for atmospheric attenuation and then converted to brightness temperature using emissivity normalization method given in ENVI software.

5.4.1.2 Spectral analysis and contrast enhancement

The reflectance and the brightness temperature images have been stacked together to form an integrated dataset. The variations in reflectance over different glacier classes in different spectral bands have also been studied. Figure 5.4a shows surface reflectance profiles of glacier terrain using reflectance profiles in different ASTER bands. It is particularly observed that the reflectance of IMD and debris conflates in different bands at several places. This shows that redundant or very similar spectral information may be present in different ASTER bands.

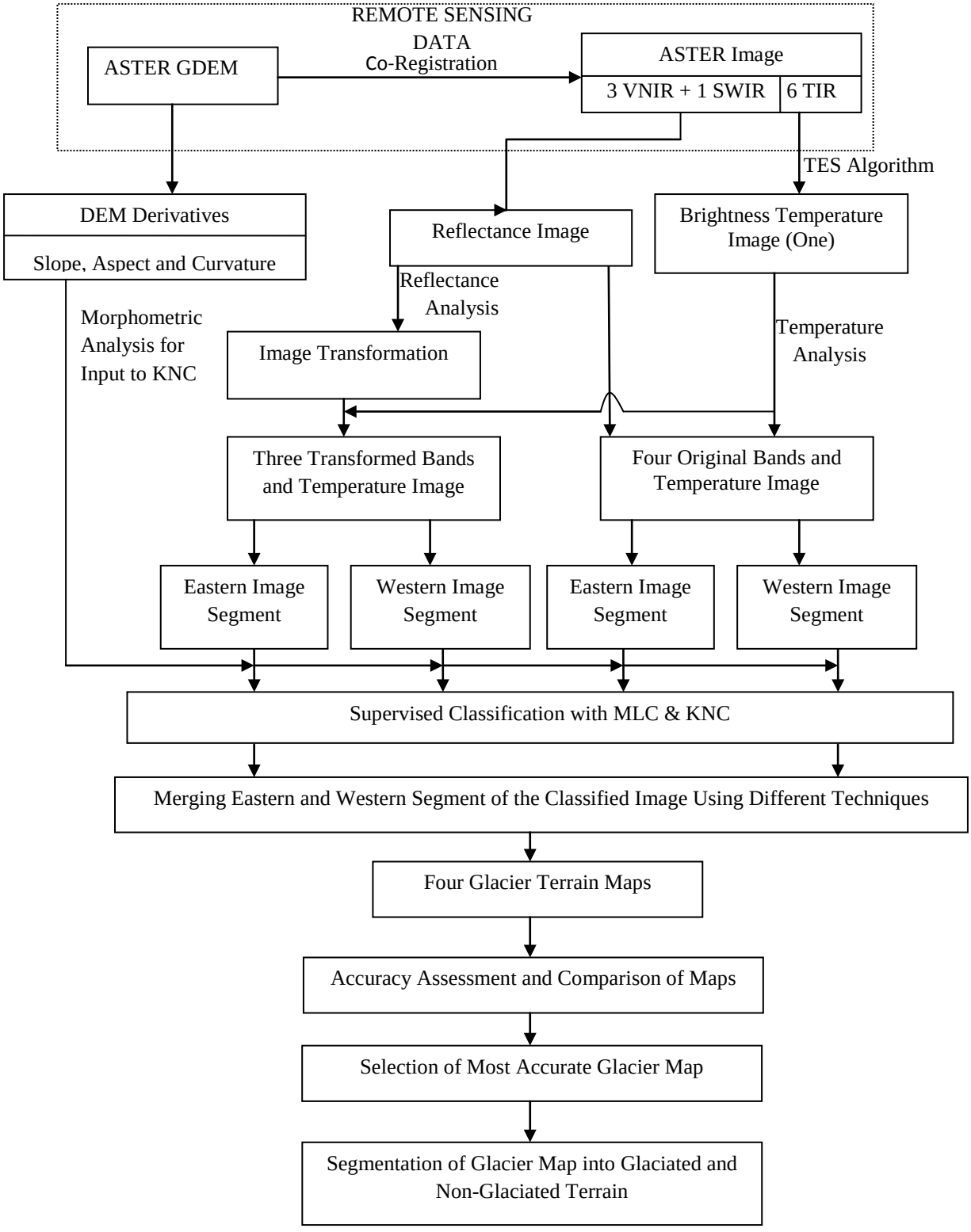

Figure 5.3: Schematic workflow for delineation of debris-covered glacier boundary.

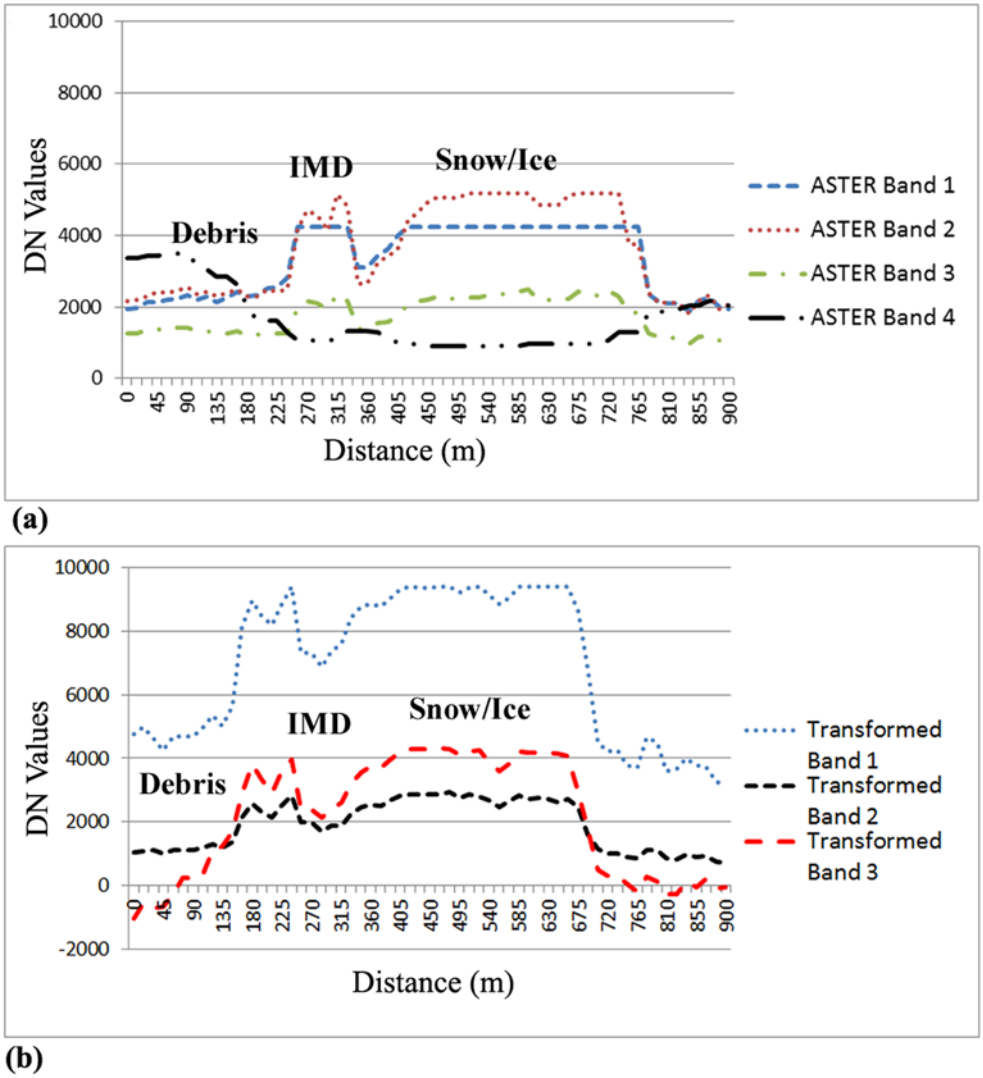

Figure 5.4: Surface reflectance profile (a) ASTER band 1 (green), band 2 (red), band 3 (NIR) and band 4 (SWIR); and (b) Transformed bands (TB) B1 + B2 = TB1, B2 - B3 = TB2 and B2 - B4 = TB3. Note: the surface reflectance profiles in (a) and (b) are taken at same location.

To remove this redundant information and to increase the difference between the reflectance of different classes, an image enhancement based on band transformation using simple addition and subtraction of bands (equations 5.1-5.3) has been proposed here:

$$B1 + B2 = TB1 \quad (5.1)$$

$$B2 - B3 = TB2 \quad (5.2)$$

$$B2 - B4 = TB3 \quad (5.3)$$

where B1, B2, B3 and B4 are the data acquired in ASTER optical bands and TB1, TB2 and TB3 denote transformed bands. Band transformation may lead to increase/decrease in the dynamic range of the reflectance thereby producing increased contrast between the image objects, which results into or highlighting the spectrally 'off-beat' objects (Gupta, 2003).

Figure 5.4b shows the reflectance profiles in different transformed bands at the same location as in Figure 5.4a. An increase in the contrast (difference in reflectance) between the glacier classes in different transformed bands can be seen. Due to this increased contrast, glacial classes (IMD and debris) and the cloud present in the image may become more separable than those observed in original optical bands. Hence, accuracy of classification is expected to increase.

5.4.1.3 Generation of DEM derivatives

It is observed in the eastern side of the valley that some pixels of SGD, PGD and valley rock exhibit similar temperature (see section 5.4.2 for details). Due to this, it was difficult to formulate the rules based only on temperature information to classify these classes using KNC. To resolve this issue, additional information in the form of geo-morphometric parameters has been used as an input to the KNC (details in section 5.4.3.2). Geo-morphometric parameters have been derived using DEM derivatives like slope, aspect and elevation.

5.4.1.4 Optical and thermal data integration

The existing temperature difference (discussed in section 4.2) between the SGD and PGD is the key to classify the debris cover part of the glacier. Therefore, three new transformed bands and ASTER original (VNIR and SWIR) bands have been stacked separately with the temperature image to form different sets of images for classification. Thus, two sets of images have been used for the classification of glacier terrain:

(i) Transformed bands with thermal image,
(ii) Original ASTER bands (VNIR, SWIR (band 4) with thermal image.

5.4.2 Temperature analysis

Other studies have reported that the SGD and the PGD have distinct temperature variations due to the presence of cooler ice beneath the SGD. The temperature difference

between both the classes has also been observed in the shaded and illuminated areas (Shukla *et al.* 2010). Using this assumption, the dataset has been segmented into shaded and illuminated areas using the method given by Shukla *et al.* (2010).

The temperature distribution over the shaded and illuminated areas has been analyzed and it has been observed that in the eastern part of the glacier even the PGD has cooler temperature than the SGD of the western part (Table 5.2 and Table 5.3). Similarly, comparatively lower temperatures may be seen for the valley rocks and the SGD of the eastern side. Further, in the eastern side, the temperature distributions have been found to be obscuring. Some pixels of the SGD, PGD and the valley rocks have similar surface temperature. But in general, the eastern side of the valley is cooler than the western side of the valley (Table 5.2 and Table 5.3). The probable reason may be the orientation and the narrowness of the glacier valley with high and steep valley walls, which prevents solar radiation to reach in the eastern part during most of the sunny day. The other reason may be the wind circulation system within the glacier valley which needs to be further studied. Therefore, the method given by Shukla *et al.* (2010) fails to explain the temperature distribution over this glacier.

To resolve this ambiguity, general observations of the temperature have been used to divide the glacier into cooler and relatively hotter zone. Based on the temperature distribution, all the images have been divided into two parts i.e. eastern side and western side. The signature for each class has been taken from both sides separately for image classification.

5.4.3 Image classification and delineation of glacier boundary

MLC and KNC has been widely used technique in the field of land use/land cover mapping. MLC has been earlier used for mapping snow and glacier classes but as the literature suggests KNC has never been used for classification of glacier cover. Therefore, in this chapter, the glacier cover mapping has been carried out utilizing both methods of classification:

(i) MLC based classification,

(ii) Hybrid classification (MLC and KNC together).

Table 5.2: Temperature distribution over selected pixels of supraglacial debris type

Sl. no.	Western side Temperature (°C)	Eastern side Temperature (°C)
1	12.3	8.1
2	7.8	6.3
3	8.8	6.7
4	7.1	4.7
5	10.7	3.9
6	9.8	3.5
7	10.8	5.9
8	10.5	5.2
9	10.7	4.6
Average	9.8	5.4

Table 5.3: Temperature distribution over selected pixels of periglacial debris type.

Sl. no.	Western side Temperature (°C)	Eastern side Temperature (°C)
1	13.3	11.7
2	21.5	8.9
3	14.6	8.6
4	19.3	8.5
5	19.3	8.9
6	11.5	9.6
7	16.0	8.2
8	18.6	4.0
Average	16.8	8.5

5.4.3.1 MLC based classification.

Based on the field knowledge and visual image analysis of the area (refer chapter 4 for details), the glacier terrain has been divided into snow/ice, IMD, SGD, PGD, valley rocks, shadowed area and cloud cover classes. The image has then been classified using MLC. Signatures or the training data for each class have been collected and later a separability analysis has been performed for both the datasets (i.e. transformed bands along with temperature image and the ASTER original bands plus temperature image) and for each image segment (i.e. eastern and western). Based on the training data statistics, the signature separability for both the eastern and the western sides of the valley has been determined (Table 5.4).

The separability analysis clearly shows that the classes are more separable when transformed bands are used in comparison to using the original ASTER bands. The best average separability has been observed for the two transformed bands and the temperature image (TB2+TB3+Temperature image; referred as image set 1 (IS 1) afterwards) than for ASTER original bands (B1+B3+B4+ temperature image; referred as image set 2 (IS 2) afterwards). Table 5.4 shows the best average separability for the two datasets used in this study. These selected bands have then been used as an input in the classification of glacier terrain. The accuracy of the classification has been assessed using the field data, visual interpretation and conventional error matrix based measures, namely overall accuracy, user's and producer's accuracy (Congalton, 1991).

Table 5.4: Selected image dataset having the best average separability

Separability measure	**DataSet**	**Value of the separability measure**	
		Eastern Valley segment	**Western Valley Segment**
Transformed divergence	IS 1	2000	1995
Transformed divergence	IS 2	1954	1947

5.4.3.2 Hybrid classification

For hybrid classification, both MLC and KNC have been used in an integrated manner and hence has been referred here as hybrid classification. Firstly, MLC has been used

to classify the clean glacier classes (debris free part of the glacier) like snow/ice and IMD along with the shadow, cloud and the rocks using only optical data. Rock class includes SGD, PGD and the valley rocks which are then separated using the temperature information and geo-morphometric parameters in KNC of ERDAS software.

KNC is a new and advanced technique for integrating information (knowledge) derived from data like satellite images, thematic maps and other spatial data to produce a final and desired output. Users' knowledge about the different variables (i.e. data from multiple source i.e. different images, maps and/or ancillary information) which influences the distribution of the spatial objects or the image classes are taken as input. These inputs are then used to frame production rules which are then used in the classification or to produce a final output.

Since the temperature variation of the two debris classes (i.e., SGD and PGD) has already been examined, KNC has been used to map the distribution of these two classes. It is observed that the temperature distribution is sufficient enough for identification of the classes in the western side but not in the eastern side due to the similar temperature of some pixels of different classes. Therefore, geo-morphometric data have been used as inputs in the eastern side to further refine the extent of classes. The rocks having temperature between -1.43^{o}C to 10.63^{o}C; aspect angle 300^{o} to 360^{o}; and elevation above 4350 m have been classified as SGD and remaining as PGD. The valley rock class has been included in the PGD class; because the KNC has not been able to separate valley rock from the other two classes even after combining temperature and geo-morphometric data. This may be due to similar morphometric characteristics and temperature of the PGD and the valley rocks classes. This may not have bearing on the ultimate objective of delineating the glacier boundary, as the glacier boundary includes only SGD class. Further, the accuracy of the classification has also been assessed.

5.4.4 Accuracy assessment

The goal of this study is to demonstrate and test two different methods for classification of the debris covered glacier terrain. Therefore, two-stage accuracy assessment has been done - first to test the quality of classification and second to test the accuracy of information contained in the final output thematic layer.

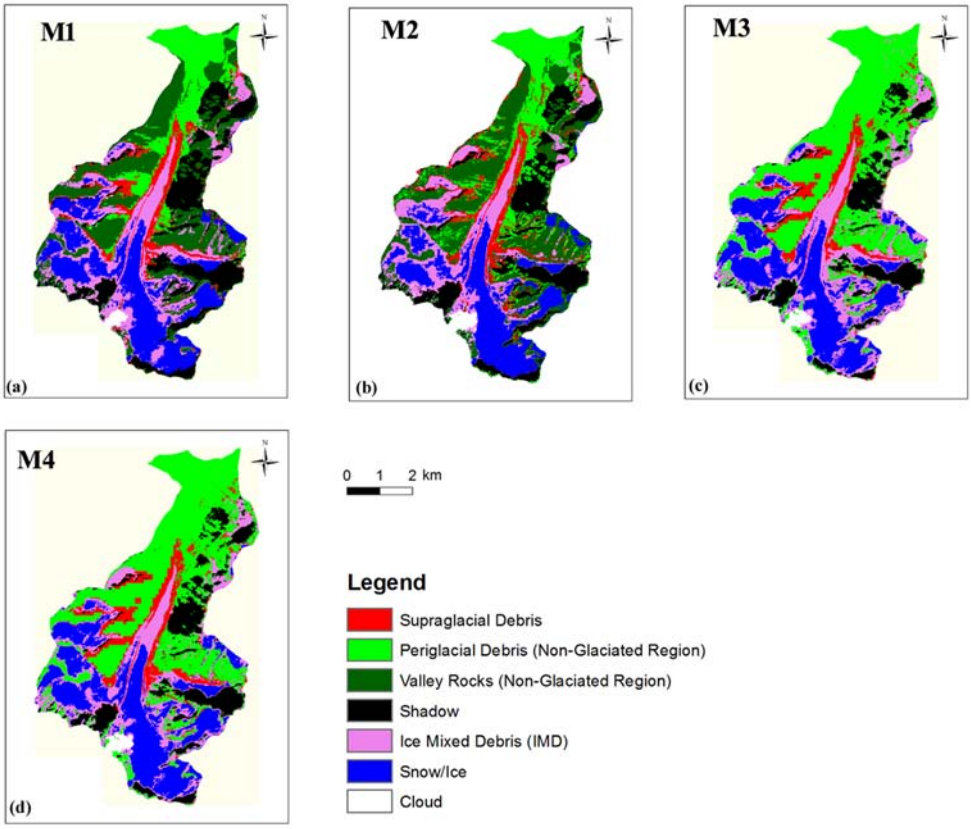

Figure 5.5: Thematic maps (a) M1 map prepared using IS 1 using MLC; (b) M2 map prepared using IS 2 using MLC; (c) M3 map prepared using IS 1 using hybrid classification; and (d) M4 map prepared using IS 2 using hybrid classification. Note, in M3 and M4 maps, periglacial debris and valley rocks are merged to single class i.e. non-glaciated region.

The two image classification methods have been applied on two sets of data; first set is of transformed bands and thermal image (IS 1) and the second set is of ASTER original bands including thermal image (IS 2). Thus, four thematic maps (Figure 5.5) referred as M1, M2, M3 and M4 from here on, have been produced.

First, the thematic maps have been visually inspected by swiping them over the FCC of the area. Then, error matrix based measures have been applied to determine the overall, user's and producer's accuracy. A testing dataset consisting of 256 pixels has been selected using stratified random sampling for each map. The reference data have been collected from the visual interpretation of the ASTER image to generate the error matrix.

Thus, finally two accuracy reports have been obtained,

a) classification accuracy report

b) accuracy report of glacier terrain map.

As mentioned earlier, the idea behind the extraction of debris-covered glacier boundary is based on the separation of SGD and PGD. Thus, the overall accuracy and individual accuracies of only SGD and PGD for all the glacier terrain maps have been discussed in detail later (Table 5.5).

5.4.5 Post-processing of thematic maps

Post-processing is done to remove the misclassified pixels in the classified images. These pixels are often seen studded into other classes and give a patchy look to the thematic map. In the complex glacier terrain, these corrections may include detailed correction of debris covered part, shadow regions, local cloud cover etc. (Paul *et al.*, 2013).

Post-processing of the classified image having the highest classification accuracy (M1) (Figure 5.5) has been corrected for these errors using manual editing and by applying majority filter to the classified map. The indecipherable outline of the glaciated region such as in the shadowed region can be corrected by manual digitization of the boundary by keeping shaded DEM or high resolution image in the background (Paul *et al.*, 2013). The areas under the shadow have been removed by manual digitization of boundary using a shaded DEM and a high resolution WorldView-2 image of the area. A 3x3 pixels majority filter has been applied to the output thematic layer to remove the studded misclassified pixels. These simple but highly valuable exercises may lead to further increase in the accuracy of the classified thematic layer and help in producing a finer outline of the glacier.

5.4.6 Delineation of the glacier boundary

The thematic map produced after post-processing and having the highest accuracy has been used to create the glacier boundary map. For this purpose, first, the non-supraglacial cover classes (i.e. PGD, valley rock, cloud and shadow) and supraglacial cover classes (i.e. SGD, snow/ice, and IMD) in the glacier terrain map have been merged separately. This results in a binary glacier terrain map with two classes, namely, glaciated area and non-glaciated area (Figure 5.6). The binary glacier terrain map, thus obtained, has been vectorised to extract the boundary of the debris covered glacier. The glacier boundary from toposheet has also been extracted using simple on-screen digitization.

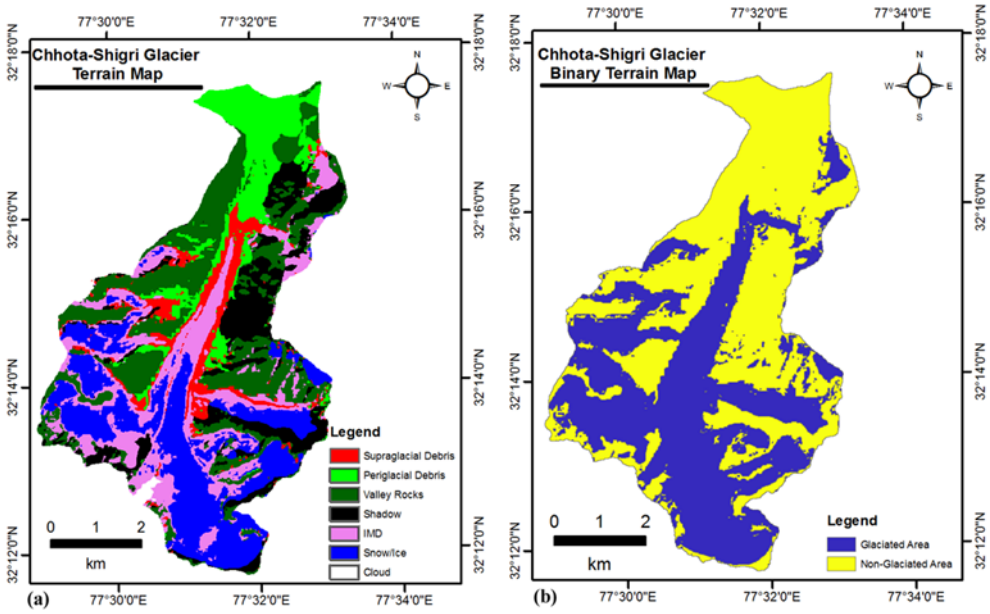

Figure 5.6: Chhota-Shigri glacier terrain map prepared using thematic map M1. (a) All glacial terrain classes after post-processing. (b) Binary glacier terrain map with two classes namely - glaciated area and non-glaciated area prepared after merging of appropriate classes from map M1.

5.5 Results and Discussion

The efficacy of the two classification methods (i.e., MLC and hybrid classification) used here for delineation of the debris-covered glacier boundaries has been discussed in this section. First, the accuracy assessment of the thematic maps has been described. Later, the validation of the debris-covered glacier boundary, delineated using the glacier terrain map having highest accuracy with that obtained from manually digitized boundary of the glacier (by visual interpretation of ASTER VNIR image and SOI Toposheet; Figure 5.7) has been carried out.

Table 5.5 shows the overall accuracy of all the glacier terrain maps produced from different datasets using the two methods. It also shows the individual accuracy (i.e., user's and producer's accuracy) of the SGD and PGD classes. The overall accuracy has been found to range from 84.50% to 89.75%. The highest overall accuracy (i.e. 89.75%) has been obtained for the glacier terrain map (M1) derived from the dataset IS 1 and the MLC. This clearly justifies the utility of contrast enhancement proposed in this study. The user's and producer's accuracies of SGD have been found to be 91.40% and 92.10% respectively and for

Table 5.5: Overall accuracy and individual (user's and producer's accuracies) accuracies of supraglacial and periglacial debris for four thematic maps obtained from two classification schemes from two image sets. UA =User's Accuracy, and PA= Producer's Accuracy.

Thematic map	Image set used	Classification method	Overall accuracy (%)	Supraglacial debris		Periglacial debris	
				UA (%)	PA (%)	UA (%)	PA (%)
M1	IS 1	MLC	89.75	91.40	92.10	91.25	92.23
M2	IS 2	MLC	84.50	81.64	80.66	83.78	82.32
M3	IS 1	Hybrid classification	86.65	85.50	85.50	89.63	90.10
M4	IS 2	Hybrid Classification	84.89	83.12	84.76	89.63	90.10

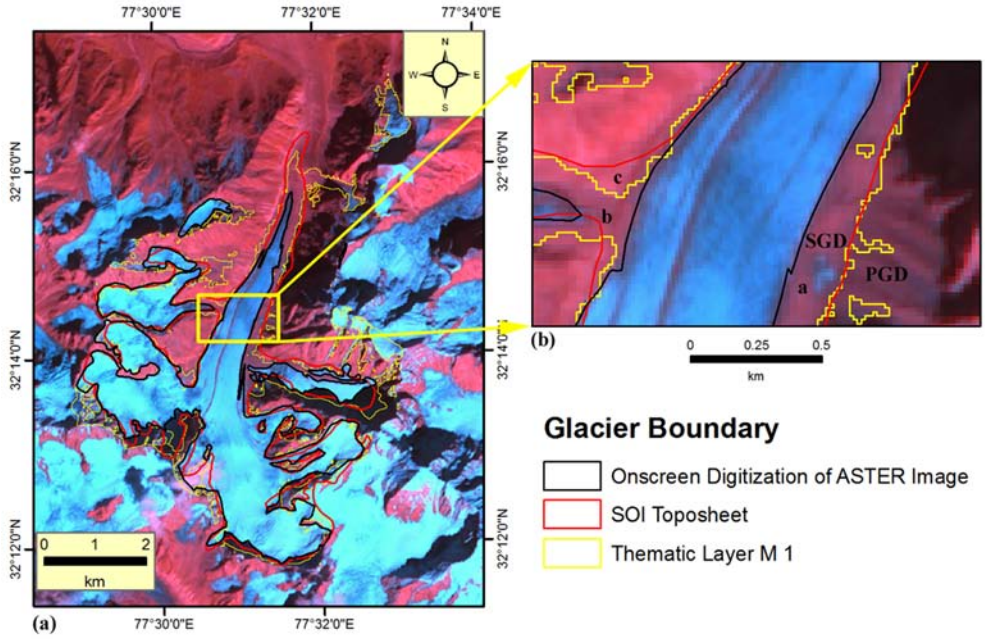

Figure 5.7: Comparison of the glacier boundary derived from the thematic map M1 (yellow outlines) with the visually interpreted boundary from ASTER image (black outlines) and visually interpreted boundary from toposheet (red outline). (a) Boundaries overlaid on the ASTER (R=4, G=3, and B=2) image of the area. (b) Detailed view of the boundaries in a part of the ablation area of the glacier. Regions marked as ‘a’, ‘b’ and ‘c’ show how the use of integrated thermal and optical data is able to resolve ambiguity between boundaries of supraglacial and periglacial debris.

the PGD the user's and producer's accuracies have been found to be 91.25% and 92.23% respectively. These accuracy values are above the acceptable value of 85% as suggested in the USGS classification scheme. Thus, the dataset IS1 comprising of two transformed bands and one thermal image has been able to accurately separate SGD and PGD as well as map the glacial terrain classes using MLC classification more accurately (Table 5.5).

The extent of cloud cover have been visually analysed for all the classified images. It was observed that cloud has been classified more accurately with IS 1. Near the junction of cloud and snow, the snow has been properly classified. Therefore, it can be said that the transformed bands may be more useful for classification of cloud in respect to ASTER images.

Hybrid classification also produces the terrain maps with higher overall accuracy (86.65%) when IS1 is used (M3). Accuracies of SGD and PGD classes have also been found within the acceptable value i.e. 85%. In the eastern side of the glacier, it has been observed that the temperature information is not sufficient enough for delineating supraglacial part from the non-supraglacial part of the terrain using KNC. Other morphometric parameters (i.e. aspect and elevation) have been incorporated to correctly identify the SGD. The most significant benefit of using hybrid classification is that it does not require much post-processing as the knowledge about the terrain can be incorporated during the classification process. The major drawback in this technique is that it requires prior knowledge of the terrain and some tedious trial and error method to refine and formulate the parameters to set the rules.

Since, thematic map M1 has been found to have the highest accuracy; it has been post-processed using the shaded DEM of the area. The validation of glacier boundary extracted from this thematic map and the one digitized from the toposheet and the visual interpretation of ASTER FCC has also been performed. The glacier boundary prepared from the visual interpretation of ASTER FCC completely fails at the lower and lateral part of the glacier to give the extent of glacier. The main reason for this is the presence of heavy debris cover in the lower part and in lateral sides (Figure 5.7a).

The boundary extracted from the toposheet matches quite well in the western side with few meters of SGD outside the boundary. The boundary derived from the toposheet and the multispectral classification also matches well in the eastern side of the glacier. The visually interpreted boundary in the eastern part lies behind both the boundaries in many parts

i.e. the toposheet boundary and the boundary from multispectral classification due to the heavy debris cover in this side (Figure 5.7b).

The width of SGD ranges from ~130 m in the ablation area to ~200 m in the lower part near the snout in the eastern side of the glacier whereas in the western side the width of SGD ranges from ~50 m in the ablation area to ~100 m near the snout. The large amount of SGD in the eastern side may be due to the increase in the debris supply and less load carrying capacity of the glacier ice flowing in the eastern part. The other reason may be the occurrence of heavy rockslides (Figure 1d) in the eastern side of the glacier.

The current position of the snout with respect to the one which is mapped using toposheet clearly indicates the recession of the glacier during the last 42 years. The visually interpreted terminus (Figure 5.7a) clearly indicates the limitation of mapping glacier terrain using visual interpretation or the conventional ratio based methods.

The classified glacier terrain map produced from the proposed method is able to map the extent of glacier to the position from where the water channel is visible in the high resolution WorldView-2 panchromatic image thus confirming the utility of this advance method for mapping glacier terrain. The field observations also support the fact that the lower portion is completely covered with the SGD.

5.6 Summary and Conclusion

In this chapter, Chhota-Shigri glacier has been mapped using two methods. The efficacy of MLC and Hybrid classification has tested for mapping the debris covered part of the glacier. Both methods produced maps with accuracy above the acceptable limits. Based on the results of this study following major conclusions may be derived:

1. The thermal information of the debris may vary within different parts of the glacier which can obscure the delineation of the glacier boundary. Therefore, careful examination of the existing temperature difference between the SGD, PGD and the valley rocks may be required to correctly map the SGD and PGD distribution.

2. The band transformation leads to an increase in the separability between the glacier cover classes and non-glacier class, like cloud, thereby increasing the accuracy of the thematic maps.

3. Based on the inputs required and the time required during classification, it can be concluded that although the use of MLC is much easier than the hybrid classification, the latter does not require post-processing of the output maps since the user knowledge about the classes are inherently taken care of during the classification.

Finally, it is felt that the availability of a high resolution DEM and TIR data may further improve the quality of the results with hybrid classification. The eastern side of the glacier show significantly high amount of debris cover which could affect the health of this glacier. More debris is brought in everyday in this glacier by different tributary glaciers and the rockfall. This may lead to complete debris cover over this glacier through time. The snout of the glacier is also receding which indicates poor health of the glacier. Thus, long term monitoring of this glacier is required to further investigate the effect of climate change on this glacier.

CHAPTER 6
LANDFORMS OF CHHOTA-SHIGRI GLACIER

6.1 Introduction

Landforms and their development in an area give an insight about the key geomorphic activities of that region. In glacier environment, landforms can give an idea about the nature of the glacier like retreat, advancement, surging, etc. Additionally, they can render information about the health of the glacier. Landform studies and mapping dates back to early geological research (Close,1867; Smith *et al.*, 2006), as can be seen from a number of studies in the 1960s and 1970s (Rose and Letzer, 1975; Prest *et al.*, 1968; Punkari, 1982; Smith *et al.*, 2006). Typically, in the past, contours and hill-shading have been used to depict glacial landforms (Rose and Letzer, 1975). A few studies on mapping landforms based upon topographic base maps have also been reported (Close, 1867; Charlesworth, 1928, Chaujar, 1987, 1991, 1992; Rose and Letzer, 1977, Dhobal *et al.*, 1991, 1995). With the increased availability of remote sensing data, mapping of landforms is now being carried out done generally by aerial photography (Prest *et al.*, 1968), satellite imagery (Punkari, 1982) and the application of digital elevation models (DEMs) (Clark and Meehan, 2001).

This chapter describes the various landforms present in the study area. First, a brief review of various landform studies conducted in this glacier by previous workers is presented. Then the processes which shape glacial landforms have been described. This is followed by a short description of the various landforms observed in the Chhota-Shigri glacier. The definitions and description of landforms and glacial process presented in the

sections 6.3 and 6.4 are based on the studies of Goudie (2004); Bennett and Glasser (2009) and Singh *et al.* (2011). The description and identification of various landforms is based on the observations made during the field visits, and analysis and interpretation of high resolution satellite images and DEM of the area. Based on these observed landforms and the satellite image interpretation, a geomorphological map at large scale has also been prepared for the glacier watershed.

6.2 Previous Landform Studies in Chhota-Shigri Glacier

Chaujar (1987) carried out field investigations in the Chhota-Shigri glacier during 1984-85 and described the landforms of the area, particularly mentioning about the presence of cirques, crevasses, moraines, till, etc. Advance and retreat of the Chhota-Shigri glacier was described based on the field observation of landforms (Chaujar, 1991). The presence of various loops of lateral and terminal moraines in the inactive zone of the glacier, i.e. below the snout was also reported. The five distinct loops of moraines were identified. The presence of loops as the terminal ridges indicated that these were the push moraines, having been pushed from the south toward the north. Based on remnants of the loops, observations on the retreat history of the glacier were also made.

Slope variation in the glacier and the glacier valley was examined using SOI toposheets by Dhobal *et al.* (1991) who divided the area into three categories *viz* gentle slope (<15°), moderate slope (15° to 40°) and steep slope (>45°). Different geomorphic process and the mechanism of debris flow were explained based on the slope distribution. It was found that most of the features have developed due to mechanical weathering as a result of intense variation of temperature. Morphology of Chhota-Shigri glacier has been described based on the field based surveys (1987-89) and SOI toposheet (Dhobal *et al.*, 1995). They also prepared a large scale (1:10,000) geomorphological map of the Chhota-Shigri glacier.

A detailed review of the landforms and geomorphological studies has been presented in chapter 2 (section 2.3.1). It is observed that the literature is silent on these types of studies in this glacier for almost two decades. The available literature shows that most of the studies are based on field surveys. Further, due to the precarious terrain

presented by the study area, the earlier studies were only limited to the visual description of the features and some measurements.

6.3 Erosional Processes in Glacial Terrain

The erosional processes in the glacial terrain can be distinguished into two types:
i) erosion by glacier melts

ii) erosion by glacier ice.

i. Glacier melt water erosion

Glacier melt water erosion may occur beneath the ice sheets and glaciers, and may be a mechanical or chemical process. The actions and the effects of glacier melt water depend on several physical and chemical properties of bedrock such as structural weakness or its susceptibility to chemical attack. Melt water erosion also depends on the velocity, turbulence and amount of sediments present in the melt discharge.

ii. Glacial ice erosion

Glacier erosion involves the processes by which a glacier detaches, picks up and transports rocks and sediments as it moves over the earth's surface. As glacier ice moves towards the terminus, it erodes the bed rock, transports the debris and deposits the same at the terminus.

Two principal mechanisms of sub-glacial erosion are recognized: (a) glacial erosion and, (b) glacial plucking or quarrying. *Glacial abrasion* is the erosion of bed rock by the sliding of debris-entrained ice. *Glacial plucking* or *quarrying* is the process of removal of sediments or block of rocks from the glacier bed.

Glacier abrasion is caused by the sliding of basal debris over the bed rock. As ice slides, it polishes, creates striations and grooves in the bed rock. Clasts (>= 0.01 m) embedded in the glacier erode the bed primarily by scratching, creating striations and grooves, whereas finer material (<= 0.01m) such as silt causes polishing of bedrock surfaces.

Glacial plucking or *glacial quarrying* is the process of removal of larger chunks of rock from the glacial bed. The bedrock beneath the glacier is fractured and crushed and then the material gets entrained into the ice and gets transported. A complex mechanism of

Figure 6.1: Sheet joints in valley wall of Chhota–Shigri glacier formed by glacial quarrying.

Figure 6.2: Rocks entrained (sandwiched) into the ice.

fracture formation operates at the base of glacier surface. Sometimes fracture and cracks are present in the bedrock or they may be produced by the periglacial freeze-thaw weathering. Fractures are also produced by the glacier as they flow. Sometimes due to the unloading of rock surface, rocks expands and fractures parallel to the flow or erosional surface are produced (such as sheet joints in valley wall) (Figure 6.1).

Debris entrainment (Figure 6.2) into the ice is mainly caused by the effect of melting of basal ice and re-freezing of water due to the change in the pressure and temperature condition. It is the process by which bedrock or sediments are detached from the glacier bed and get incorporated into the basal ice.

At the contact of the bedrock and glacial ice, sometimes the basal pressure is increased near obstacles leading to the generation of melt water. The melt water may migrate into the cracks or joints and again re-freeze later. Thus, the rock mass or debris may get entrained into glacial ice.

6.4 Glacial Landforms

6.4.1 Glacial erosion and associated landforms

Erosional work of glaciers is accomplished mainly through two mechanisms namely abrasion and plucking/quarrying. Both abrasion and plucking leave erosion markers or evidences which become visible after ice has disappeared. Based on their scale, the erosional landforms can be divided into small-scale features and large-scale features.

6.4.1.1 Small-scale erosional features

The small scale features may develop as a result of the erosive actions of the glaciers and have been meticulously described by Embleton and King (1975). These include striations, grooves, polished surfaces, chatter marks, lunate fractures, crescentic gouge, crescentic fractures, conchoidal fractures, sichelwannen, potholes, and roches moutonnées. Small scale erosional feature of glacial origin found in the study area are as follows:

i. Striations/Grooves

Striations consist of lines, usually short but very occasionally a meter or more in length, carved into the bedrock by pebbles and cobbles carried at the bottom of a glacier (Figure 6.3). The clarity of their development depends largely on the character of the rock as soft, coarse-grained or brittle rocks do not take markings well and on exposed or easily weathered rocks, the markings are rapidly erased. The larger striations are known as *grooves* (Embleton and King, 1975).

ii. Glacial polish

Glacial polish is the name given to smooth rock surfaces created as glaciers flow over bedrock (Figure 6.4a, b). Rock surfaces which appear smooth and polished to the naked eye are seen to possess innumerable small scratches under the microscope. The degree of polishing depends on the fineness of the abrading material, namely the rock floor (Embleton and King, 1975).

Figure 6.3: Striation in the rock present over the median moraine of Chhota–Shigri glacier.

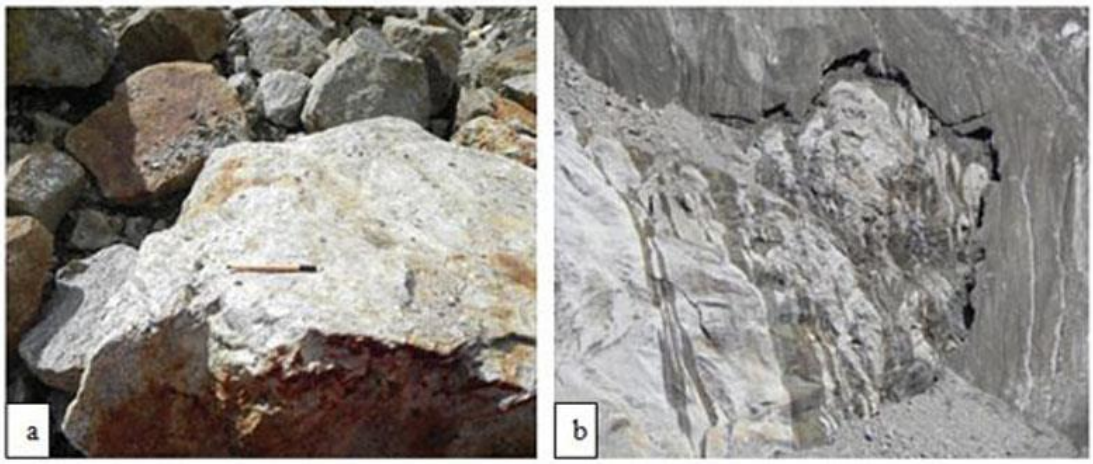

Figure 6.4: Polished surface (a) rock; and (b) valley wall due to glacial ice.

6.4.1.2 Large-scale erosional features

Large-scale landforms developed as a result of glacial erosion include cirques, horns, arêtes, U-shaped valleys, and hanging valleys (Embleton and King, 1975; Singh, 1998; Kale and Gupta, 2001). The large-scale forms of glacial erosion found in the study area are as follows:

i. Cirque

Cirques, found in the mountains and uplands, are deep and semicircular erosional basins with a high headwall, a scooped out floor and a raised still at the lower end (Kale and Gupta, 2001). Cirques expand by erosion. Initially, snow accumulates in small pre-existing depression to forms firn and later into ice. During the periods of high temperature, the melt water wedges out the rock fragments by plucking. These rock fragments are then moved down the depression to form a ridge of deposition at the bottom called protalus rampart. The sum of all processes that operates at this stage is called nivation. As more and more snow accumulates, true glacial ice is formed and its erosive action transforms the nivation cirque to cirque glacier. The erosion is carried out by both headwall recession and basal sliding of the cirque ice. The headwall recedes by frost shattering and rock failure. Cirques can be also clearly identified and marked using satellite imagery (Figure 6.5 (b)). In satellite images, they appear to originate from another adjoining small valley similar to the main glacial valley. Usually, a large amount of debris may be seen at the junction of

the main glacier and the tributary glacier contained in the cirque. A DTM can therefore be more useful in identification of such features due to its unique geometry.

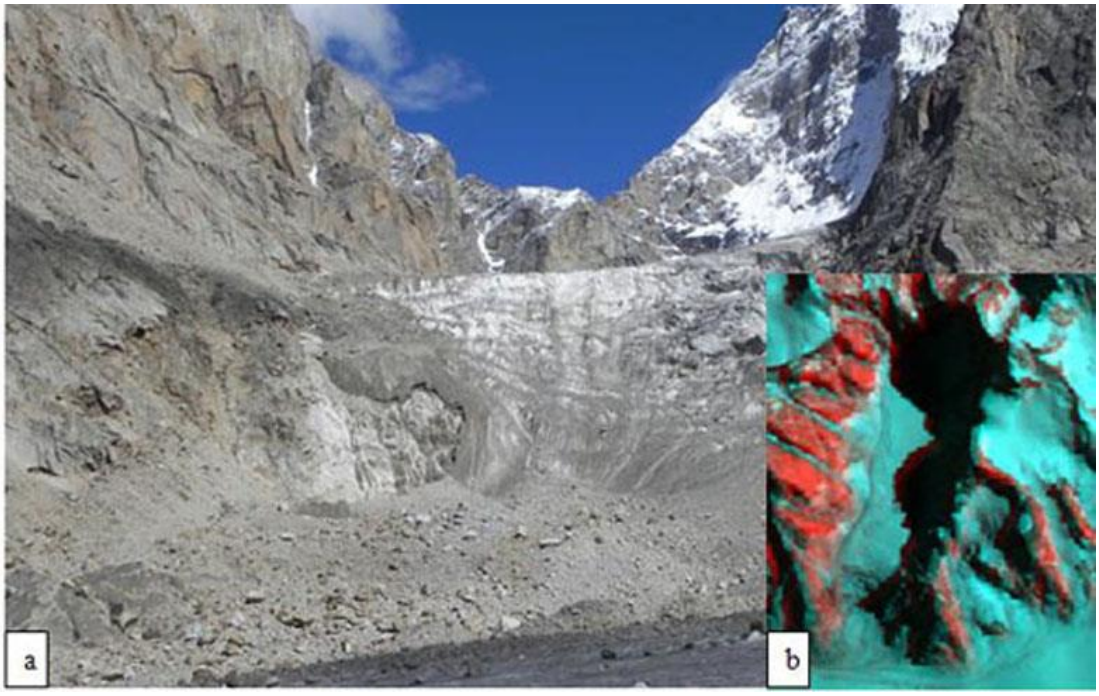

Figure 6.5: Cirque developed in the eastern side of the main glacier (a) Field photograph showing Cirque in the eastern side of the valley; and (b) Inset: ASTER FCC (R=4, B=3 and G=2) showing the same area.

ii. Horns and Arêtes

As mentioned above, cirques increase in dimension by eroding the head and sidewalls. In a mountainous region, neighboring cirques are separated from each other by intervening ridges. As the cirque increases in area, these ridges are progressively eroded to a steep narrow form called *arêtes* (Kale and Gupta, 2001) (Figure 6.6). Several arêtes converge to a peak whose sides stand as headwalls to several cirques. Such pointed peaks are called *horns* (Kale and Gupta, 2001) (Figure 6.6). Almost all high Himalayan peaks are horns. Horns and arêtes can be well demarcated on the DEM and remote sensing images.

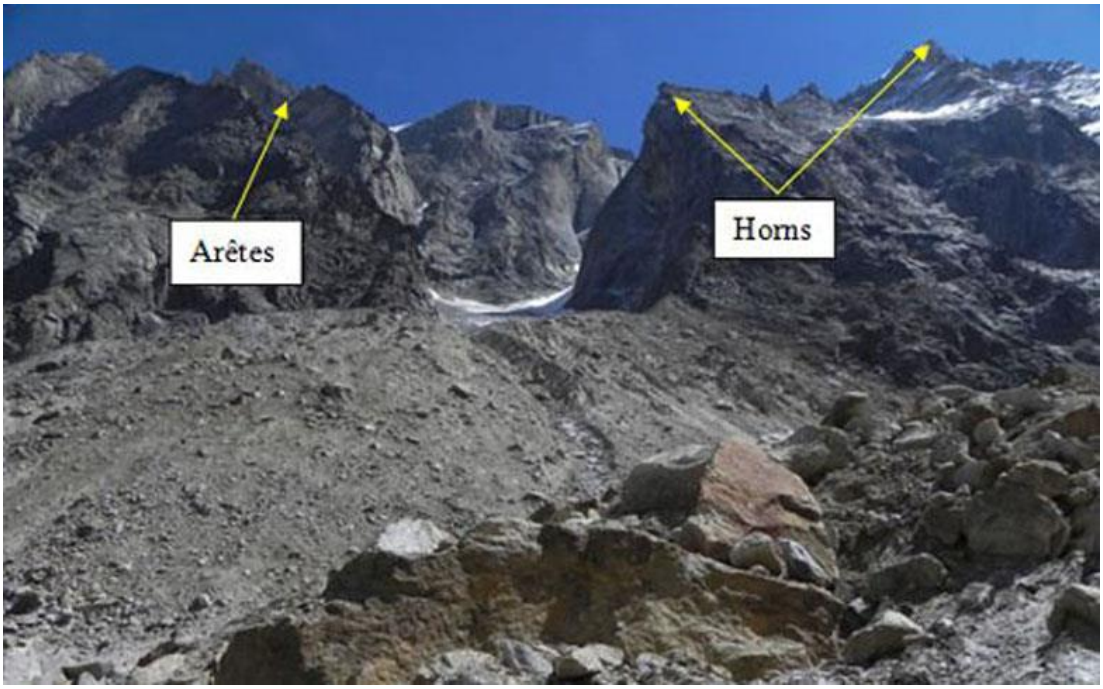

Figure 6.6: Horns and Arêtes in the eastern side of the main glacier valley.

iii. U-Shaped valley

Valleys, which carry or in the past did carry a glacier, are often described as glaciated trough. The cross-section of glacial trough is U-shaped (Figure 6.7) which is characterized by steep valley walls with concave slope and broad and flat valley floor (Singh, 1998).

6.4.2 Glacial deposition and associated landforms

The erosive action of glaciers generates a considerable amount of sediment. The sediments are carried through the ice and is deposited at its end, or at the sides, or underneath between the ice and the bedrock. The general term for glacial sediment is *drift.* Drift may be deposited by ice, by a combination of melt-water and ice or reorganized completely by melt-water. Drift is commonly subdivided into two broad classes: *non-stratified* and *stratified drift*. Non-stratified drift is commonly known as *till* (Figure 6.8) and is essentially ice-deposited. Grain size of the till sediments may range from boulders to clay resulting in a wide textural range. Till is further classified as *lodgement till* and

ablation till. Lodgement till is transported inside the ice (englacial) and then deposited at the base of the ice. It is commonly fine grained and densely packed. *Ablation till* (Figure 6.8) consists of material accumulated either on top of the glacier (supraglacial) or inside the ice and later deposited on the bedrock as the glacial ice disappears by ablation. It is therefore coarser, angular and more loosely packed than the *lodgement till*. Stratified drift is a glacial deposit that has been moved and re-deposited by water even though it originally started as ice-deposited sediment. These are also referred to as glaciofluvial deposits and involvement of water produces sorting, stratification and some rounding of the constituent grains. They are deposited in channels inside the glacier ice, inside local depressions in contact with the glacier ice such as between the rocky valley wall and the side of the glacier, and in a washed out form in front of the glacier snout.

It is also important to recognize the difference between glacial sediments and the forms produced by their deposition. Both non-stratified and stratified drifts produce a variety of depositional forms of different sizes and internal structure (Table 6.1). Glacial and glaciofluvial deposits are two types of the glacial depositional forms. In the study area, mainly the glacial deposits are found which are described here.

Figure 6.7: U-Shaped valley of Chhota–Shigri glacier.

Figure 6.8: Glacial Till (Ablation till) near the Chhota–Shigri glacier.

Table 6.1: Glacial and glaciofluvial deposits (after Kale and Gupta, 2001).

Processes	Environment	Type of deposit	Depositional forms
Glacial	Inside ice	Lodgement till	Ground moraines
		Till (varieties)	Lateral and Medial moraine
		Till (varieties)	Rogen moraine
		Till (some glaciofluvial)	End moraines (varietes)
		Lodgement till	Drumlins
Glaciofluvial	Marginal ice-contact	Deposition by water after reworking of former glacial sediment	Kames (varietes)
	Proglacial (in front of the glacier)		Eskers
			Sandur (outwash plains)

i. Moraines

The term '*moraine*' covers a wide range of depositional features associated with glaciers and normally consists of unstratified material. Moraines may be categorized on the

basis of their position (lateral, medial and end moraines), their state of activity (active-in contact with ice and inactive-not in contact with ice) and their method of formation (ablation and ground moraine) (Embleton and King, 1975). The surface of Chhota-Shigri glacier near its snout and up-to about 1 km upstream is heavily debris covered (Figure 6.9). The debris-cover has a considerable influence on the process of glacier melting and hence estimation is considered important for the determination of glacier runoff and evaluation of the water resources of the area. The temporal variation of debris-cover over the glaciers is correlated with the changing regional climate and hence considered as an important indicator of glacier health and a parameter of the climatic changes in the area (Michalcea *et al.*, 2006; Stokes *et al.*, 2007).

Lateral moraines are generally long, narrow, steep sided parallel ridges of till on either side of a glacier and can vary greatly in character. They may be derived from the valley rocks or deposited as a result of ablation (Figure 6.10). *Median moraines* constitute most conspicuous type of active moraines. They form where two glaciers meet and their lateral moraines come together to form a ridge in the middle of the joint glacier (Figure 6.11). These are made of the valley rocks and, therefore, exhibit similar contrast in the multispectral satellite images (Figure 6.11 (b)). These appear as dark red in the ASTER image FCC (R=4, B=3 and G=2). Median moraines are associated with ice on its both sides.

In chapter 7, the paleo-moraines have been mapped using the remote sensing method. Paleo-lateral moraines are clearly visible in both side of the glacier valley. Additionally, seven distinct morainic loops (Figure 7.6) have also been identified in the inactive zone of the glacier. These loops imply seven different stages of glacial retreat.

Figure 6.9: Supraglacial debris upstream of the Chhota–Shigri glacier snout.

Figure 6.10: Lateral moraine in the ablation zone of the Chhota–Shigri glacier

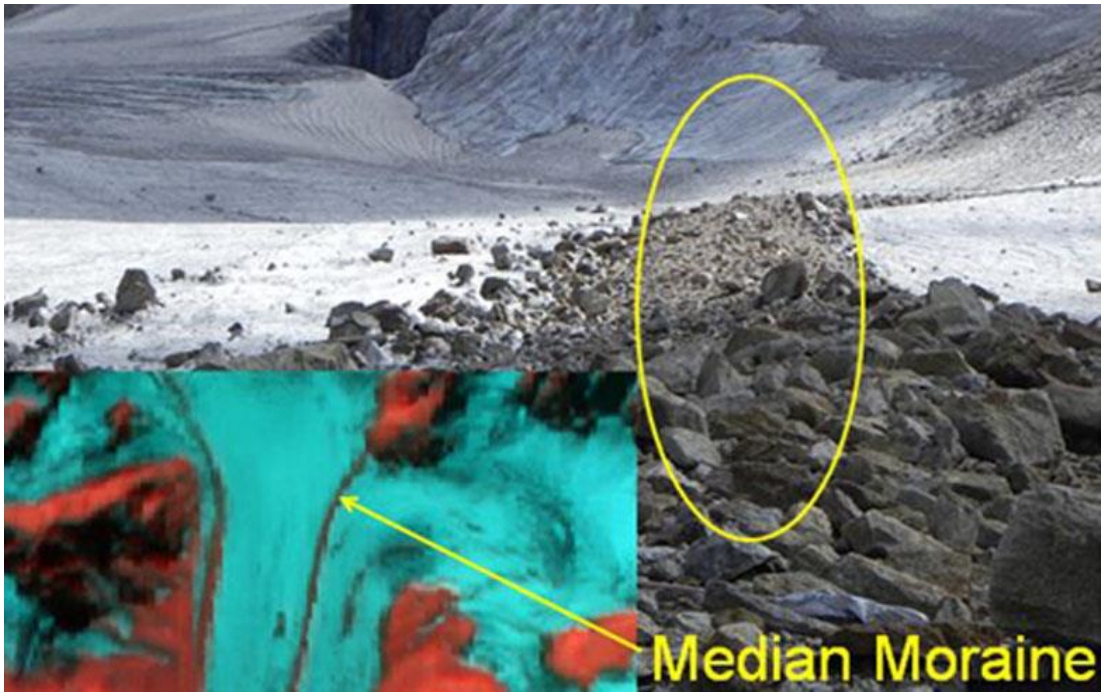

Figure 6.11: Median moraine in the ablation zone of the Chhota–Shigri glacier (a) Field photograph showing median moraine confined between the ice on both sides; and (b) Inset: ASTER FCC (R=4, B=3 and G=2) showing the same median moraine.

6.4.3 Special glacial landforms and features

i. Moulin

Sometime crevasses are also found to be the factors driving the development of peculiar epiglacial forms which reach the inner and deeper glacier sectors. In fact, crevasse-traces produce planes of weakness which allow melt-water to create vertical holes into ice called glacier mills or moulins (Figure 6.12), analogous to the potholes in karst regions. Several moulins have been seen in the Chhota-Shigri glacier which may penetrate deep into the glacier for many tens of meters; they in fact appear to form the most important way for the glacier surface melt-water to reach the bed or for the internal drainage network.

ii. Supraglacial melt channels

Several melt-water channels are prominently visible on the upper ablation zone, and these may converge into the crevasses or the moulins. Glacier surface ice melts in day-time

due to heating of the snow and ice present. If a slope is found, melt-water drains away, forming rills (Figure 6.13). These develop in the ablation areas like a surface stream network owing to the low primary permeability of glacier ice.

Figure 6.12: Moulin in the lower ablation zone.

Figure 6.13: Supraglacial melt channels in ablation zone of Chhota-Shigri glacier.

iii. Cryconite holes and dirt cone

Sometimes, small depressions in the ice surface barely a few centimetres deep are formed that riddle the ice giving it a honeycombed appearance. Clusters of small pebbles and/or dust may be found at the bottom of the holes. The dark patches absorb solar radiation leading to snow/ice melting creating a cryoconite hole (Figure 6.14).

When the fine debris collected in a hollow by surface stream becomes thicker than a certain critical value, differential ablation tends to remove more ice from surrounding areas than from below the debris layer, producing an upstanding dirt-mound. It is called *dirt cone*, and is formed by a relatively thin veneer of debris, almost sand, covering a cone of ice (Figure 6.15).

iv. Glacier table

Isolated large boulders are brought over the glacier surface by the sliding of valley wall or glacier ice. These rocks are sometime even decimeters thick and protect the ice below from melting and as a result it tends to be perched on the top of a pedestal of ice. These are known as *glacier tables* (Figure 6.16).

v. Crevasses

Crevasses are cracks of variable width on the surface of glacial ice and are manifestations of tensile stresses caused due to glacier movement. The effect of local tension is seen in the alignment of crevasses. Therefore, these may be categorized into transverse, longitudinal, radial and marginal types. Near the snout, crevasses are radial as ice spreads out. Along the margins, crevasses are at high angle to the valley walls. These are described as chevron or en-echelon crevasses. Where the flow is extending in character, transverse crevasses develop across the surface of the glacier. Crevasses of all types can be very well mapped using satellite images (Figure 6.17). On satellite images, these are seen as elongated dark linear features mainly in the middle of bright glacial ice. These features can be seen parallel or perpendicular to the glacial flow direction depending upon their type. They are mainly present where the glacier ice bends. In Chhota–Shigri glacier, transverse crevasses have been frequently seen in the ablation zone. They appear to indicate bed-rock control in their formation.

Figure 6.14: Cryoconite holes in the ablation zone of Chhota–Shigri glacier.

Figure 6.15: Small dirt cone formed in the ablation zone of Chhota–Shigri glacier.

Figure 6.16: Glacier table in the ablation zone of Chhota–Shigri glacier.

Figure 6.17: Crevasses present in the accumulation zone as seen on the (a) field photograph; (b) Inset: WorldView-2 multispectral FCC (R=8, G=5 and B=1).

6.4.4 Other feature/non-glacial features.

Some features found in the glacier watershed are not associated with the glacial activity. They are formed due to the activities of other geomorphic agents such as water. Rills (Figures 6.18) have been seen in the slopes of lateral moraines and paleo-lateral moraines. Rills are linear features and can be identified by the textural changes over the rocky part in the satellite images. These are mainly found associated with the debris deposited near the valley wall. The synoptic nature of satellite images may be very helpful in identification of these features. These are formed due to the seasonal water channels which have developed in the area during the rainy season or when the seasonal snow melts in the start of ablation season.

Freeze-thaw weathering of the valley rock and highly unstable slope causes rock-fall (Figure 6.19). These rock-falls are common in the valley mostly in the eastern side segregated around ablation zone of the glacier. Rock-fall also contributes to the debris cover over the glacier. Eastern margin of glacier valley in the inactive zone is also filled with the debris cone. The presence of these debris cones indicates that this area is highly unstable. Debris in this area may have been deposited by the landslide or the mass wasting or the seasonal water flow.

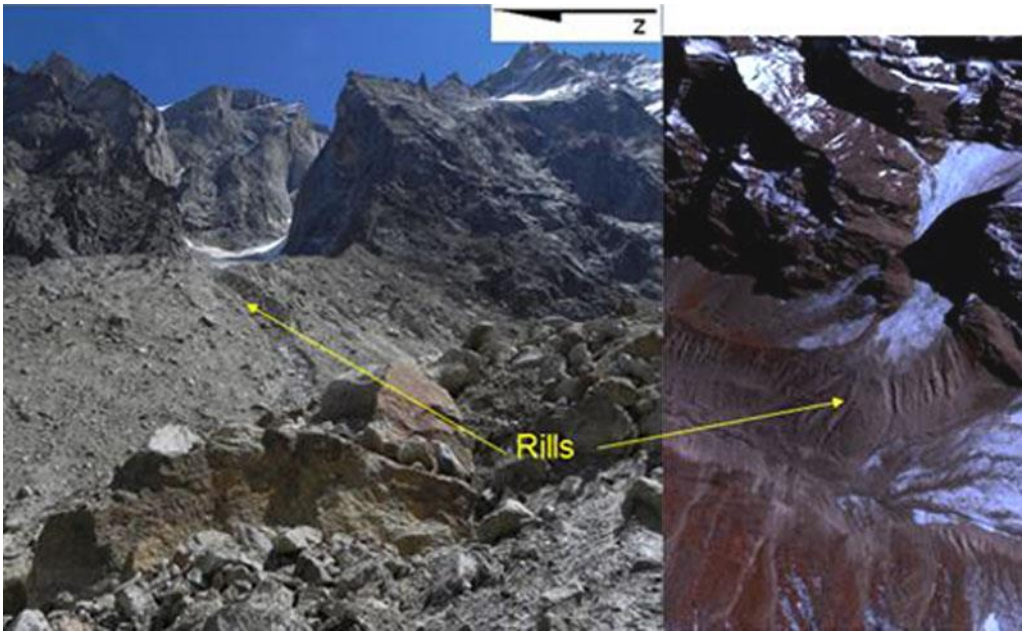

Figure 6.18: Rills present near the terminus of the glacier as seen on the (a) field photograph; (b) Inset: WorldView-2 multispectral FCC (R=8, G=5 and B=3).

Figure 6.19: Sudden rockfall as seen in the eastern side of the glacial valley.

6.5 Large Scale Geomorphological Mapping

Detailed study and analysis of the glacial geomorphology can provide vital clues regarding evolutionary history of the glacier. Different stages of glacial retreat or advancement can be determined by studying various glacial features. Conventional field surveys have long been used for detailed mapping of the glacial landforms. However, advancement in the remote sensing sensors onboard a number of satellites (e.g. GeoEye-1, Quickbird, Cartosat-1, IRS-P6 LISS-IV, Terra ASTER etc.) together with other geospatial tools (e.g., GoogleEarth and Bhuvan) have led to a new era in mapping of glacial features (Butler and Walsh, 1998; Bishop *et al.*, 1998; Brown *et al.*, 1998; Phillip and Sah, 2004). In recent years, it has been seen that remote sensing and geographic information system (GIS) has enhanced and broadened the opportunities in geomorphological mapping. Integrating remote sensing with field studies offer a robust synergistic model to explore research questions associated with landscape mapping (Vitek *et al.*, 1996; Walsh *et al.*, 1998; Butler and Walsh, 1998; Bishop *et al.*, 1998; Brown *et al.*, 1998; Allen, 1998; Boelhouwers and Meiklejohn, 2002; Phillip and Sah, 2004).

In the present study, high and medium resolution satellite images have been used to minimize the field work required in mapping of glacial landforms. The synoptic nature of remote sensing provides detailed view of landforms. DTM prepared by draping WorldView-2 panchromatic satellite image over a ASTER DEM also adds to the visualization of landforms in three dimensions (3D) (Figure 6.20). DTM is also helpful in delineation of the paleo-lateral moraines of the glacier.

Table 6.2: Details of data and mapping methods used for geomorphological mapping.

Sl. no.	Data used	Utility	Mapping method
1.	SOI Toposheet (Surveyed in Oct. 1961)	Glacier boundary	Onscreen digitization
1.	ASTER image	Glacier boundary mapping; terrain classification	Visual image interpretation; classification of glacier terrain
2.	WorldView-2	Large and medium scale features (e.g. crevasses, debris cone, etc.); Paleo morainic loops mapping	Onscreen digitization
3.	DEM	Glacier boundary mapping; Paleo-morainic loops mapping	Image processing and analysis of different derivative products
4.	Field data	Validation and small scale feature mapping.	GCPs processed in GIS environment

Details of the data used along with its purpose and mapping method are given in Table 6.2. The boundary of the glacier has been first traced using georeferenced SOI toposheet. Then the traced outline has been modified further using visual interpretation of the ASTER FCC (R=4, G=3 and B=2) and DTM. . It is observed at several places that the glacier extent has shrunk and the snout has retreated from its position in 1961. After that, GPS points showing locations of small the glacial landforms which have been collected during two field visits to the Chhota-Shigri glacier (during September 2011 and 2012)have been overlaid in the watershed boundary. Then the orthorectified satellite images from ASTER and WorldView-2 have been used to transpose exact position and orientation of

various landforms onto a large scale map. The orthorectified images have been used in this process as they provide geographical positions and measurements as existing on the ground surface Image interpretation elements, namely, like shape, size, association etc. have been used to infer these classes on the image. The extents of the landforms have been redefined and verified using DTM of the area which presents the geomorphometry of the features in three dimensions. Finally, a large scale geomorphology map (1:10,000) of the Chhota-Shigri watershed has been prepared (Figure 6.21).

Earlier, Dhobal *et al.*, (1995) also prepared a very detailed geomorphological map containing many small scale features, based on field surveys. But in the present case, the map has been prepared by precise onscreen digitization at a scale larger than 1:2500 over the high resolution orthorectified WorldView-2 image and the output has been taken at a scale of 1:10000. Therefore, it presents a very accurate representation of the glacial features. However, no quantitative assessment of the accuracy has been done for this map as it contains several features and has been digitized by integrating data from varied sources such as SOI toposheet, ASTER and WorldView-2 images.

It, however, presents updated information about the area of the glacier and many debris covered parts. The map shows an increase in the debris cover and also shrinking of the area of the glacier. The new information depicted in this map may be effectively used to assess the health of this glacier which is in bad shape. Although, it does not include some of the features described by Dhobal *et al.*, (1995) especially small scale such as Moulin, it highlights the different types of debris deposits and other important features describing its recessional history.

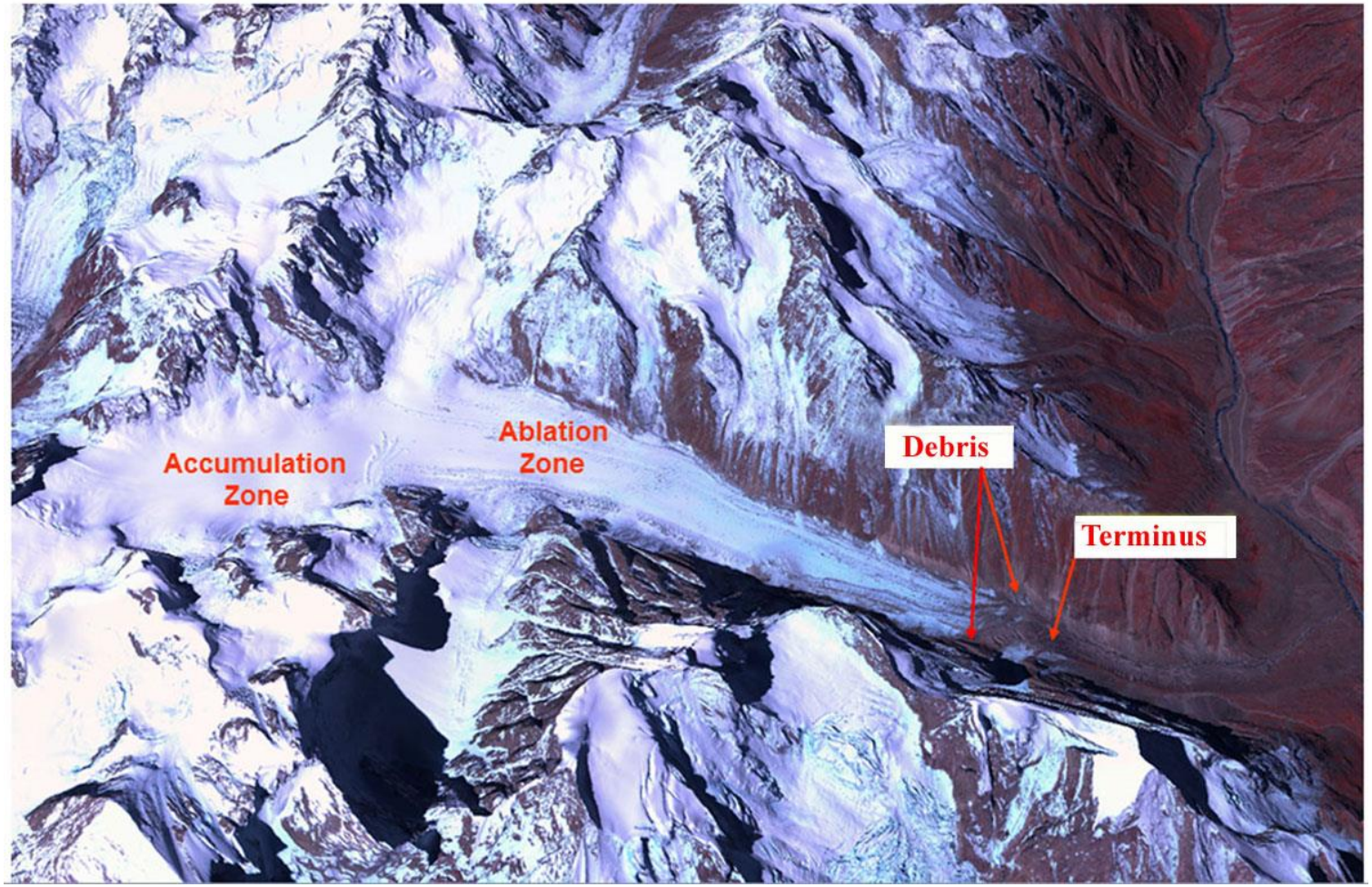

Figure 6.20: A DTM of the Chhota-Shigri glacier produced by draping WorldView-2 image over the ASTER DEM showing accumulation zone, ablation zone, debris and terminus of the glacier.

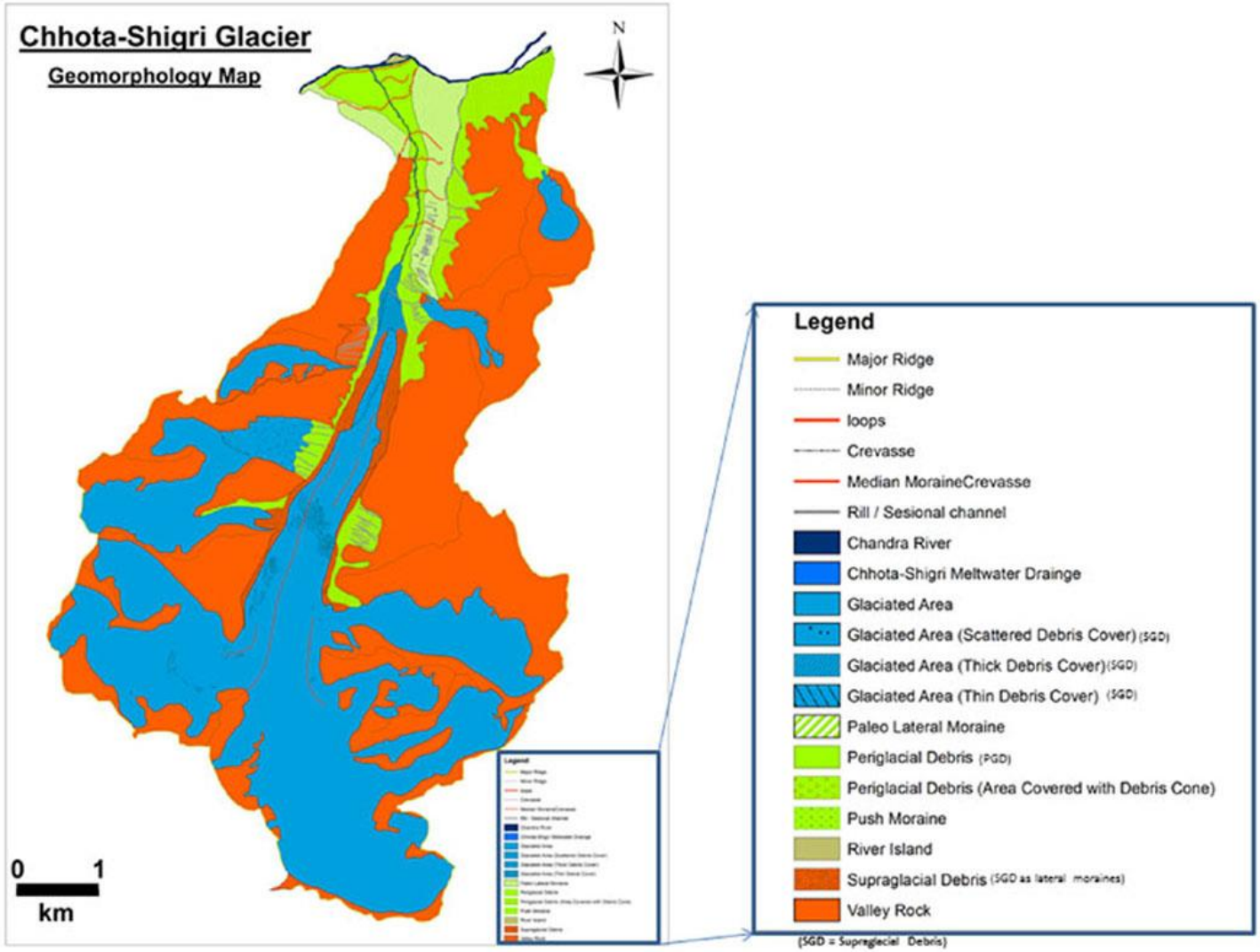

Figure: 6.21: Large scale geomorphological map (1:10,000) of the Chhota-Shigri glacier watershed.

CHAPTER 7
MAPPING OF PALEO-MORANIC DEPOSITS AND GLACIAL RETREAT

7.1 Introduction

Moraines (typically *lateral* and *terminal moraines*) and snout positions have long been used to as markers for chronological analysis of glacial action, *i.e.*, to study glacial advance and retreat (Sharma and Owen, 1996; Kulkarni *et al.,* 2006). Several stages of glaciation of the Chhota-Shigri glacier can be identified on the basis of well-preserved terminal moraine data in the field (Chaujar, 1991,1992). Further, field surveyed maps and repetitive satellite data can reveal variations in glacial snout positions with time.

In this study, paleo-morainic loops of the Chhota-Shigri glacier have been mapped using high resolution satellite images and DEM. Further, changes in glacial snout positions have been located based on repetitive satellite images and past field records. These aspects and salient results are described in this chapter.

7.2 Mapping of Paleo-Morainic Loops

Chaujar (1991), based on field data, was the first to map the paleo-morainic loops of Chhota-Shigri glacier and presented the proof of glacier retreat through time. The five stages of glacier retreat were described based on the field evidences of morphology and textural material in moraines (Figure 7.1). However, as remote sensing data provides a synoptic view, this type of interpretation can be better accomplished based on high-

resolution satellite image data and satellite derived digital elevation model. This is described in the following paragraphs.

7.2.1 Methodology adopted

The mapping of morainic loops in the inactive zone of glacier valley has been done by remote sensing method using DEM, high resolution panchromatic and multispectral images and thermal images. An overall methodology adopted is shown in the Figure 7.2. Thermal IR images have been analyzed to check for the composition variation in the inactive zone of the glacier valley; however, these images have failed to reveal any reliable thermal variation that could indicate variation in material composition of different morainic loops.

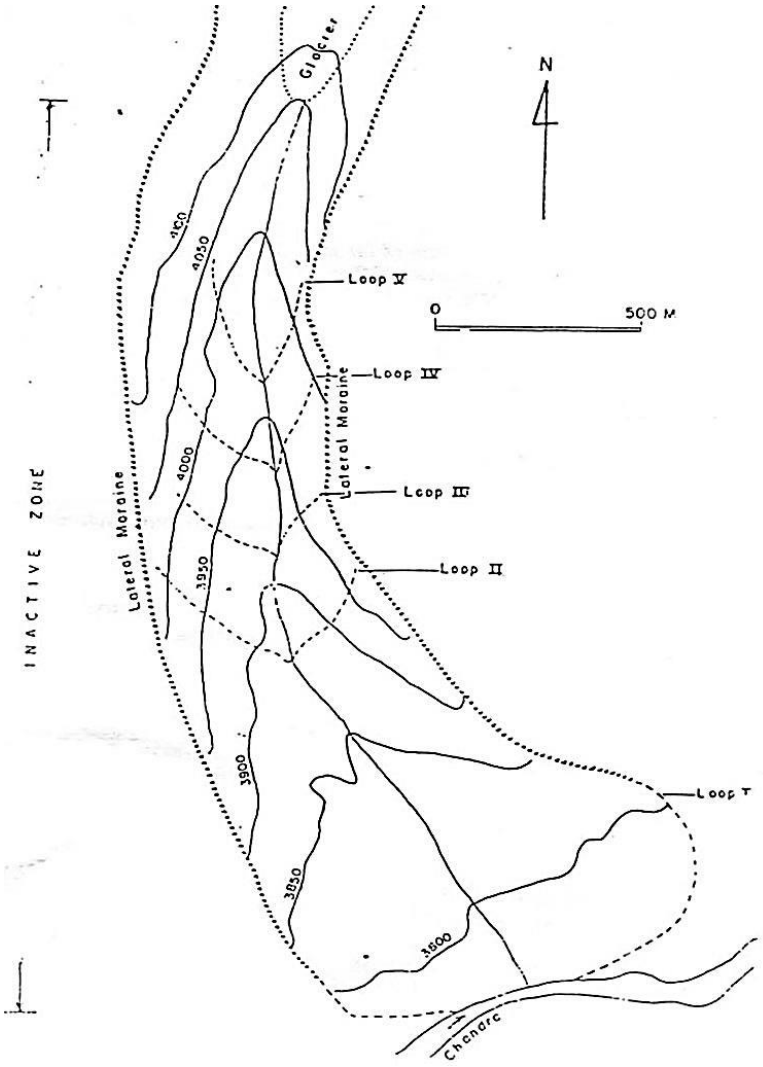

Figure 7.1: Field morainic loops (Mapped by Chaujar, 1991).

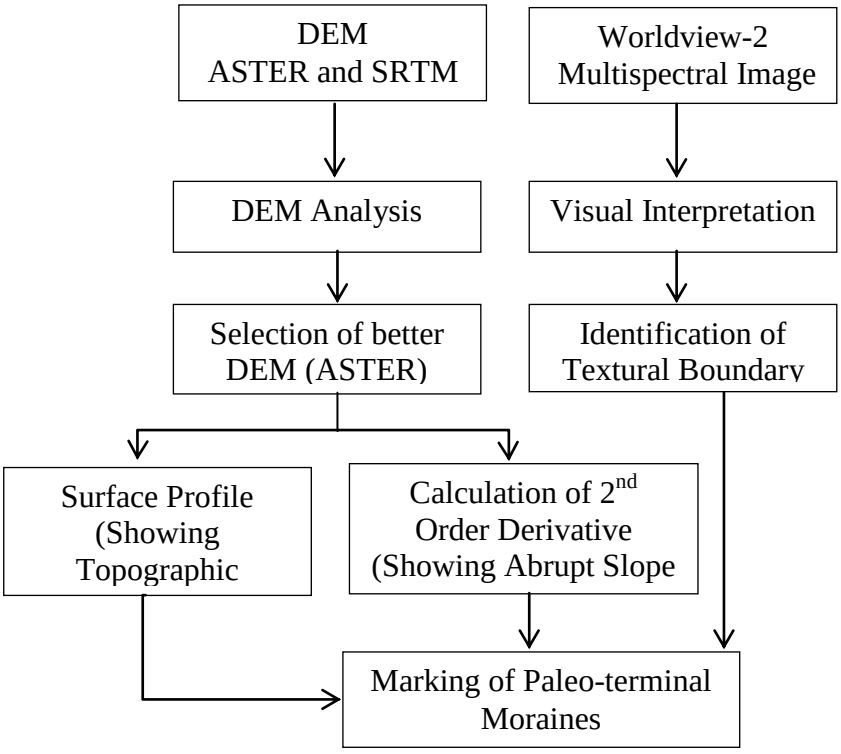

Figure 7.2: Flowchart of overall methodology for mapping paleo-morainic loops.

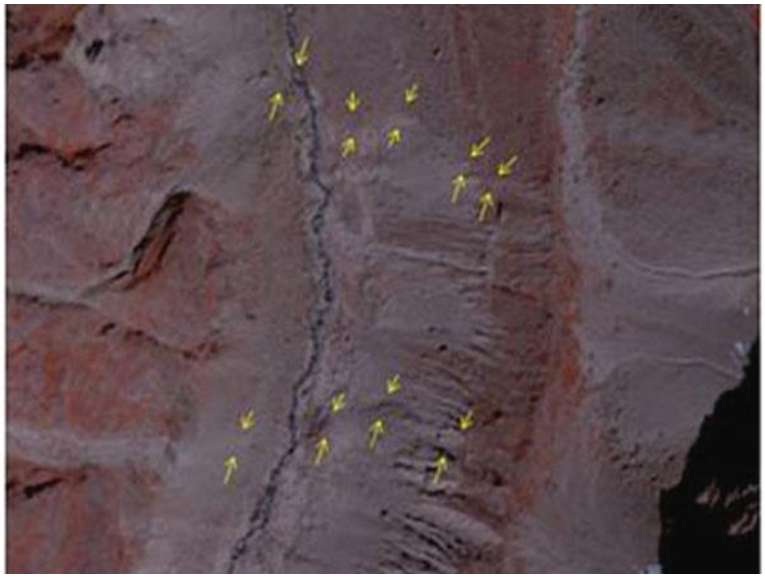

Figure 7.3: Textural difference as seen in the WorldView-2. Note the yellow arrow points to the observed textural difference in the inactive zone.

Later, high resolution images (panchromatic and multispectral) have been analyzed for textural variation. It has been observed that the textural differences do exist indicating different morainic loops (Figure 7.3). However, these morainic loops may not be mapped continuously based on only textural changes for the simple reason that subsequent fluvioglacial activity has modified these loops over time.

Further, with a view to study topographic changes in terms of gradients and rate of change of gradient that could possibly help detect the location of different morainic loops, the DEMs derived from SRTM and ASTER data have been analyzed. The SRTM DEM being at 90 m ground resolution is rather inferior for this purpose. Although, the SRTM DEM shows topographic breaks at some points, it is not reliable where the boundaries are thin and broken. Subsequently, the ASTER DEM of 2011 created from the stereo images of 30th October 2011 has been analyzed. This DEM has 30 m ground resolution and is much better. A topographic profile along line A-B has been created (Figure 7.4). It clearly shows the topographic breaks at several places in the inactive zone of the glacier valley. The location of surface profile A-B has been shown in the Figure 7.5. To demarcate changes in topography (inflexion points), second-order derivative (rate of change of slope) has been generated from the ASTER DEM to provide valuable insights (Figure 7.5). This image shows the abrupt change of slope in the inactive zone of the glacier. The change of slope is observed at the point where the remains or paleo-terminal moraines terminate and a flat surface is observed. Finally, in ArcGIS, lines are drawn to mark the position of the paleo-terminal moraines by connecting all the observed breaks in different images.

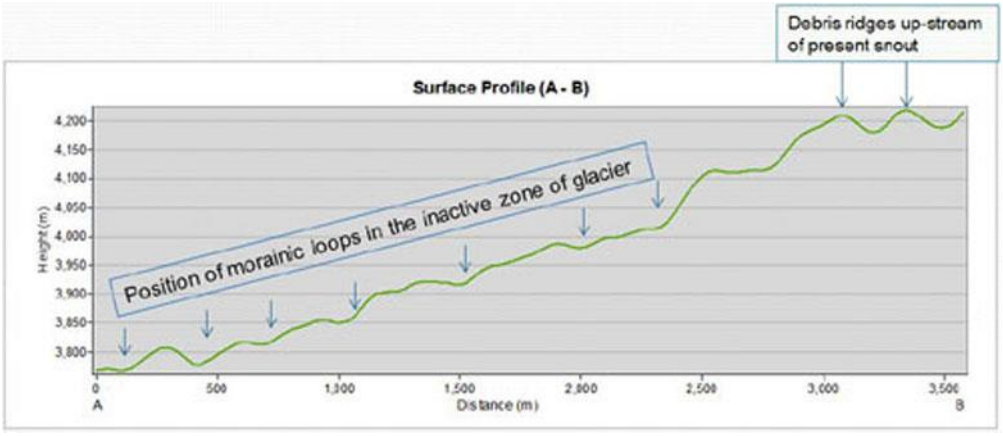

Figure 7.4: Observed break in topography as seen in the ASTER DEM surface profile.

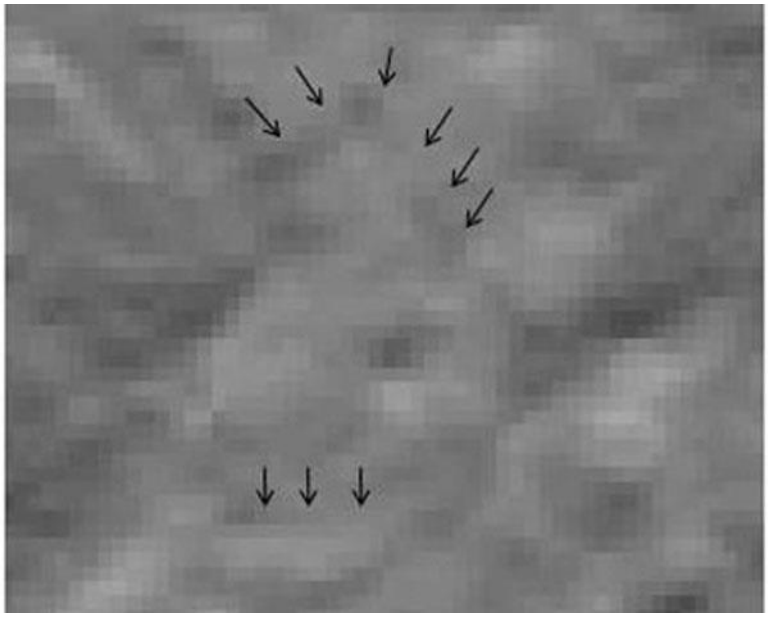

Figure 7.5: Textural difference as seen in the 2nd order derivative of ASTER DEM. Note the arrows point to the observed change of slope in the inactive zone.

7.2.2 Results and Discussion

Based on the above data interpretation, seven distinct morainic loops (Figure 7.6) have been identified in the inactive zone of glacier. These loops imply seven different stages of glacial retreat. The results appear to be quite consistent with the map prepared by Chaujar (1991) based on field surveys that indicated the presence of five morainic loops in the area. Four morainic loops mapped from remote sensing method appear to more or less coincide with these results. It appears that the other three loops may also be better mapped from remote sensing and DEM for obvious reasons of difficulty in field delineation due to undulating terrain etc.

Based on the position of the oldest morainic loop, it can be said that the glacier, at some point of time, might be flowing upto the current extent of the Chandra River. In the field, two distinct paleo-lateral moraines are visible. These moraines are about 100 m high from the vacated glacier bed. A 3D view of the lower portion of the glacier clearly shows the two paleo-lateral moraines (Figure 7.7). The current position of the Chandra River is also marked in the Figure 7.7. Besides the above, this method of integrated interpretation of high resolution satellite images and ASTER DEM has enabled delineation of two debris

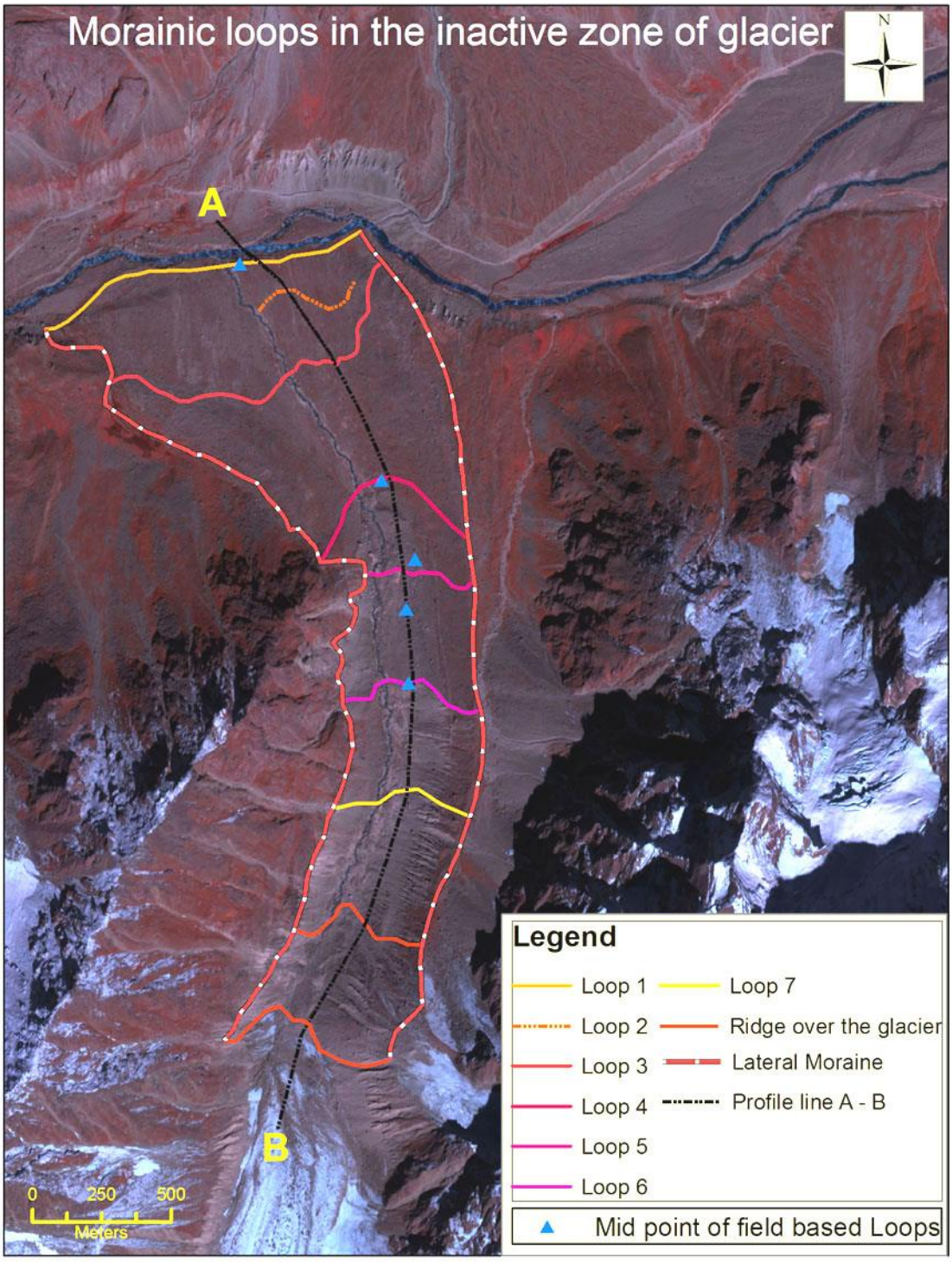

Figure 7.6: Morainic loops and the lateral moraines (based on WorldView-2 image and ASTER DEM).

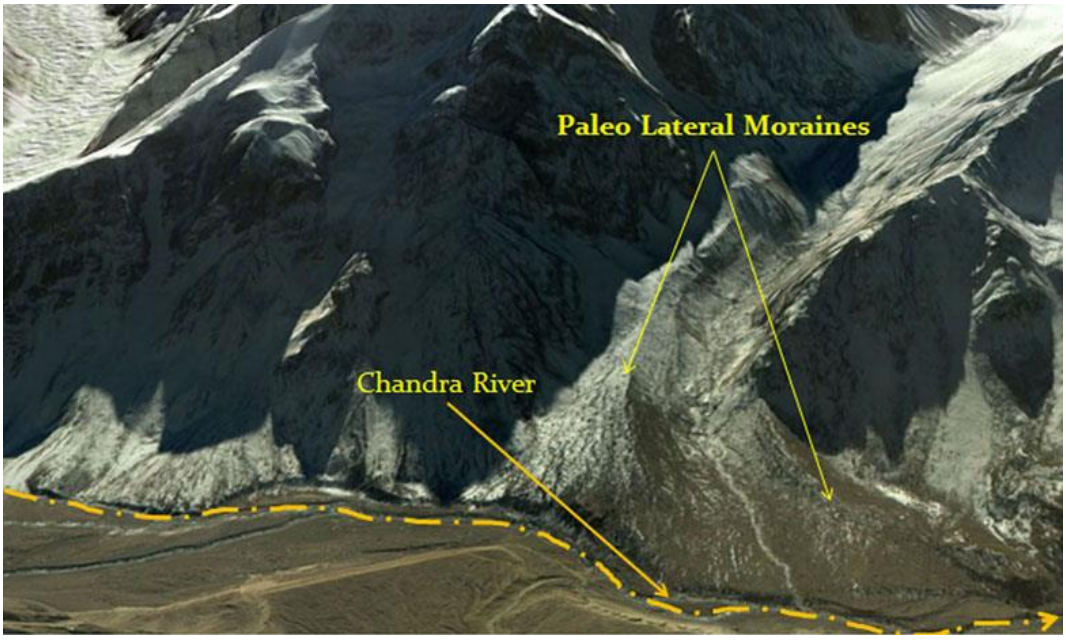

Figure 7.7: 3D view of paleo-lateral moraines in the inactive zone of the glacier and the current extent of Chandra River.

Figure 7.8: Debris ridge upstream of snout.

ridges existing upstream of the present snout (Figure 7.6). These ridges can very well be seen in the field also (Figure 7.8). It seems that these debris ridges have developed due to excessive mass wasting along the glacier and want of adequate disposal of debris due to lack of proper load carrying capacity by the glacier.

Presence of the paleo-morainic loops in the inactive zone of the glacier suggests past recession of the glacier. Remote sensing data has provided a valuable insight into the presence and location of these loops thereby signifying the use of remote sensing in such types of studies. Further, to map the recession of the glacier in the recent years, SOI toposheet, ASTER VNIR image and WorldView-2 panchromatic image have been used. Results of which have been discussed in the next section.

7.3 Mapping Snout Position (1961-2006)

In this study, ASTER images (2002-2006) and WorldView-2 image (2010) have been used for the mapping of snout positions (Figure 7.8). Often, it is found that the snout is not clearly visible in the satellite images as the lower part of the glacier is heavily debris covered. Therefore, to map the position of snout, the point where-from the water channel appears to start in the image has been considered. The high resolution WorldView-2 panchromatic image gives a clear view. On this image, the 2010 position of snout has been well marked. However, in the moderate resolution images of ASTER, the snout positions are somewhat difficult to mark. All the images used for mapping the snout position have been first orthorectified. This process removes the biasness or error that could be induced by the image geometry. The orthorectified image also gives the true position and location of any ground object, because it is an accurate representation of the earth's surface, having been adjusted for topographic relief, camera lens distortion, and sensor tilt.

Based on the position of snout marked from the visual interpretation of ASTER images (Table 3.1), the shift in the position of snout from 2002-2006 has been found to be 56 m giving an average recession of 14 my^{-1}. The position of snout measured from WorldView-2 image is very clear due to the high spatial resolution of the data but it has not been incorporated in the analysis because of the probability of error in comparison of different resolution images. Otherwise, observed snout position from WorldView-2 image

The SOI toposheet at the scale of 1:50000, published in 1966 and prepared from aerial survey of 1961, has been georeferenced and the glacier area has been digitized from it using ArcGIS. Thus, the snout position of 1961 is also available. The 2006 snout and 1961 snout has been compared and shift in the position of snout from 1961-2006 has been found to be 540 m giving an average recession of 12 my^{-1}. For comparison purposes, the average rate of retreat as recorded by other workers for the Chhota-Shigri glacier is given in Table 7.1.

Table 7.1: Relative advance/retreat of snout position of Chhota-Shigri glacier (1962-2006) (revised after Ramanathan, 2011).

Year	**Altitude (m msl)**	**Snout fluctuation (m)**	**Period of Interval considered (years)**		**Advance/ Retreat (my^{-1})**	**Remarks**
1962	4050	-	- -		-	Initial position taken from SOI toposheet *
1984	-	-165.0	1962-84	22	-7.5	Position per SOI Air Survey Map of Chhota-Shigri *
1986	4055.15	-5.2	1984-86	2	-2.6	Co-ordinates fixed by WIHG*
1987	4051.40	+17.5	1986-87	1	+17.5	Co-ordinates fixed by WIHG*
1988	4052.60	-22.1	1987-88	1	-22.1	Co-ordinates fixed by WIHG*
1989	4055.65	-19.0	1988-89	1	-19.0	Co-ordinates fixed by WIHG*
1995		-35.5	1989-95	6	-5.9	Recalculated from WIHG & GSI data *
2003		-800.0	1988-03	15	-53.3	Kulkarni *et al*. (2007)**
2006		-850.0	NA	34	-25.0	Shruti (2008) **
2006		**-56.0**	**2002-06**	**4**	**-14.0**	**This work*** **
2006		**-540.0**	**1961-06**	**45**	**-12.0**	**This work**** **

* field based; ** remote sensing based; ***based on R.S. data analysis in this work; ****based on snout position of 2006 R.S. data and 1961 SOI toposheet

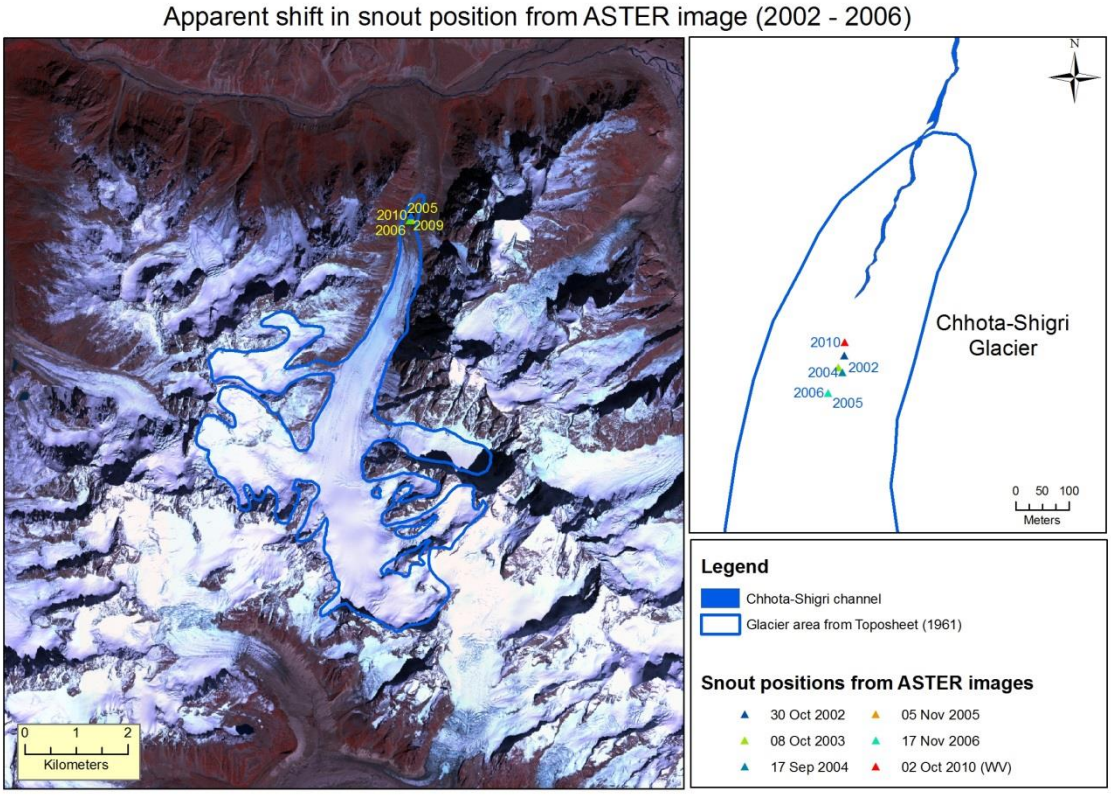

Figure 7.9: Snout positions from ASTER images (2002-2006). Note the snout position from the WorldView-2 image has not been used for the computation of retreat.

From the study, it has been is observed that there is a wide variation in the rate of retreat of Chhota-Shigri glacier as reported by various authors. The reported retreat rate ranges from 2.6 my^{-1} to 53.3 my^{-1}. This large mismatch may be due to various reasons such as:

(1) Use of different methods for snout location: some estimates are based on field methods and some on remote sensing observations, which has led to a mismatch.

(2) Even where only remote sensing methods have been used, the sensor resolution has varied for data of different years, which affects accuracy of locating features. This has led to mismatch.

(3) Even if georeferenced images have been used, if these are not orthorectified, the results may have high probability of error.

(4) There may be some natural variation in rates of retreat over some periods of time.

However, there is a distinct trend that the Chhota-Shigri glacier is retreating and generally, the overall rate of retreat may be in the range of around 5-15 my^{-1}. In this approach of mapping, snout position measurements from same resolution data have been used which removes the uncertainties in the measurements. Further, continued monitoring over long duration is required for a realistic assessment of glacier retreat.

CHAPTER 8

ESTIMATION OF SURFACE ICE VELOCITY USING SUB-PIXEL IMAGE CORRELATION

8.1 Introduction

Glaciers all over the world have been experiencing recession at varying rates (Haeberli *et al.*, 1999; Oerlemans, 2005; Paul *et al.*, 2007; IPCC, 2013). Therefore, the need of generating glacier inventory and dynamics data at global scale cannot be overemphasized. A comprehensive review on the Himalayan glaciers was made by Bolch *et al.* (2012) emphasizing the need of their continued monitoring. Glaciers move, or flow, downhill due to gravity and associated internal deformation of ice. Ice can move as plastic material due to high pressure of thick accumulated ice/snow or due to basal sliding. Measurement of ice flow velocity can help in modeling the glacier dynamics. A glacier's surface ice velocity is a measure of how fast the surface ice is flowing toward the terminus of the glacier. The flow can be faster or slower, depending on how much the glacier is melting. Faster moving glacier brings more ice towards the terminus for melting, which in turn is one of the important factors governing mass balance of the glacier. Another important aspect which is governed by surface velocity is the load carrying capacity of a glacier. The denudational force exerted by the glacier and the transport of generated debris depend on the load carrying capacity. Thus, the surface ice velocity has a high impact on the health and fate of the glacier.

Conventionally, surface ice velocity is measured in the field by monitoring the position of stakes, which are installed by drilling into the glacier ice, by Differential Global

Positioning System or total station surveys. It is, however, very difficult to obtain sufficient velocity data to investigate processes and the stability of glaciers using conventional glaciological techniques (field measurements) due to the frequent loss of stakes and difficulty in handling of measuring instruments at site. Considering the vastness and inaccessible nature of mountain glaciers, and the various difficulties and limitations commonly associated with field glaciological studies, satellite remote sensing technology now offers a highly viable tool for various glaciological studies (Racoviteanu *et al.,* 2008). Details of various techniques used for glacier velocity measurement are listed in Table 8.1.

In this chapter, the surface ice velocity of the Chhota-Shigri glacier has been estimated using optical image correlation method utilizing multitemporal ASTER images from year 2003-2009. COSI-Corr (an add-on module of ENVI), based on the algorithms described by Leprince *et al.,* (2007) and Ayoub *et al.,* (2009), has been used for this study. This software allows precise co-registration, orthorectification and sub-pixel correlation of remote sensing images, all in one package and in a more user friendly-environment. The estimation of velocity largely depends on the precise co-registration and orthorectification of two images being used in the pair. Further, during processing (correlation), the errors from different sources tend to combine and result in relatively higher error in the final result. COSI-Corr includes different filtering algorithms to remove such errors. Precise orthorectification is obtained by applying the optimized model for registration and resampling (Leprince *et al.,* 2007). An iterative unbiased processor that estimates the phase plane in the Fourier domain is also introduced in the COSI-Corr for image registration and correlation (Leprince *et al.,* 2007).

8.2 Mechanism of Ice Flow

The glacier moves downhill due to the action of gravity and sometimes due to the pressure of ice itself. Bennett and Glasser (2009) and Cuffey and Paterson (2010) have described the mechanism of ice flow in detail. Based on their work, mechanism of ice flow is described below in brief. Any glacier can be divided into two zones:

(i) an accumulation zone, where accumulation exceeds ablation

(ii) an ablation zone, where ablation exceeds accumulation.

Table 8.1: Comparison of various techniques for estimation of glacier surface ice velocity.

Sl. No.	Broad category	Sub category	Technique used	Merits	Demerits	Cited reference
A	Field based method	----	Repeated measurement of stakes in the field using DGPS	Accurate up to cm level	Time taking; Difficult due to rugged glacier terrain; Only few point could be collected so do not give overall picture of ice dynamics.	Dobhal *et al.* (1995); Wagnon *et al.* (2007); Azam *et al.* (2012)
	Remote sensing based methods	1. Using SAR data	(i) SAR intensity tracking	Not effected by cloud	Due to oblique viewing angle of SAR images data presents high shadowing and layover in mountainous terrain; High cost of data.	Strozzi *et al.* (2002); Kumar *et al.* (2009); Gray *et al.* (1998); Pritchard *et al.* (2005); Strozzi *et al.* (2008)
			(ii) SAR interferometry	Very accurate ; Not effected by cloud	Due to oblique viewing angle of SAR images data presents high shadowing and layover in mountainous terrain; Fails in high speed glacier due to de-correlation of data; High cost of data; Tandem missions with only a few days between the acquisitions are often required which limits its application	Rao *et al.* (2004); Kumar *et al.* (2009); Fatland and Lingle (1998), Strozzi *et al.* (2002)

		2. Using optical data	(i) Manual Feature tracking		Easily to implement and cost effective; Large time series data available	Effected by cloud and shadow; not very accurate; user dependent	Lucchitta & Ferguson (1986)
			(ii) Correlation of time series data	(a) Normalized cross-correlation	Easily to implement and cost effective	Effected by cloud and shadow; accuracy is dependent on the data resolution but the results are found to be very accurate.	Berthier *et al.* (2003); Bindschadler *et al.* (1996); Copland *et al.* (2009); Kääb, (2002); Rack *et al.* (1999); Skvarca *et al.* (2003)
				(b) Cross-correlation operated in the Fourier domain			Rolstad *et al.* (1997)
				(c) Least squares matching			Kaufmann & Ladstädter (2003)
				(d) Phase correlation			Leprince *et al.* (2008); Quincey and Glasser (2009); Scherler *et al.* (2008)
				(e) Orientation correlation			Haug *et al.* (2010)

The line dividing the two zones is called equilibrium line along which accumulation is balanced by ablation. In the accumulation zone (higher altitude), the snow is added by precipitation and is taken away at the snout and at the ablation zone (lower altitude). This process increases the gradient of the glacier surface. With this increase in the slope of the glacier surface, stress builds up in the accumulated ice and when the sufficient stress has built up, the ice from the accumulation zone starts flowing towards the ablation zone. The transfer of ice from the higher zone to the lower zone reduces the slope, thereby balancing the stress and maintaining the slope at a constant level. This slope gradient is called net balance gradient. In an idealized condition, the ablation will be equal to the accumulation (Figure 8.1), thus maintaining the constant glacier surface ice velocity and slope. Thus, variation in the surface ice velocity can convey more about the health of the glacier.

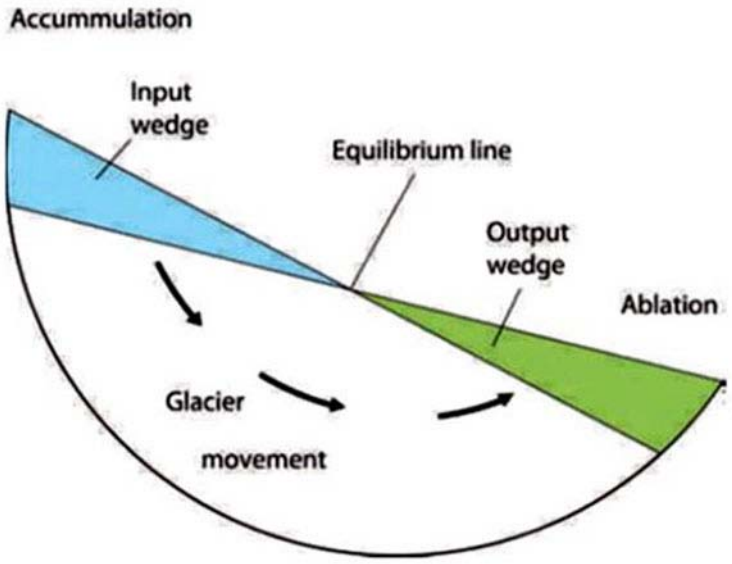

Figure 8.1: Idealized glacier with net accumulation or input 'wedge' and net ablation or output 'wedge'. Glacier flow from the accumulation zone to the ablation zone is necessary if the glacier is to maintain a constant slope. [After Bennett and Glasser (2009), Glacial Geology: Ice Sheets and Landforms, Figure 3.4, p. 45].

The glacier flows downwards due to the ice deformation because of the gravitational force which is derived from the slope towards the snout of the glacier. If there is no surface slope, there will be no imbalance between the accumulation and ablation zone and the glacier will not flow. Shear stress is the force per unit area set up within a mass of

ice by gravity which causes it to deform. Ice thickness and the surface slope of the glacier govern the shear stress experienced within an ice mass at any point. This can be summarized in the equation (8.1):

$$\tau = \rho g\,(s-z)\sin\alpha \qquad (8.1)$$

where τ is the shear stress at a point within the glacier, ρ is the density of ice, g is the acceleration due to gravity, α is the surface slope of the glacier, s is the surface elevation and z is the elevation of a point within the glacier. Glacier ice can flow in response to the shear stress through three different mechanisms: (i) by *internal deformation*; (ii) by *basal sliding*; and (iii) by *sub-glacial bed deformation*.

The *internal deformation* in the ice is achieved by two processes: (i) by *creep*; and (ii) by *folding and faulting*. In creep, ice crystals may undergo deformation or mutual displacement relative to one another due to higher temperature. The rate of ice creep is a function of the shear stress applied; the greater the shear stress, the greater the rate of ice creep. This relationship is known as *Glen's flow law*. In certain temperature and pressure conditions of the glacier ice, creep does not adjust sufficiently fast to the stresses set up within the ice. As a result, faults and folds may develop transferring ice from one place to other.

Another mechanism is the *basal sliding* by which glacier ice moves. In basal sliding, ice sheets or the glacier ice slides over the base rock over which it is sitting. There are two main processes in basal sliding: (i) *enhanced basal creep*; and (ii) *regelation slip*. The glacier base over which it is situated is not a smooth surface instead it contains irregularities such as bedrock bumps or lodged boulders, which protrude into the bottom of the moving glacier. Large stress builds up upstream of these points increasing the ice deformation, allowing more efficient creep, thus this type of movement is called *enhanced basal creep*. If the ice near the base is subjected to a series of irregularities or bumps, the pressure on the upstream side increases causing melting point of ice to fall and as a consequence, basal ice melts on the upstream side of the obstacles. The meltwater produced flows around the bump to the downstream side where the pressure is lower and

refreezes which is called *regelation ice*. This causes the transfer of mass from one point to another and this process is called *regelation slip*.

In *sub-glacial bed deformation,* the glacier moves over the continuously deforming slurry like material of unconsolidated sediments. If the glacier bed is made up of unconsolidated and unfrozen sediments, the weight of ice over it increases the water pressure in the pores, allowing the sediments to drift like slurry-like mass and the glacier ice moves with it.

8.3 Techniques for Measurement of Surface Ice Velocity- A Review

As said earlier, glacier surface ice velocity can be measured in field or using satellite remote sensing. From satellite data, ice velocity can be measured using *SAR interferometry, SAR image data intensity tracking* or *feature tracking* from optical data. Although SAR interferometry is a widely used technique for deformation and velocity mapping, this method has limitations in highly rugged terrains like the Himalayas and especially in glaciers possessing fast moving velocities. The visibility of the target glacier is affected in such rugged terrain conditions due to oblique viewing SAR images (Goldstein *et al.,* 1993; Kwok and Fahnestock, 1996; Joughin *et al.,* 1998; Joughin *et al.,* 2002; Strozzi *et al.*, 2002; Bolon *et al.,* 2007; Luckman *et al.*, 2007; Trouvé *et al.*, 2007; Kumar *et al.,* 2009). In this study, feature tracking from optical data has been used to derive the velocity of the Chhota-Shigri glacier. Therefore, detailed review of work employing different techniques for *optical image correlation* has been presented in the following paragraphs.

Optical image correlation is another promising technique used to deduce deformation or displacement of a moving object. The principle involved in this technique is that two images acquired at different times are correlated to find out the shift in the position of any moving object, which is then treated as displacement between different times. Surface velocity fields of glaciers and other moving ice bodies using optical satellite images matching have been studied since mid-1980s using manual tracking of features (Bindschadler and Scambos, 1991; Scambos *et al.*, 1992; Heid and Kaab, 2012). Different

methods for correlating image to derive velocity have been developed and applied in glaciology, like normalized cross-correlation (Bindschadler *et al.*, 1996; Rack *et al.*, 1999; Kääb, 2002; Berthier *et al.*, 2003; Skvarca *et al.*, 2003; Copland *et al.*, 2009), cross-correlation operated in the Fourier domain (Rolstad *et al.*, 1997), least squares matching (Kaufman and Ladstädter, 2003), phase correlation (Leprince *et al.*, 2008; Scherler *et al.*, 2008; Quincey and Glasser, 2009) and orientation correlation (CCF-O) (Haug *et al.*, 2010).

A few open source image processing software are available e.g. CIAS, IMCORR, COSI-Corr, etc. which utilize the above principle but their applications are limited due to tedious and time consuming processing. However, it has been reported that CCF-O and COSI-Corr are relatively more robust matching methods for global-scale mapping and monitoring of glacier velocities (Heid and Kaab, 2012).

8.3.1 Normalized cross-correlation

Scambos *et al.* (1992) measured glacier flow velocity in Siple coast area, West Antarctica using image-to-image correlation algorithm. They used two Landsat images of 1987 and 1988 to measure velocity in this low slope glacier and were able to measure velocities as low as 30 my^{-1}.

Kääb (2002) extracted ice velocity by tracking the displacement of features in repeat optical imagery. A DEM was generated from ASTER imagery using PCI Geomatica Orthoengine software. Two ASTER images of 2000 and 2001 were processed using Correlation Image Analysis (CIAS) software to measure horizontal displacement in Tasman glacier, New Zealand. The maximum ice velocity was reported to be 250 my^{-1}. The ice velocities were compared with some terrestrial and photogrammetric velocity measurements available. The velocity at the terminus was reported to be within the measurement accuracy to those observed in 1971-1986 and 1957-1971.

An accurate velocity field for Mertz glacier, Antarctica, was calculated using Landsat ETM+ images of 2000 and 2001 by Berthier *et al.* (2003). New estimates of the ice discharge flux, 17.8 km^3 a^{-1} and of the basal melting of the tongue, 11m of ice per year were also given. This glacier was reported to present a highly symmetric flow, with a strong increase in velocity when it reaches the grounding line. A Landsat TM image of

1989 was also acquired to give an estimate of the mean velocities in the nineties. They also compared their estimates of discharge fluxes, basal melting and the mass balance with previous studies and discussed the uncertainty of the imbalances and problems with accumulation mapping for this region.

Skvarca *et al.* (2003) derived velocity measurements over a fast flowing calving glacier namely Lago Argentino, Southern Pantagonia using four Landsat scenes covering a full year (Oct 2000 - Oct 2001). Annual and daily velocities were calculated using cross-correlation technique and it yielded a maximum velocity of 1600 my^{-1}. These values were validated using the field data of Nov 1993 and were found to be similar. The derived velocities showed no seasonal variations for the calving termini under study.

Copland *et al.* (2009) measured surface velocities of Baltoro glacier, South Skamri glacier and Chaktoi/Panmeh glacier in Pakistan using feature tracking technique. Two image pairs of ASTER (2006 and 2007) were used for the analysis. Co-registered images were processed in the VisiCORR and ArcGIS software. The average velocity of Baltoro glacier was measured to be 50 my^{-1}, highest being at 75 my^{-1} in the upper part of the glacier to lowest at < 15 my^{-1} at the terminus. The accuracy assessment of the feature tracking technique was done through field measured velocities. A good correspondence was reported between the two methods with <5% variation in the measured direction. In the case of South Skamri glacier, feature tracking revealed that the glacier is surging and pushing Skamri glacier aside. The velocity was reported to be as high as > 250 my^{-1} over an icefall in the upper part of the ablation area. On comparison with earlier imagery, it was observed that prior to 1978, Skamri glacier provided the main driver of ice flow which is now taken over by South Skamri glacier. Chaktoi/Panmeh glacier showed an average velocity of 100 my^{-1} over the central part of the ablation area which gradually decreases to zero approximately 8 km from the termini of the glacier. In these glaciers, the velocity increases away from the glacier margins and towards the center, suggesting that basal sliding is the dominant motion mechanism in the basin.

8.3.2 Cross-correlation operated in the Fourier domain

Rolstad *et al.* (1997) used Fourier chip cross-correlation technique to measure average velocity of Osbornebreen glacier, Svalbard using SPOT and Landsat ETM+

images. The glacier is surging so an elevation change study was also carried out by means of remote sensing. The average velocity vectors were measured for one month and one year interval between 1987-1988. A DEM was prepared using aerial photographs of 1990 and was compared with a map published in 1966. The velocity measurements of 1988 indicated a decrease in the western part and an increases in the eastern part. Along the mountain ridge, the velocity fields showed that the ice flowed like a block indicating that the bedrock formed a smooth channel along the mountain ridge.

8.3.3 Least squares matching

Kaufman and Ladstädter (2003) developed a new software namely ADVM (Automatic Displacement Vector Measurement) using which they applied digital photogrammetric method for detecting, mapping and quantifying, rock glacier creep in the Hochebenkar and Hinteres Langtalkar glaciers in Austria. Here, the correlation of images was not carried out in original photos, instead image matching was carried out in quasi-orthophotos derived from the use of rough and preliminary digital terrain models. For Hochebenkar rock glacier, aerial photographs from 1953-1997 were used to measure the velocities. The maximum mean velocity reported for the time period was 130 cmy^{-1}. For Hinteres Langtalkar rock glacier, aerial photographs ranging from 1954-1999 were used to derive surface ice velocities. The speed was reported to be increasing from 130 cmy^{-1} for 1969-1974 to 280 cmy^{-1} for 1997-1998.

8.3.4 Phase correlation

Leprince *et al.* (2008) used COSI-Corr to measure glacier ice velocities over mountainous terrain. COSI-Corr is a new software for measuring horizontal displacement of earth surface in the east-west and north-south direction. It consists of two tasks: first is to precisely orthorectify, co-register and correlate the images followed by post-processing of correlation results. The second task involves filtering and assessing the quality of results. They used two date SPOT 5 panchromatic data (dates of acquisition 23 Aug 2003 and 18 Sep 2003) of Mer de Glace area in French Alps to measure surface ice velocity over the 26 days period. They assessed the accuracy of the results using different techniques like flow direction and magnitude cross verification with the flow features present over the glacier and strain analysis. The accuracy of the velocity data was reported to be very high

with very few areas of decorrelation were observed. A displacement of 55 m was observed over the 26 day period. They concluded that these accurate measurements could be used to validate the ice flow models and thus help in studies related to fate and health of the glaciers as regards to the changing global warming scenario.

Schlerer *et al.* (2008) used ASTER data from Sep 2001 to Nov 2006 to obtain surface ice velocities in Gangotri galcier in Garhwal Himalayas. After processing the images using the COSI-Corr software, velocity measurements were done from the correlated images to study the recent velocity history of the glacier. A profile was picked from the central flow line of the glacier and the annual velocity was plotted. It was observed that the annual velocity was higher from Oct 2003 to Jul 2004 as compared to velocity from Jul 2004 to Oct 2005. They detected seasonal velocity variations of 10-20 my^{-1} in the lower part of the Gangotri glacier. They used same techniques as Leprince *et al.* (2008) to assess the accuracy and found that the results were very accurate.

Quincey and Glasser (2009) studied surface morphological and ice-dynamical changes on the Tasman Glacier, New Zealand using remote sensing data from various sensors such as Landsat TM, ETM+, ASTER from 1990 to 2007. COSI-Corr module was run on multi-temporal ASTER data and was used to extract contemporary velocity data of three distinct glacier flow units *viz* upper catchment, middle region comprising of ice and debris and lowermost region comprising the tongue of Tasman glacier. They reported that horizontal glacier velocities decline from 150 my^{-1} in the upper catchment area to almost zero at the glacier terminus. Moreover, at some points in the head of the catchment anomalously high velocities (200 my^{-1}) could also be detected. Surface elevation changes near the terminus and at upper areas were measured from multi-temporal elevation data (acquired from Land Information New Zealand) ranging from 1986 to 2007. Surface lowering was most pronounced at terminus at areas adjacent to lateral moraine ridges (4.2 $\pm$ 1.4 my^{-1}) than at the upper areas (1.9 $\pm$ 1.4 my^{-1}). An incremental increase in the areal extent of the lateral moraines was also reported between 1990 and 2007.

Herman *et al.* (2011) calculated the ice velocities of three glaciers in Southern Alps, New Zealand namely Fox, Franz Josef and Tasman glaciers. COSI-Corr software was used for precise orthorectification, co-registration and correlation of ASTER optical

imagery ranging from 2002 to 2006. Ground based velocity measurements using a network of GPS stakes were done in Franz Joseph glacier between Nov 2001 and Apr 2002. ASTER-inferred velocities were compared with the ground-based velocity measurements on Franz Josef glacier and a systematic overestimation of the velocities in the satellite data was reported. Small changes in velocities along most of Franz Josef and Fox Glaciers were also observed, while large changes in velocities were observed at the snouts of the glaciers during the advancing phase. Tasman glacier however, showed no measurable velocity. The contrasting behavior of velocity increases on the steeper glaciers as a result of an observed thickening and steepening of the glacier tongues as they moved from a retreat phase in 2002 to an advance phase in 2006 was found to be consistent with the historic terminus position changes.

8.3.5 Orientation correlation

Haug *et al.* (2010) studied the velocity field of Larsen C ice shelf, Antarctica over the periods 2002-2006 and 2006-2009 using MODIS and Landsat ETM+ pan data. They used two methods for correction of images: a) orientation correlation operating in frequency domain, and b) normalized cross-correlation in spatial domain. Two different validation sections were chosen on the ice shelf for measuring the velocity. For 2002-2006 the velocities were calculated to be -15.4 my^{-1} and 13 my^{-1}. For 2006-2009 the speed were -26.7 my^{-1} and 27.9 my^{-1} for MODIS and Landsat respectively. On comparing the two methods of image correlation, they concluded that orientation correlation is faster, more accurate and not sensitive to information restricted to few frequencies as compared to normalized cross-correlation. However, normalized cross-correlation produces higher resolution velocity field where velocity varies over short distances.

8.4 Data Used

The unprocessed level 1A of ASTER images have been used in this study. Band 3N (nadir viewing) infrared band image of ASTER images from 2003-2009 have been used to estimate the surface ice velocity on an annual basis. All the ASTER images have nearly similar incidence angles resulting in good correlation without requiring corrections for

attitude. Details of ASTER image pairs used in this study are given in Table 8.1. All the images used are almost of the same month from different years.

This glacier has been monitored in field by several groups of glaciologists for quite some time (Dhobal *et al.*, 1995; Wagnon *et al.*, 2007; Azam *et al.*, 2012) and limited field data for glacier velocity are also available which have been used as reference data.

Table 8.2: List of ASTER image pairs used in the study.

Sensor	Type of data	Resolution	Image date and pair used for correlation
SRTM	DEM	90 m	2000
ASTER NIR band 3N	NIR band 3N	30 m	08 Oct 2003 – 17 Sep 2004
			17 Sep 2004 – 07 Nov 2005
			07 Nov 2005 – 17 Nov 2006
			17 Sep 2004 – 17 Nov 2006
			17 Nov 2006 – 20 Nov 2007
			20 Nov 2007 – 01 Dec 2008
			01 Dec 2008 – 01 Oct 2009

8.5 Methodology

The methodology of data processing followed is outlined in Figure 8.2. As mentioned earlier, co-registration of Optically Sensed Images and Correlation (COSI-Corr) is a relatively new and advanced method given by Leprince *et al.* (2007) and, this package is bundled and provided as an add-on module for ENVI software. COSI-Corr is starting to become a commonly used program within glaciology. The methodology for studying glacier dynamics is provided by Scherler *et al.* (2008). After that other studies have followed (Quincey and Glasser, 2009; Herman *et al.*, 2011; Scherler *et al.*, 2011a,b). This methodology reduces the effect of inaccurate DEMs, errors due to satellite attitude during scanning and also increases the accuracy of co-registration of images.

8.5.1 Pre-processing and correlation

Before correlation of images, firstly raw satellite images have to be co-registered and orthorectified. The quality of the co-registration and orthorectification limits the accuracy of the displacement field (Leprince *et al.*, 2007). In COSI-Corr, images are projected and resampled onto a reference system that is independent of the satellite viewing geometry, such as ground projection. This produces a better co-registration irrespective of the viewing angle and geometry of the different images.

In COSI-Corr, orthorectification is achieved without having any external information such as GPS measurements of ground control points (GCPs). GCPs are generated from an automated process incorporated in this software and is based on the knowledge of the topography and the ancillary data provided with the satellite image (positions, velocities, attitudes variations and pointing directions for spacecrafts, or calibration reports for aerial photographs (Leprince *et al.*, 2007 a, b). For this, tie-points have been manually selected from pre-orthorectified image or a shaded DEM (master image) with respect to a raw image. Then the GCPs have been refined and used for automatic registration and orthorectification of the base image. The orthorectified image is further used as base image for rectifying other images. Here, band 3N of AST14DMO (orthorectified image) has been taken as master image with respect to the raw image (ASTER L1A).

After orthorectification, two selected time series images are correlated to sub-pixel level using COSI-Corr. The correlation gives horizontal displacement with two components (two images) i.e. East-West and North-South. SNR has also been calculated along with the displacement field defining the confidence of the results.

As discussed earlier, there are different mathematical ways used in glaciology to measure the glacier velocity like: (1) normalized cross-correlation operated in the spatial domain, (2) cross-correlation operated in the frequency domain using Fast Fourier Transform, (3) phase correlation operated in the frequency domain using FFT, (4) cross-correlation operated in the frequency domain using FFT on orientation images, (5) phase correlation operated in the frequency domain using FFT on orientation images , and (6) the phase correlation algorithm used in COSI-Corr.

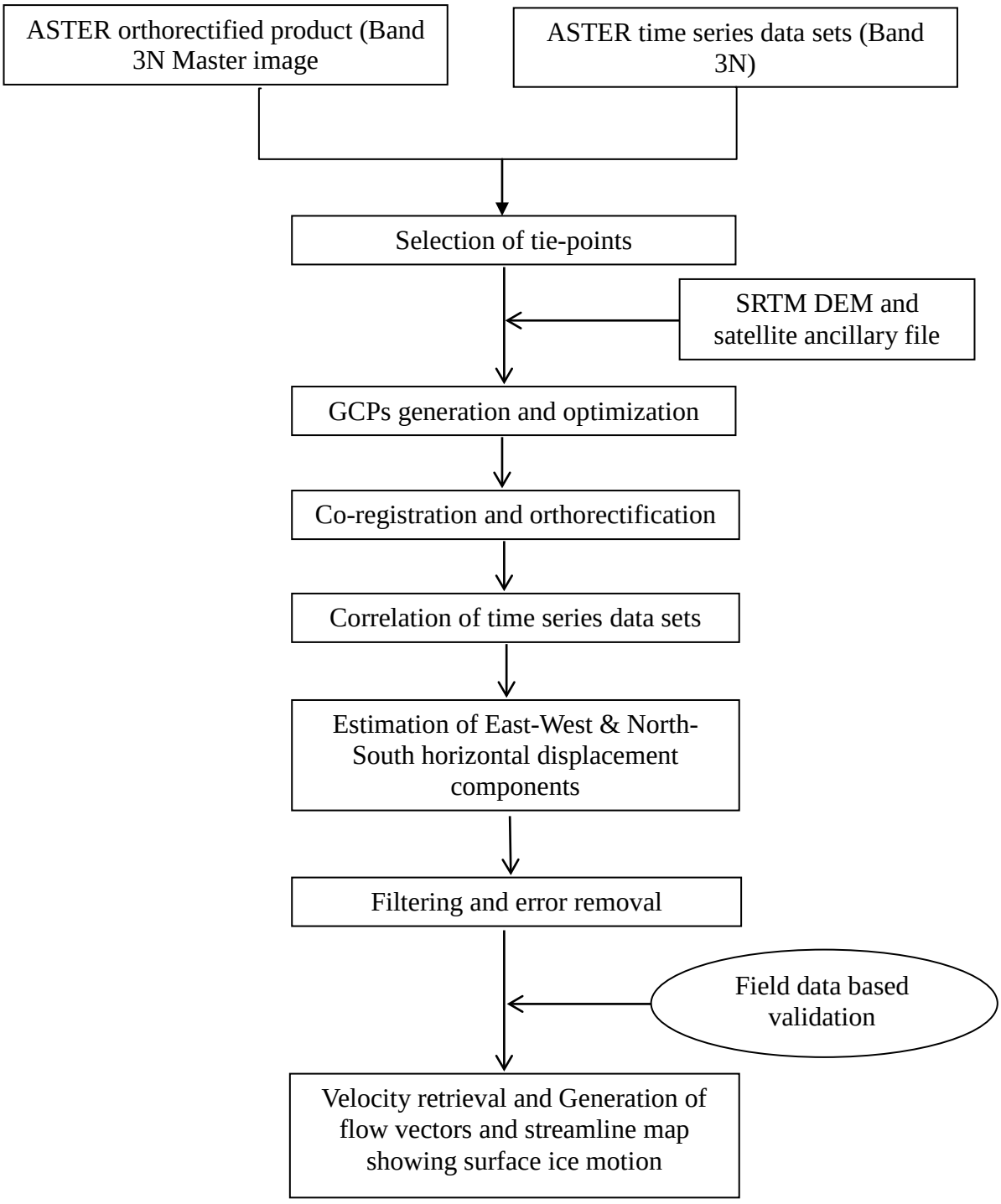

Figure 8.2: Overview of methodology.

Heid and Kaab (2012) evaluated all the methods and found that the COSI-Corr is the most robust for the measurement of the glacier velocity globally. The velocities derived using COSI-Corr is from the center coordinates of the matching window providing a more realistic idea of velocity (Heid and Kaab, 2012). Therefore, this method has been used here.

8.5.2 Sources of error and post-processing

A very important step is the filtering of correlated results before any meaningful interpretation can be drawn. Three filters to refine data processing involving SNR, direction and magnitude have been used here. The correlated results contain many errors which arise from pre-processing, from image matching and from any surface change that would have occurred between the two image acquisitions period. Errors from pre-processing (orthorectification) and from image correlation are easy to quantify whereas errors due to surface change are more difficult to quantify. Errors due to pre-processing may arise due to errors in orthorectification not the co-registration. This error may occur due to the wrong information about the camera geometry, incidence angle, atmospheric effect or errors in the DEM. The wrong information about the sensor orientation can lead to the attitude effect and present wave like effect in the correlated results. This can be removed using simple thresholding or destriping tool of COSI-Corr. In this study, a threshold of -10 m to +10 m has been applied to remove this effect.

If a same DEM is used to orthorectify all the images with near similar incidence angle ($<10^0$), the error will be of similar type in all the images and can be ignored. Also, if the time gap between the two image acquisitions is larger and same DEM is used to orthorectify both the images, then the horizontal shift may arise due to elevation change in glacier surface over time. The relationship between the elevation change (*de*) and horizontal shift (*dx*) is given by equation (8.2).

$$\frac{de}{dx} = \frac{h_1 - h_2}{x} \tag{8.2}$$

where $h_1 - h_2$ is the sensor height above ground and x is horizontal distance of a terrain point from sensor nadir (Heid, 2011).

Scheler *et al.* (2008) proposed another way to measure the DEM related errors (equation 8.3)

$$D = H \times (\tan(\theta_1) - \tan(\theta_2)) \tag{8.3}$$

where DEM elevation error is H, θ_1 and θ_2 are the incidence angle of two images used for correlation and D is the measured ground disparity. They found that if the difference in the incidence angle of the two images being correlated is $< 10^0$, then the DEM related errors are very less significant and can be ignored. Therefore, in this study, where all the image pairs used for correlation has $< 10^0$ difference in incidence angle, these corrections have been ignored.

The error from the image correlation are automatically calculated and given as one of the outputs i.e. SNR file. The pixels which are poorly correlated return low SNR. Therefore, pixels having SNR value less than 0.98 have been removed using SNR filtering option in the COSI-Corr. Directional filters have been used to further filter out those points which do not match with the general flow direction of the glacier ice. In this study, the flow directions have been defined from the flow features visible in the orthorectified images and then compared with the computed horizontal displacement (velocity vectors). One of such examples is presented in Figure 8.3. The last filter used is the magnitude filter. In case of glaciers, the movement rate may not change abruptly but gradually; this fact has been used as a parameter for filtering. These filtering operations are done manually and have to be in small patches, and also require some *a-priori* knowledge of the area.

The estimated horizontal displacements (EW and NS components), which have been computed by feature tracking from a pair of images (different temporal coverage), are first converted into net displacements using Euclidean norm equation (8.4).

$$Displacement\ (d) = \sqrt{b1^2 + b2^2} \tag{8.4}$$

where $b1$ and $b2$ are the east west and north south images. To calculate velocity, displacement is divided with a time gap between the two image acquisitions. All time interval data have been normalized for 365 days interval (annual basis).

8.6. Results and Discussion

8.6.1 Quality and accuracy assessment

It is important to mention a few words about possible errors in the remote sensing derived results. The image correlation accuracy is of the order of 1/20-1/10 of the pixel size (Scherler *et al.*, 2008), which would imply error of about ± 1.5 my^{-1} in image deduced velocity computations.

In this study, the velocities derived from image matching have been compared with the field collected velocity estimates (Figure 8.4; Table 8.3) as obtained from the published results. Other than this, Scherler *et al.* (2008) proposed several other tests to check the consistency of the results with regard to the displacement direction and magnitude in absence of the field data. These include,

1. Checking of the displacement direction by using velocity vectors, i.e., ice displacement paths, which can be checked against flow features present on the glacier surface (Figure 8.3)

2. A test of the displacement magnitude by comparing the sum of incremental measurements (e.g., comparison of velocity computed by sum of results of image correlation of 17 Sep 2004 *vs*. 07 Nov 2005 and 07 Nov 2005 *vs.* 17 Nov 2006 with velocity from image correlation of 17 Sep 2004 *vs.* 17 Nov 2006 (after normalizing all velocities to 365 days)) (Figure 8.5).

Figure 8.4 shows comparison of the remote sensing derived glacier surface ice velocities vis-à-vis field measurements for the years 2003-04 and 2004-05. The velocity profiles derived from the image matching is a near continuous profile line (Figure 8.6) near the median glacier, whereas the field data are the point data. It can be seen that there is a general agreement between the remote sensing estimates and the field data. It may however be appreciated that field stake locations are selected on constraints of accessibility and therefore field data should be taken only as an indicator for comparison. Further, it can be seen from Figure 8.4 that at several locations such as 2400, 3500, 4150, 6150 and 6600 m positions from the snout, correspondence between the field data and remote sensing estimates is very good. Both sets of data indicate that the glacier surface ice velocity is relatively high at ~3 km and ~6 km distances from the snout.

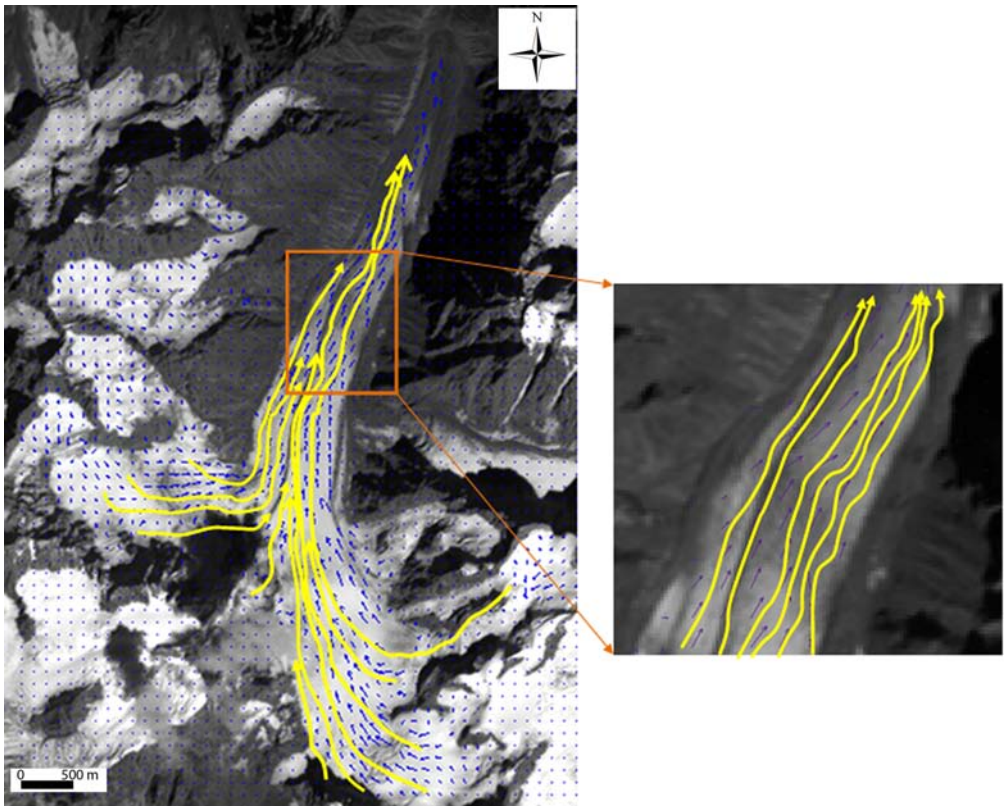

Figure 8.3: Example of velocity vectors derived from image pair 2003-04. Streamlines are shown in yellow and have been constructed using the retrieved velocity vectors and general flow pattern as observed over the glacier (vector length not to scale).

Table 8.3 shows the highest and the lowest glacier surface ice velocity data as derived from image matching and published field results. The highest and lowest velocities derived from remote sensing for the years 2003-04 and 2004-05 differ from field measurements by less than 10 per cent. For the years 2005 to 2009, no published field data are available. For the year 2009-10, no good remote sensing image pair for velocity estimation could be obtained; however the field data giving velocities of 19 my^{-1} (lowest) and 35 my^{-1} (highest) appear to be quite close to the remote sensing estimates of 2008-09. These lower values can be attributed to several factors like (1) the data collection time is different for the field measurements than the correlation images, (2) errors in the correlation results and the field measurements may be attributed to these disparities, and (3) presence of some missing values (discarded results after filtering) in the correlation results. Nevertheless, results from correlation of remote sensing images match closely with the field data with almost 90 per cent accuracy.

Table 8.3: Lowest and highest surface ice velocity measured using remote sensing and field based methods from 2003-2010 (Part A).

Year	Lowest velocity (my^{-1})		Highest velocity (my^{-1})	
	Remote sensing estimates	Field measured	Remote sensing estimates	Field measured
2003-04	20	24	41	45
2004-05	19	22	38	42
2005-06	19	NA	36	NA
2006-07	21	NA	35	NA
2007-08	20	NA	41	NA
2008-09	16	NA	36	NA
2009-10	NA	19	NA	35

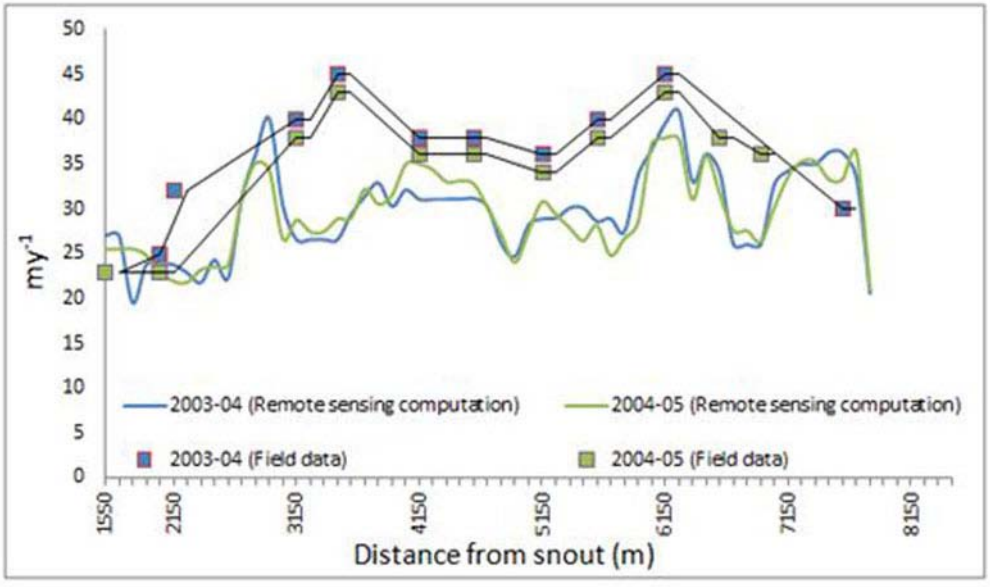

Figure 8.4: Comparison of remote sensing derived glacier velocity *vis-à-vis* field measurements for years 2003-04 and 2004-05 in part A of the glacier. The continuous curves show the remote sensing computation results; points pertain to field measurements (published data from Wagnon *et al.*, 2007). X-axis is distance from the snout.

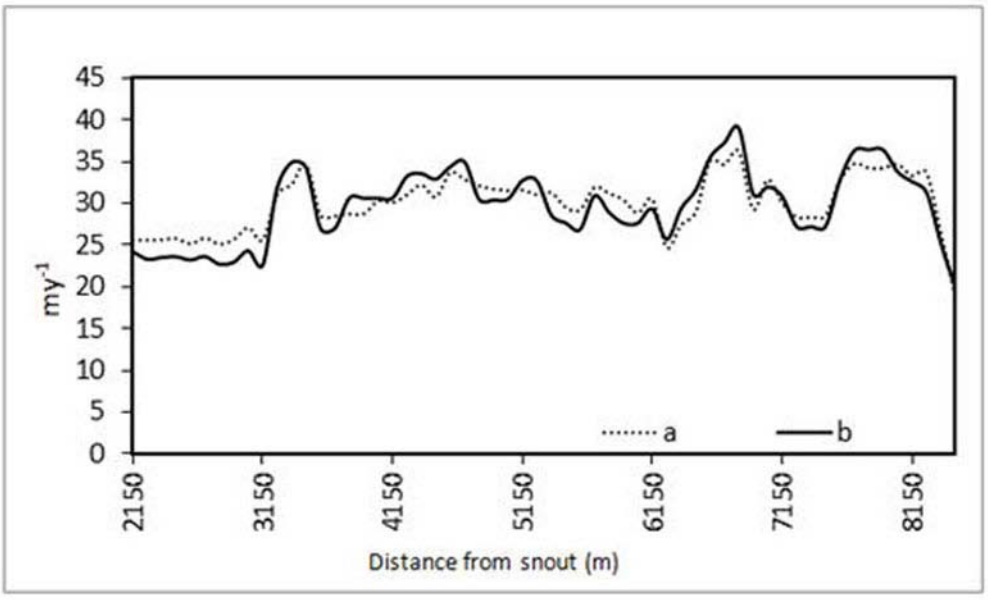

Figure 8.5: Comparison of velocity computation. (a) Velocity computed by averaging results of image correlation of 17 Sep 2004 *vs.* 07 Nov 2005 and 07 Nov 2005 *vs.* 17 Nov 2006; (b) Velocity from image correlation of 17 Sep 2004 *vs.* 17 Nov 2006 (two year difference). All computations are normalized for 365 days interval (one year).

To test the accuracy of displacement magnitude obtained after image matching, a separate exercise has been carried out in which images of 17 Sep 2004, 07 Nov 2005 and 17 Nov 2006 are used. Velocities have been computed from the pairs (i) 17 Sep 2004 *vs.* 07 Nov 2005, (ii) 07 Nov 2005 *vs.* 17 Nov 2006, and (iii) 17 Sep 2004 *vs.* 17 Nov 2006. Figure 8.5 shows the recomputed yearly surface ice velocities for the period 2004-06. It is observed that the average annual velocity is in the range 23 my^{-1} to 39 my^{-1}. The result also shows similar trends in both the cases with residual error of ± 2.5 my^{-1}. This indicates that the correlation algorithm in the COSI-Corr works well and return correct displacement magnitudes within the acceptable range.

The velocity vectors and the constructed streamlines match quite well (Figure 8.3). The velocity vectors have been generated using the displacement retrieved from the correlation of image pair 2003-04. The streamlines have been manually drawn to show the general flow pattern of the glacier surface ice using the field knowledge and the flow features as seen in the orthorectified ASTER images. The match in the direction of the

velocity vectors and the streamlines suggests that the direction retrieved from this technique is correct and it agrees with the general pattern further suggesting the consistency in image correlation results.

8.6.2 Analysis of glacier velocity

A total of seven image pairs have been used for calculating the velocity. Out of these, six pairs are separated by a year each, and one pair has a gap of two years. A comparison of the surface ice velocity derived from remote sensing and the published field data has also been made.

The Chhota-Shigri glacier has two main accumulation zones – parts A and B (terminology used by Wagnon *et al.,* 2007) (Figure 8.6). All the velocities reported here are for part A of the glacier. The velocities have been taken pixel wise along the central profile line, as most of the field measurements pertain to this part of the glacier.

The average velocity between years 2003-09 in different zones (distance from snout) as computed from image to image correlation of remote sensing data has been shown in Figure 8.7. It is observed that the highest average velocity is in the 4000 – 5000 m zone, and therefore it can be said that this (mid-ablation zone) is the fastest moving part of the glacier. The slowest moving zone is in 5000 – 6000 m (distance taken from snout) zone. This inference is in correspondence with the field data (Figure 8.5). The cause of this reduced velocity in 5000 – 6000 m distance zone may be attributed to the topographic factor, as in this zone the glacier is forced to change its direction to follow the valley orientation. Further, velocity is relatively high in the accumulation zone (Figure 8.7), which may be due to high topographic gradient and greater weight of the accumulated ice there.

In different years, velocity variations have been observed in different zones of the glacier. To give an overall view of the changes in different years in different snout zones, Figure 8.8 has been plotted. Each line pertains to a distance zone from the snout. It can be said that the average velocity in all the zones range between ~20 to 40 my^{-1}. It can also be inferred that for all the zones, the velocity is higher for the years 2005-06 and 2007-08 and lower for 2006-07 and 2008-09. Therefore, it can be said that the velocity exhibits

pulsating pattern, which may be due to the hydro-metrological parameters including change in mass balance, variation in seasonal snowfall, etc.

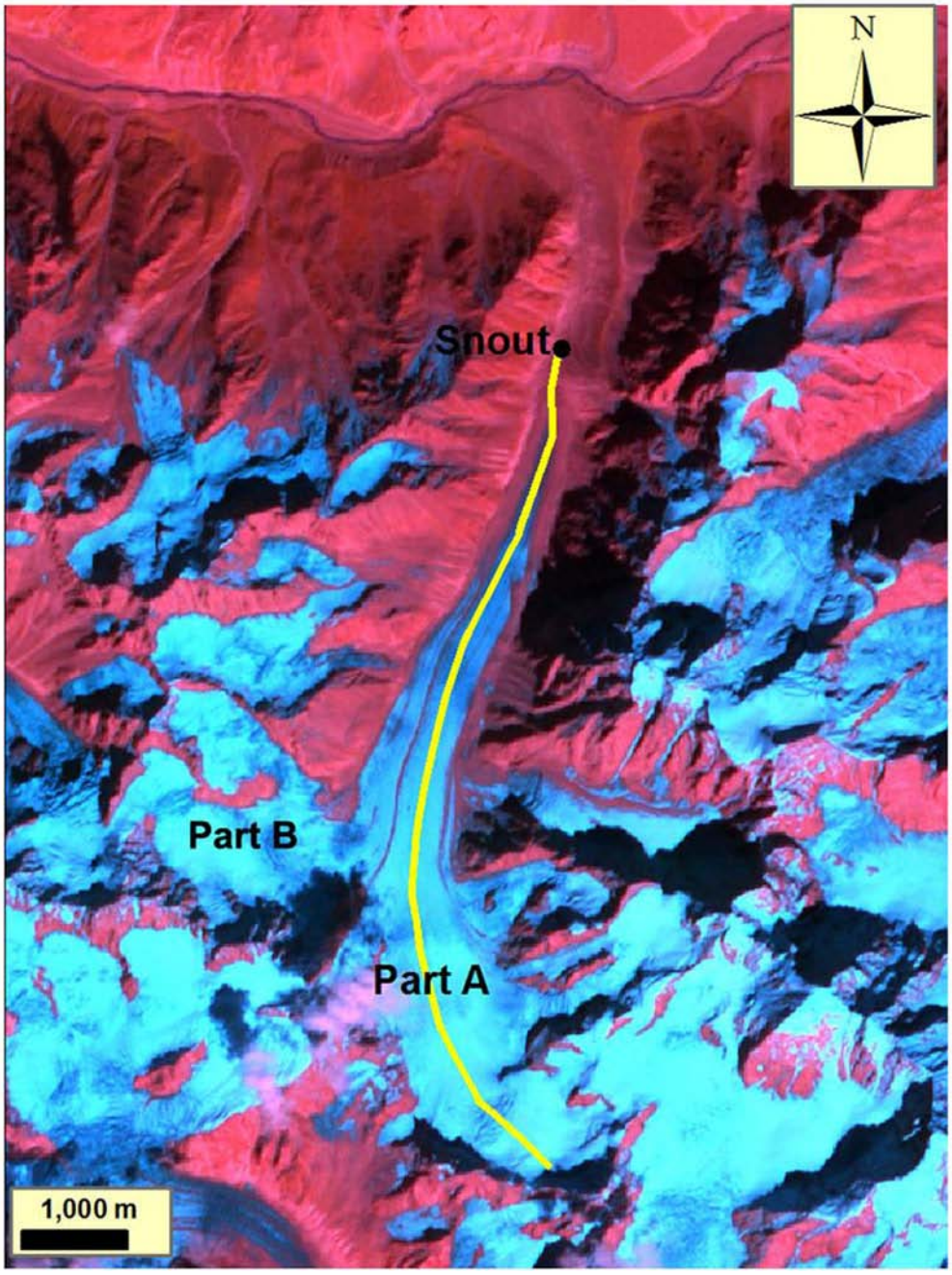

Figure 8.6: ASTER FCC (R=4, G= 3 and B= 2; image (8^{th} Oct 2003) of the Chhota-Shigri glacier. There are two main accumulation zones, part A and part B. All the data reported in this work is for part A. The figure also shows location of the snout and the central profile line.

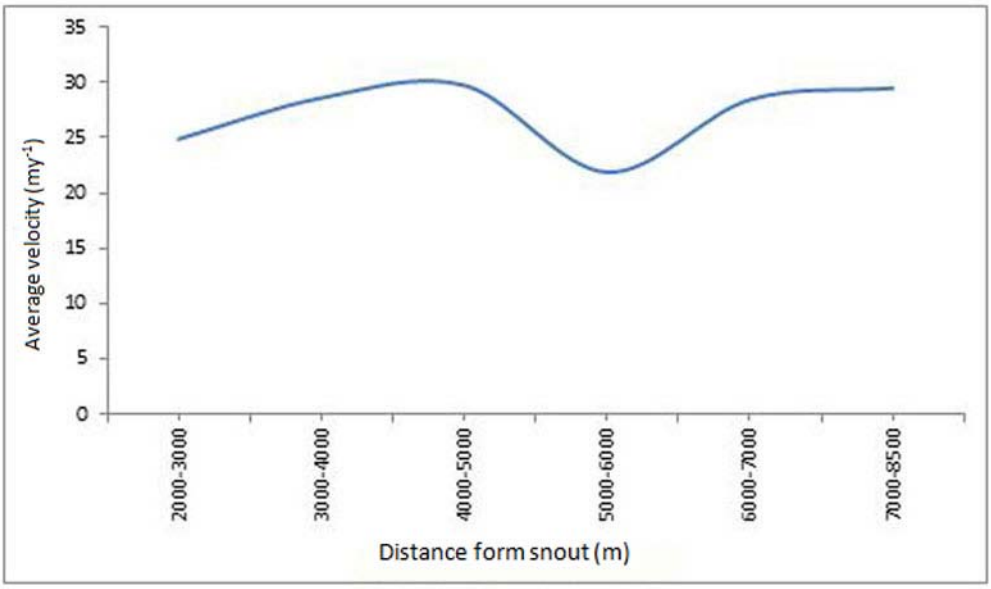

Figure 8.7: Average velocity of all the years in different distance zones from the snout. Average velocities pertain to average of all the years, i.e. 2003-09.

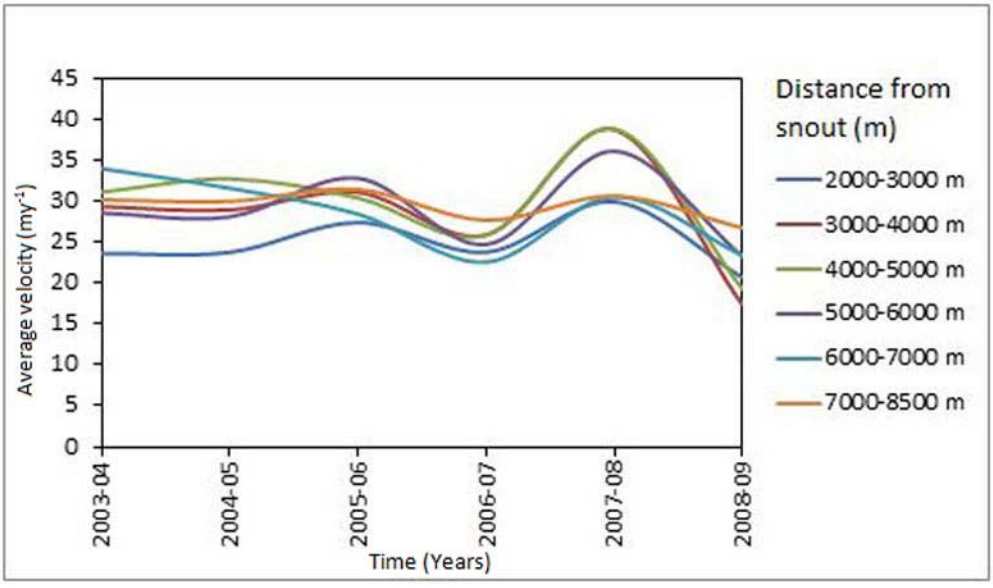

Figure 8.8: Year-wise variations of average velocity in different zones of the glacier. Each coloured line pertains to a distance zone from the snout.

Some possible causes of variation/source of error in computed results could be due to mismatch in image correlation, DEM-related error, and minor difference in incidence angle of the two images of a pair. Another factor could be that various images of different dates (17 Sep to 1 Dec) of different years have been used which have been normalized for all the vector displacements from image pairs to 365 days, based on the assumption that ice velocities are the same throughout the year, a generalization which may not be true. However, overall results from the image correlation by feature tracking technique (image to image correlation) appear to be acceptable.

The data presented here is very limited. Therefore, a very conclusive trend of glacier dynamics could not be ascertained. However, this study has clearly demonstrated the utility of image to image correlation method based on remote sensing data for deriving velocity of glaciers without field data. This type of study can be used to create glacier dynamics inventory with less effort over a large temporal and spatial scale.

8.7 Concluding Remarks

In view of the general concern of global warming and glacier recession, it is extremely important to monitor glacier dynamics on global scale. COSI-Corr utilizes the method of feature tracking (image to image matching) and is a powerful open-source software useful for such studies. Velocity data of the Chhota-Shigri glacier using COSI-Corr software was generated using time series ASTER satellite images for the period 2003-09. The image data were orthorectified, co-registered and adequately processed in COSI-Corr to generate displacement vectors. To assess the accuracy of the results it was compared with field data as available.

The results clearly indicated that the velocity data obtained from remote sensing images matched very well with the field measurements. Also, the accuracy and consistency of the results was found satisfactory. In different parts of this glacier, the surface ice velocity appeared to vary such that the mid-ablation zone and accumulation zone are relatively fast moving parts and the area near the snout and ELA are slow moving. This pattern of spatial variation in velocity was exhibited in all the years. Further, the glacier velocity also appeared to vary from year to year such that there are some years of higher

velocity and some years of relatively lower velocity. This variation could be possibly related to hydro-meteorological factors.

The need of monitoring glacier and their dynamics has been very well outlined by Bolch *et al.* (2012). In view of the vastness and inhospitable terrain conditions in the Himalayas, the above approach of optical image to image correlation can be very valuable in generating surface ice velocity data of the Himalayan glaciers.

CHAPTER 9
SUMMARY AND CONCLUSION

9.1 Introduction

Glaciers and their environmental significance have got the attention of scientists globally in last few decades. In the past, many reports by various global organisations and scientific research have suggested that the need for long term monitoring of glaciers to derive any conclusion regarding state and fate of the global glacier cover. Himalayas being the largest snow-covered area outside the poles have grabbed special attention of scientists all round the globe. In India, various government agencies have selected Himalayas and particularly the Himalayan glaciers as one of the main thrust area of research. It has also been emphasised that for Himalayan glaciers no complete inventory is available with all the aspects of glacier research meeting global standards.

It has been found that the Himalayan glaciers are mostly debris covered in the lateral and terminal parts. This debris poses difficulty in mapping of the glaciers. Also, the glacial landform studies in India are mainly restricted to field based studies. Because of this, no or very scanty data is available about the glacial processes over the Himalayas.

Glacial dynamics plays an important role in determining the glacial discharge and in terms of the availability of fresh water to the snow-fed perennial rivers originating from the mountainous regions like the Himalayas. Glacial velocity is one of the major components of glacial dynamics. Study on this aspect of glaciers is restricted to mainly field based studies in India. Therefore, very little data about the glacial dynamics over Himalayas are available and these datasets are not even continuous.

The above described facts about the Himalayan glaciers led to the evolution of this thesis. In this research, focus has been placed on studying various aspects of a single

glacier Therefore, the main objective of the present research was to examine the usage of various remote sensing techniques for different types of glaciological studies and their validation using field data. Some new methods have also been proposed.

9.2 Summary of the Research

Different remote sensing techniques have been employed to accomplish the objectives of this research. The Chhota-Shigri glacier has been selected as the study area in this research. It is a small debris-covered glacier in Himachal Himalayas. This glacier has been selected because it has been monitored in the field by different research groups for a long time and a lot of field data are available for validating the research outcome. A detailed review of all the previous studies has also been presented in this thesis.

Glacier terrain can be divided in several land cover classes which includes snow/ice, IMD, SGD, PGD and valley rocks. An attempt has been made to map the distribution of these classes using advanced remote sensing techniques. A novel methodology has been proposed here. The developed methodology has been tested for accuracy and quality of classification with the most commonly used classification algorithm i.e. MLC. Integrated use of ASTER optical and thermal bands has been done along with the geomorphometric parameters.

The landforms of the glacier have been mapped using the field collected information and their subsequent validation from satellite imageries. High spatial resolution WorldView-2 multispectral images provide useful information about the landforms and the same has been used for preparing large scale geomorphological map of this area. DTM and DEM of the area have been very useful to map and validate the geomorphological map.

The recessional history of this glacier has been studied and measured using the high spatial resolution WorldView-2 multispectral and panchromatic images. The elevation data derived from ASTER DEM has also been found to be very useful in this study. The textural information derived from the WorldView-2 images and the DEM derivatives have been used to map the paleo-morainic loops present in the inactive zone of the glacier. DEM derivatives have been particularly found very informative for providing such information. Recent recession of the glacier has also been studied using orthorectified time series ASTER images. Image correlation technique has been used for estimating the

surface ice velocity of this glacier using ASTER time series images. An add-on module of ENVI (COSI-Corr) has been used for co-registration, orthorectification and image correlation. The glacier surface ice velocity derived from the image correlation has been validated using the published field data.

The results of this research can be used to fill several gaps in the database of Chhota-Shigri glacier. The studies conducted in this research have led to several significant conclusions.

9.3 Conclusion

From the analysis of the results from this research, following conclusions have been drawn.

i. In this research, detailed investigation about the glacier terrain of the Chhota-Shigri glacier has been made using the field data and satellite images. The terrain has been categorized into five classes i.e. snow/ice, IMD, SGD, PGD and valley rocks. ASTER optical and thermal images have been used to map the extent of these glacier terrain classes. A final map containing all the glacier terrain classes has been produced with high (> 85%) accuracy.

ii. A novel methodology has been developed for the mapping of debris-covered glacier classes. This methodology includes the combined use of MLC and KNC. The developed methodology has been tested against MLC. Contrast enhancement of ASTER images by band transformation has also been proposed to increase the accuracy of classification results. The accuracies of the classified maps with the proposed classification scheme have been higher than the generally acceptable accuracy of 85%.

iii. Different types of debris have been mapped successfully using the proposed methodology. Four different classified maps have been prepared, and the best classified map is produced from transformed band and MLC in which user's and producer's accuracies of SGD have been found to be 91.40% and 92.10% respectively and for PGD they are 91.25% and 92.23% respectively.

iv. The classified image produced from hybrid classification (MLC + KNC) proposed in this research has been tested for accuracy and against the map produced from the popular MLC based classification. The accuracy of the glacier terrain map produced from hybrid classification has an overall accuracy of 86.65% which is above the general acceptable value. Further, post-processing of the output maps is not required when this method is applied, since the user knowledge about the classes are inherently taken care of during the classification process.

v. The landforms of this glacier have been studied in detail using field and satellite images and a large scale (1:10000) geomorphological map has been prepared. This updated landform information fills the long gap in the knowledge about the active geomorphological processes of the Chhota-Shigri glacier.

vi. Seven paleo-morainic loops have been mapped using the satellite images, DEM and DEM derivatives. The locations of these loops have been verified using the published maps prepared using field survey and a good correlation has been found between the two. The published map shows only five morainic loops whereas in this study seven distinct loops have been mapped using remote sensing data. Therefore, it can be concluded that remote sensing mapping has a clear advantage over field based mapping in such precarious terrain.

vii. Surface ice velocities of this glacier have been derived using ASTER time series images (2003-2009) and COSI-Corr software. The derived velocity matches quite well with the published field data with 90% accuracy. The average velocity in different zones of the glacier ranges between ~20 my^{-1} to ~40 my^{-1}. Different distinct trends of the velocity have been observed in different zones of the glacier. For example, mid-ablation zone and accumulation zone have higher velocity than lower ablation zone (near ELA) and upper ablation zone. Year-wise variations in velocity have also been observed, the velocity is higher for the year 2005-06 and 2007-08 and lower for 2006-07 and 2008-09. Therefore, it can be said that velocity exhibits pulsating pattern which may be due to hydro-meteorological parameters including change in mass balance, variation in seasonal snowfall etc.

viii. Finally, it can be concluded from the results of overall research that the Chhota-Shigri glacier is showing,

   a. increase in debris cover in lower and lateral parts of the glacier
   b. retreat over the years
   c. fluctuating velocities over the years

In general, this suggests the poor health of this glacier. Further, it can be stated that this glacier may become fully debris covered over a period of time.

9.4 Future Scope

The work presented in this thesis fills major gaps in the database of Chhota-Shigri glacier. The high correlation of the field data and remote sensing derived results clearly indicate the advantage of remote sensing technique for glaciological studies. The melt-water of Chhota-Shigri glacier feed Chenab River, which is one of the major rivers in Northern India. Based on the results of this research and the importance of this glacier, following future scope of work has been identified,

i. Regular mapping and change detection of Chhota-Shigri glacier terrain classes has to be done to keep a check on the diminishing health of the glacier using remote sensing techniques. This may particularly be important for the planning and utilization of available water resources in this basin.

ii. Long term and regular monitoring of the surface ice velocity of this and other glaciers of this basin for better understanding of glacial dynamics in the region may be carried out.

iii. Regular geomorphological studies are required to be carried out to better understand the glacial denudational processes.

iv. Further, the methodology developed here for glacial mapping needs to be tested on other larger areas to establish its utility.

REFERENCES

1. Ahluwalia, R. S., Rai, S. P., Jain, S. K., Dobhal, D. P., Kumar, B. (2013). Assessment of snowmelt runoff modelling and Isotope approach, case study from western Himalaya, India. *Annals of Glaciology*, 54, 299-304.
2. Ahmad, N. and Rais, S. (1998). *Himalayan Glaciers*. A.P.H. Publishing Corporation, New Delhi, India, 160 p.
3. Ahmad, S., Hasnain, S. I., Arha, C. D., Ramamurthy, V. S., Mathur, K. N. and Bassi, U. K. (2004). Analysis of satellite imageries for characterization of glacio-morphological features of the Gangotri Glacier, Ganga headwater, Garhwal Himalaya. In: Srivastava, D., Gupta, K. R. and Mukerji, S. (Eds.) *Proceedings of Workshop on Gangotri Glacier Special Publication Series - Geological Survey of India*, 80, 61–67.
4. Allen, T. R. (1998). Topographic context of glaciers and perennial snowfields, Glacier National Park, Montana. *Geomorphology*, 21, 207-216.
5. Aniya, M., Sato, H., Naruse, R., Skvarca, P. and Casassa, G. (1996). The use of satellite and airborne imagery to inventory outlet glacier of Southern Patagonian Icefield, South America. *Photogrammetric Engineering and Remote Sensing*, 62, 1361-1369.
6. Arendt, A., Bolch, T., Cogley, J. G., Gardner, A., Hagen, J.-O., Hock, R., Kaser, G., Pfeffer, W. T., Moholdt, G., Paul, F., *et al.* (2012). Randolph Glacier Inventory [v2.0]: A Dataset of Global Glacier Outlines. Global Land Ice Measurements from Space, Boulder Colorado, USA, 35 p.
7. Ayoub, F., Leprince, S. and Avouac, J. P. (2009). Co-registration and correlation of aerial photographs for ground deformation measurements. *ISPRS Journal of Photogrammetry and Remote Sensing*, 64, 551-560.
8. Azam, M. F., Wagnon, P., Ramanathan, A. L., Vincent, C., Sharma, P., Arnaud, Y., Linda, A., Pottakkal, J. G., Chevallier, P., Singh, V. B. and Berthier, E. (2012).

From balance to imbalance: a shift in the dynamic behaviour of Chhota Shigri Glacier (Western Himalaya, India). *Journal of Glaciology*, 58, 315–324.

9. Azam, M. F., Wagnon, P., Vincent, C., Ramanathan, A., Linda, A., and Singh, V. B. (2014a) Reconstruction of the annual mass balance of Chhota Shigri glacier, Western Himalaya, India, since 1969. *Annals of Glaciology*, 55, 69–80.
10. Azam, M. F., Wagnon, P., Vincent, C., Ramanathan, A. L., Mandal, A., and Pottakkal, J. G. (2014b). Processes governing the mass balance of Chhota Shigri Glacier (Western Himalaya, India) assessed by point-scale surface energy balance measurements, The Cryosphere Discussion, 8, 2867–2922.
11. Bahr, D. B. (1997). Global distributions of glacier properties: A stochastic scaling paradigm. *Water Resources Research*, 33, 1669–1679.
12. Bahr, D. B. and Dyurgerov, M. (1999). Characteristic mass-balance scaling with valley glacier size. *Journal of Glaciology*, 45, 17–21.
13. Bahuguna, I. M., Kulkarni, A. V. and Nayak, S. (2004). DEM from IRS-1C PAN stereo coverages over Himalayan glaciated region—accuracy and its utility. *International Journal of Remote Sensing*, 25, 4029–4041.
14. Bahuguna, I. M., Kulkarni, A. V., Nayak, S., Rathore, B. P., Negi, H. S. and Mathur, P. (2007). Himalayan glacier retreat using IRS 1C PAN stereo data. *International Journal of Remote Sensing*, 28, 437–442.
15. Bajracharya, S. R., Mool, P. K. and Shrestha, B. R. (2008). Global climate change and melting of Himalayan glaciers. In: Ranade, P. S. (Ed.), *Melting Glaciers and Rising sea levels: Impacts and implications.* The ICFAI University Press, India, pp. 28–46.
16. Bamber, J. L. and Kwok, R. (2004). Remote-sensing techniques. In: Payne, R. (Ed.), *Mass balance of the cryosphere: Observations and modelling of contemporary and future changes*, Cambridge University Press, Cambridge, pp. 59-116.
17. Bamber, J. L. and Rivera, A. (2007). A review of remote sensing methods for glacier mass balance determination. *Global and Planetary Change*, 59, 138–148.
18. Bamber, J. L., Griggs, J. A., Hurkmans, R. T. W. L., Dowdeswell, J. A., Gogineni, S. P., Howat, I., Mouginot, J., Paden, J., Palmer, S., Rignot, E., and Steinhage, D. (2013). A new bed elevation dataset for Greenland. *The Cryosphere*, 7, 499–510.

19. Bayr, K. J., Hall, D. K., and Kovalick, W. M. (1994). Observations on glaciers in the eastern Austrian Alps using satellite data. *International Journal of Remote Sensing*, 15, 1733–1742.
20. Bennett, M. R. and Glasser, N. F. (1996). *Glacial Geology: Ice sheets and landforms*. 2nd Ed., Wiley-Blackwell, West Sussex, U.K., 364 p.
21. Berthier, E., Arnaud, Y., Baratoux, D., Vincent, C. and Remy, F. (2004). Recent rapid thinning of the "Mer de Glace" glacier derived from satellite optical images. *Geophysical Research Letters*, 31, L17401, pp. 1-4.
22. Berthier, E., Arnaud, Y., Kumar, R., Ahmad, S., Wagnon, P. and Chevallier, P. (2007). Remote sensing estimates of glacier mass balances in the Himachal Pradesh (Western Himalaya, India). *Remote Sensing of Environment*, 108, 327–338.
23. Berthier, E., Raup, B. and Scambos, T. (2003). New velocity map and mass-balance estimate of Mertz Glacier, East Antarctica, derived from Landsat sequential imagery. *Journal of Glaciology*, 49, 503–511.
24. Bhambri, R., Bolch, T. and Chaujar, R. K. (2011a). Mapping of debris-covered glaciers in the Garhwal Himalayas using ASTER DEMs and thermal data. *International Journal of Remote Sensing*, 32, 8095-8119.
25. Bhambri, R., Bolch, T., Chaujar, R. K. and Kulshreshtha, S. C. (2011b). Glacier changes in the Garhwal Himalaya, India, from 1968 to 2006 based on remote sensing. *Journal of Glaciology*, 57, 543-556.
26. Bhambri, R., Bolch, T. and Chaujar, R. K. (2012). Frontal recession of Gangotri Glacier, Garhwal Himalayas, from 1965 to 2006, measured through high-resolution remote sensing data. *Current Science*, 102, 489-494.
27. Bindschadler, R. and Scambos, T. (1991). Satellite-image-derived velocity field of an Antarctic ice stream. *Science*, 252, 242–246.
28. Bindschadler, R., Vornberger, P., Blankenship, D., Scambos, T. and Jacobel, R. (1996). Surface velocity and mass balance of Ice Streams D and E, West Antarctica. *Journal of Glaciology*, 42, 461–475.
29. Bishop, M. P., Bonk, R., Kamp, U. and Shroder Jr., J.F. (2001). Terrain analysis and data modeling for alpine glacier mapping. *Polar Geography*, 25, 182–201.

30. Bishop, M. P., Kargel, J. S., Kieffer, H. H., MacKinnon, D. J., Raup, B. H. and Shroder Jr., J. F. (2000). Remote-sensing science and technology for studying glacier processes in high Asia. *Annals of Glaciology*, 31, 164–170.
31. Bishop, M. P., Olsenholler, J. A., Shroder, J. F., Barry, R. G., Raup, B. H., Bush, A. B. G., Copland, L., Dwyer, J. L., Fountain, A. G., Haeberli, W., Kääb, A., Paul, F., Hall, D. K., Kargel, J. S., Molnia, B. F., Trabant, D. C. and Wessels, R. (2004). Global Land Ice Measurements from Space (GLIMS): Remote Sensing and GIS Investigations of the Earth's Cryosphere. *Geocarto International*, 19, 57–84.
32. Bishop, M. P., Shroder Jr., J. F., Hickman, B. L. and Copland, L. (1998). Scale-dependent analysis of satellite imagery for characterization of glacier surfaces in the Karakoram Himalaya. *Geomorphology*, 21, 217-232.
33. Boelhouwers, J. C. and Meiklejohn K. I. (2002). Quaternary periglacial and glacial geomorphology of southern Africa: Review and synthesis. *South African Journal of Science*, 98, 47–55.
34. Böhner, J. (2006). General climatic controls and topoclimatic variations in Central and High Asia. *Boreas*, 35, 279–295.
35. Bolch, T. and Kamp, U. (2006). Glacier mapping in high mountains using DEMs, Landsat and ASTER data. *Grazer Schriften der Geographie und Raumforschung*, 41, 37–48.
36. Bolch, T., Buchroithner, M. F., Kunert, A. and Kamp, U. (2008a). Automated delineation of debris-covered glaciers based on ASTER data. In: Gomarasca, M. A. (Ed.), *GeoInformation in Europe*, Millpress, Netherlands, pp. 403–410.
37. Bolch, T., Buchroithner, M. F., Pieczonka, T. and Kunert, A. (2008b). Planimetric and volumetric glacier changes in the Khumbu Himalaya 1962–2005 using Corona and ASTER data. *Journal of Glaciology*, 54, 562–600.
38. Bolch, T., Kulkarni, A., Kääb, A., Huggel, C., Paul, F., Cogley, J.G., Frey, H., Kargel, J.S., Fujita, K., Scheel, M., Bajracharya, S. and Stoffel, M. (2012). The state and fate of Himalayan glaciers. *Science*, 336, 310–314.
39. Bolch, T., Sandberg Sørensen, L., Simonsen, S. B., Moelg, N., Machguth, H., Rastner, P. and Paul, F. (2013). Mass loss of Greenland's glaciers and ice caps 2003–2008 revealed from ICESat data. *Geophysical Research Letters*, 40, 875–881.

40. Bolon, Ph., Trouvé, E., Petillot, I., Vasile, G., Gay, M., Bombrun, L., Nicolas, J. M., Tupin, F., Landes, T., Koehl, M. and Grussenmeyer, P. (2007). Monitoring Alpine Glaciers with ALOS SAR and Optical data. In: *Proceedings of 1st Joint PI Symposium of ALOS Data Nodes for ALOS Science Program*, Japan Aerospace Exploration Agency, Kyoto, Japan, pp. 4 –7.
41. Bookhagen, B. and Burbank, D. W. (2006). Topography, relief, and TRMM-derived rainfall variations along the Himalaya. *Geophysical Research Letters*, 33, L08405.
42. Bronge, L., B. and Bronge, C. (1999). Ice and Snow type classification in Vestfold Hills, East Antarctica, using LANDSAT TM data and ground radiometer measurements. *International Journal of Remote Sensing*, 20, 225-240.
43. Brooks, R. N., Prowse, T. D. and O'Connell, I. J. (2012). Quantifying Northern Hemisphere freshwater ice. *Geophysical Research Letters*, 40, 1128–1131.
44. Brown, E. T., Bourlès, D. L., Burchfiel, B., Deng, Q., Li, J., Molnar, P., Raisbeck, G. M. and Yiou, F. (1998). Estimation of slip rates in the southern Tien Shan using cosmic ray exposure dates of abandoned alluvial fans. *Geological Society of America Bulletin*, 110, 377–386.
45. Buchroithner, M. F. and Bolch, T. (2007). An automated method to delineate the ice extension of the Debris-Covered Glaciers at Mt. Everest based on ASTER Imagery. In *Proceedings of the 9th International Symposium on High Mountain Remote Sensing Cartography*, 14–22 September, Graz, Austria, pp. 71–78.
46. Butler, D. R. and Walsh, S. J. (1998). The application of remote sensing and geographic information systems technologies in the study of geomorphology: An Introduction. *Geomorphology*, 21, 179-352.
47. Cavalieri, D. J., and Parkinson, C. L. (2012). Arctic sea ice variability and trends, 1979– 2010. *The Cryosphere*, 6, 957–979.
48. Chang, A. T. C., Foster, J. L. and hall, D. K. (1987). Nimbus 7 derived global snow cover parameters. *Annals of Glaciology*, 9, 39-44.
49. Charlesworth, J. K. (1928). The glacial retreat from central and southern Ireland *Quarterly Journal of the Geological Society of London*, 84, 293–344.
50. Chaujar, R. K. (1987). Geomorphological studies with special reference to landforms the Chhota Shigri glacier, H. P. *Geoscience Journal*, 8, 97-108.

51. Chaujar, R. K. (1991). Cycles of advance and retreat of the Chhota-Shigri glacier, Lahaul district, H.P. *Journal of Geological Society of India*, 37, 477-481.
52. Chaujar, R. K. (1992). Streamlined landforms in the inactive zone of the Chhota-Shigri glacier, Lahaul district, H.P. *Journal of Geological Society of India*, 40, 258-261.
53. Close, M. H. (1867). Notes on the general glaciation of Ireland. *Journal of the Royal Geographical Society of London,* 1, 207–242.
54. Cogley, J. G. (2009). A more complete version of the World Glacier Inventory. *Annals of Glaciology,* 50, 32–38.
55. Comiso, J. C. and Nishio, F. (2008). Trends in the sea ice cover using enhanced and compatible AMSR-E, SSM/I, and SMMR data. *Journal of Geophysical Research: Oceans,* 113, C02S07, pp. 1-22.
56. Comiso, J. C., Kwok, R., Martin, S. and Gordon, A. L. (2011). Variability and trends in sea ice extent and ice production in the Ross Sea. *Journal of Geophysical Research: Oceans*, 116, C04021, pp. 1-19.
57. Congalton, R. G. (1991). A review of assessing the accuracy of classifications of remotely sensed data. *Remote Sensing of Environment,* 37, 35–46.
58. Copland, L., Pope, S., Bishop, M., Shroder Jr., J. F., Clendon, P., Bush, A., Kamp, U., Seong, Z. B. and Owen, L. A. (2009). Glacier velocities across the central Karakoram. *Annals of Glaciology*, 50, 41–49.
59. Cruz, R.V., Harasawa, H., Lal, M., Wu, S., Anokhin, Y., Punsalmaa, B., Honda, Y., Jafari, M., Li, C. and Huu Ninh, N. (2007). Asia Climate Change 2007: Impacts, Adaptation and Vulnerability. In: Parry, M. L., Canziani, O. F., Palutikof, J. P., van der Linden, P. J. and Hanson, C. E. (Eds.), *Contribution of Working Group II to the Fourth Assessment Report of the Intergovernmental Panel on Climate Change.* Cambridge University Press, Cambridge, UK, 976 p.
60. Cuffey, K. M. and Paterson, W. (2010). *The physics of glaciers*. Elsevier, Burlington, USA, 693 p.
61. Dobhal, D. P., Gupta, A. K., Mehta, M. and Khandelwal, D. D. (2013). Kedarnath disaster: facts and plausible cause. *Current Science*, 105, 171-174.

62. Dobhal, D. P., Kumar, S. and Mundepi, A. K. (1991). Mass wasting and slope analysis of Chhota-Shigri Glacier (HP). *Journal of Himalayan Geology*, 2, 119-124.
63. Dobhal, D. P., Kumar, S. and Mundepi, A. K. (1995). Morphology and glacier dynamics studies in monsoon-arid transition zone: An example from Chhota Shigri glacier, Himachal Himalaya, India. *Current Science*, 68, 936–944.
64. Dozier, J. (1989). Spectral Signature of alpine snow-cover from the Landsat Thematic Mapper. *Remote Sensing of Environment*, 28, 9-22.
65. Duncan, C. C., Klein, A. J., Masek, J. G. and Isacks, B. L. (1998). Comparison of Late Pleistocene and modern glacier extents in central Nepal based on digital elevation data and satellite imagery. *Quarternary Research*, 49, 241-254.
66. Dyurgerov, M. (1996). Substitution of long-term mass balance data by measurements of one summer. *Zeitschrift für Gletscherkunde und Glazialgeologie*, 32, 177–184.
67. Dyurgerov, M. B. and Meier, M. F. (2000). Twentieth century climate change: Evidence from small glaciers. In: *Proceedings of the National Academy of Sciences of the United States of America 2000,* 97, 1406–1411.
68. Embleton, C. and King, C. A. M. (1975). *Glacial Geomorphology*. Edward Arnold Ltd., London, 573 p.
69. Engeset, R. V. and Weydahl, D. J. (1998). Analysis of glaciers and geomorphology on svalbard using multitemporal ERS-1 SAR images. *IEEE Transactions on Geoscience and Remote Sensing*, 36, 1879–1887.
70. ENVI User's Guide (2008). *ENVI on-line software user's manual.* ITT Visual Information Solutions.
71. Evans, A. N. (2000). Glacier surface motion computation from digital image sequences. *IEEE Transactions on Geoscience and Remote Sensing*, 38, 1064–1072.
72. Fan, Y., Held, I. M., Lin, S. J. and Wang, X. L. (2013). Ocean warming effect on surface gravity wave climate change for the end of the 21st century. *Journal of Climate*, 26, 6046-6066.
73. Fatland, D. R., and Lingle, C. S. (1998). Analysis of the 1993–95 Bering Glacier (Alaska) surge using differential SAR interferometry. *Journal of Glaciology*, 44, 532−546.

74. Foster, J. L., Chang, A. T. C. and Hall, D. K. (1997). Comparison of snow mass estimates from a prototype passive microwave algorithm and a snow depth climatology. *Remote Sensing of Environment*, 62, 132-142.
75. Fretwell, P., Pritchard, H. D., Vaughan, D. G., Bamber, J. L., Barrand, N. E., Bell, R., Bianchi, C., Bingham, R. G., Blankenship, D. D., Casassa, G., *et al.*, (2013). Bedmap2: improved ice bed, surface and thickness datasets for Antarctica, *The Cryosphere*, 7, 375–393.
76. Gao, J. and Liu, Y. (2001). Applications of remote sensing, GIS and GPS in glaciology: A review. *Progress in Physical Geography*, 25, 520–540.
77. Gardelle, J., Berthier, E., and Arnaud, Y. (2012). Slight mass gain of Karakoram glaciers in the early twenty-first century. *Nature Geoscience*, 5, 322–325.
78. Gardner, A. S., Moholdt, G., Cogley, J. G., Wouters, B., Arendt, A. A., Wahr, J., Berthier, E., Hock, R., Pfeffer, W. T., Kaser, G., Ligtenberg, S. R. M., Bolch, T., Sharp, M. J., Hagen, J. O., van den Broeke, M. R. and Paul, F. (2013). A reconciled estimate of glacier contributions to sea level rise: 2003 to 2009. *Science*, 340, 852–857.
79. GCOS/GTOS, (2004). Implementation plan for the global observing system for climate in support of the UNFCCC. *GCOS Reports - 92 (WMO/TD No. 1219)*, pp. 136.
80. Goldstein, R., Engelhardt, H., Kamb, B. and Frolich, R. (1993). Satellite radar interferometry for monitoring ice sheet motion: Application to an Antarctic ice stream. *Science*, 262, 1525–1530.
81. Goudie, A. (2004). *Encyclopedia of Geomorphology*. Routledge, New York, 1250 p.
82. Gray, L., Mattar, K., and Vachon, P. (1998). InSAR results from the RADARSAT Antarctic mapping mission: Estimation of glacier motion using a simple registration procedure. In: *Proceedings of IEEE Transactions on Geoscience and Remote Sensing Symposium* (IGARSS'98), July 6–10, Seattle, USA, 1638–1640.
83. Griggs, J., and J. L. Bamber, (2011). Antarctic ice-shelf thickness from satellite radar altimetry. *Journal of Glaciology*, 57, 485–498.
84. Grinsted, A. (2013). An estimate of global glacier volume. *The Cryosphere*, 7, 141–151.

85. Gruber, S. (2012). Derivation and analysis of a high-resolution estimate of global permafrost zonation. *The Cryosphere*, 6, 221–233.
86. Guneriussen, T., Hgda, K. A. Johnsen, H. and Lauknes, I. (2001). InSAR for estimation of changes in snow water equivalent of dry snow. *IEEE Transactions on Geoscience and Remote Sensing*, 39, 2101–2108.
87. Gupta, R. P., Haritashya, U. K. and Singh, P. (2005). Mapping dry/wet snow cover in the Indian Himalayas using IRS multispectral imagery. *Remote Sensing of Environment*, 97, 458-469.
88. Gupta, V. J. and Kumar, S. (1975). Geology of Ladakh, Lahaul and Spiti regions of the Himalaya, with special reference to the stratigraphical position of flysch deposits. *Geologische Rundschau*, 64, 540–563.
89. Haeberli, W. R., Frauenfelder, R., Hoelzle, M. and Maisch, M. (1999). On rates and acceleration trends of global glacier mass changes. *Geografiska Annaler. Series A. Physical Geography*, 81A, 585−595.
90. Haeberli, W., Hoelzle, M. and Suter, S. (Eds.) (1998). *Into the second century of world glacier monitoring—prospects and strategies*. Studies and reports in hydrology, UNESCO Publishing, Paris, France, 56, 227 p.
91. Haeberli, W., Maisch, M., and Paul, F. (2002). Mountain glaciers in global climate-related observation networks. *World Meteorological Organization Bulletin*, 51, 1−8.
92. Hall, D. K. and Martinec, J. (1985). *Remote sensing of ice and snow*. Chapman and Hall, New York, 189 p.
93. Hall, D. K., Chang, A. T. C. and Siddalingaiah, H. (1988). Reflectances of Glaciers as calculated from the Landsat 5 Thematic Mapper data. *Remote Sensing of Environment*, 25, 311- 321.
94. Hall, D. K., Ormsby, J. P., Bindschadler, R. A., and Siddalingaiah, H. (1987). Characterization of snow and ice zones on glaciers using Landsat Thematic Mapper data. *Annals of Glaciology*, 9, 104–108.
95. Hall, D. K., Riggs, G. A. and Solomonson, V. V. (1995). Development of methods for mapping global snow covers using moderate resolution imaging spectroradiometers data. *Remote Sensing of Environment*, 54, 127-140.

96. Hall, D. K., Williams, R.S. Jr. and Bayr, K. J. (1992). Glacier Recession in Iceland and Austria. *EOS Transaction of the American Geophysical Union*, 73, 129-141.
97. Haritashya, U. K., Singh, P., Kumar, N. and Gupta, R. P. (2006). Suspended sediment from the Gangotri Glacier: Quantification, variability and associations with discharge and air temperature. *Journal of Hydrology*, 321, 116–130.
98. Haug, T., Kääb, A. and Skvarca, P. (2010). Monitoring ice shelf velocities from repeat MODIS and Landsat data - A method study on the Larsen C ice shelf, Antarctic Peninsula, and 10 other ice shelves around Antarctica. *The Cryosphere*, 4, 161–178.
99. Heid, T. and Kääb, A. (2012). Evaluation of existing image matching methods for deriving glacier surface displacements globally from optical satellite imagery. *Remote Sensing of Environment*, 118, 339–355.
100. Hellmer, H. H., Kauker, F., Timmermann, R., Determann, J. and Rae, J. (2012). Twenty-first-century warming of a large Antarctic ice-shelf cavity by a redirected coastal current. *Nature*, 485, 225–228.
101. Herman, F., Anderson, B., and Leprince, S. (2011). Mountain glacier velocity variation during a retreat/advance cycle quantified using sub-pixel analysis of ASTER images. *Journal of Glaciology*, 57, 197–207.
102. Howarth, P. and Ommanney, C. S. (1986). The use of Landsat digital data for glacier inventories. *Annals of Glaciology*, 8, 90–92.
103. Huggel, C., Haeberli, W., Kääb, A., Bieri, D., and Richardson, S. (2004). An assessment procedure for glacial hazards in the Swiss Alps. *Canadian Geotechnical Journal*, 41, 1068–1083.
104. Huss, M. and Farinotti, D. (2012). Distributed ice thickness and volume of all glaciers around the globe. *Journal of Geophysical Research: Earth Surface*, 117, F04010, pp. 1-10.
105. IPCC, (2013). Climate Change 2013: The Physical Science Basis. In: Stocker, T. F., Qin, D., Plattner, G.-K., Tignor, M., Allen, S. K., Boschung, J., Nauels, A., Xia, Y., Bex, V. and Midgley, P. M. (Eds.), *Contribution of Working Group I to the Fifth Assessment Report of the Intergovernmental Panel on Climate Change*. Cambridge University Press, Cambridge, UK, 1535 p.

106. Jacobs, J. D., Simms, E. L. and Simms, A. (1997). Recession of the southern part of Barnes Ice Cap, Baffin Island, Canada, between 1961 and 1993, determined from digital mapping of Landsat TM. *Journal of Glaciology*, 43, 98–102.
107. Johnson, B. R. and Young, S. J. (1998). *In-scene Atmospheric Compensation: Application to SEBASS Data at the ARM Site.* Aerospace Report No. ATR-99(8407)-1, Parts I and II. The Aerospace Corporation, El Segundo, California, Nov 1998.
108. Joughin, I., Kwok, R. and Fahnestock, M. (1998). Interferometric estimation of the three dimensional ice-flow velocity vector using ascending and descending passes. *IEEE Transactions on Geoscience and Remote Sensing*, 36, 25-37.
109. Joughin, I., Tulaczyk, S., Bindschadler, R. and Price, S. F. (2002). Changes in west Antarctic ice stream velocities: Observation and analysis. *Journal of Geophysical Research: Solid Earth*, 107, 2289, pp. 1-22.
110. Kääb, A. (2004). Mountain glaciers and permafrost creep. Methodical research perspectives from earth observation and geoinformatics technologies. *Habilitation thesis*, Department of Geography, University of Zurich, Germany, 205 p.
111. Kääb, A. (2005). Combination of SRTM3 and repeat ASTER data for deriving alpine glacier flow velocities in the Bhutan Himalaya. *Remote Sensing of Environment*, 94, 463-474.
112. Kääb, A. (2007). Monitoring high-mountain terrain deformation from repeated airandspaceborne optical data: examples using digital aerial imagery and ASTER data. *ISPRS Journal of Photogrammetry and Remote Sensing*, 57, 39–52.
113. Kääb, A. and Haeberli, W. (2001). Evolution of a high-mountain thermokarst lake in the Swiss Alps. *Arctic, Antarctic, and Alpine Research*, 33, 385-390.
114. Kääb, A. and Vollmer, M. (2000). Surface geometry, thickness changes and flow fields on creeping mountain permafrost: Automatic extraction by digital image analysis. *Permafrost and Periglacial Processes*, 11, 315–326.
115. Kääb, A., Berthier, E., Nuth, C., Gardelle, J., and Arnaud, Y. (2012). Contrasting patterns of early twenty-first-century glacier mass change in the Himalayas. *Nature*, 488, 495–498.
116. Kääb, A., Huggel, C., Paul, F., Wessels, R., Raup, B., Kieffer, H. and Kargel, J. (2003). Glacier monitoring from ASTER imagery: Accuracy and applications.

Proceedings of EARSeL-LISSIG-Workshop Observing our Cryosphere from Space, 11-13 March, Bern, Switzerland, 2, 43–53.

117. Kääb, A., Reynolds, J. M. and Haeberli, W. (2005). *Glacier and permafrost hazards in high mountains*. In: Huber, U. M., Bugmann, H. K. M. and Reasoner, M. A. (Eds.), Global change and mountain regions: A state of knowledge overview, Springer, Dordrecht, 225– 234
118. Kale, V. S. and Gupta, A. (2001). *Introduction to Geomorphology*. Orient Longman, Calcutta, 267 p.
119. Kapadia, H. (1999). *Spiti: Adventures in the Trans-Himalaya*. 2nd Edn., Indus Publishing Company, New Delhi, 245 p.
120. Kargel, J. S., Abrams, M. J., Bishop, M. P., Bush, A., Hamilton, G., Jiskoot, H., Kääb, A., Kieffer, H. H., Lee, E. M., Paul, F., Rau, F., Raup, B., Shroder, J. F., Soltesz, D., Stainforth, D., Stearns, L. and Wessels, R. (2005). Multispectral imaging contributions to global land ice measurements from space. *Remote Sensing of Environment*, 99, 187-219.
121. Kargel, J. S., Ahlstrøm, A. P., Alley, R. B., Bamber, J. L., Benham, T. J., Box, J. E., Chen, C., Christoffersen, P., Citterio, M., Cogley, J. G., Jiskoot, H., Leonard, G. J., Morin, P., Scambos, T., Sheldon, T., and Willis, I. (2012). Brief communication Greenland's shrinking ice cover: "fast times" but not that fast. *The Cryosphere*, 6, 533-537.
122. Karimi, N., Farokhnia, A., Karimi, L., Eftekhari, M. and Ghalkhani, F. H. (2012). Combining optical and thermal remote sensing data for mapping debris covered glaciers (Alamkouh Glaciers, Iran). *Cold Regions Science and Technology*, 71, 73-83.
123. Kaser, G., Fountain, A. G. and Jansson, P. (2002). A manual for monitoring the mass balance of mountain glaciers. *IHP-VI- Technical documents in hydrology*, 59 p.
124. Katoch, K. C. (1989). *Study of moraines with special reference to metallic minerals in Chhota Shigri glacier in Lahaul and Spiti District, Himachal*. Technical Report on Multi Disciplinary glacier expedition to Chhota Shigri, Department of Science and Technology, New Delhi, 3, 299-301.

125. Kaufmann, V. and Ladstädter, R. (2003). Quantitative analysis of rock glacier creep by means of digital photogrammetry using multi-temporal aerial photographs: two case studies in the Austrian Alps. *Permafrost*, 525–530.
126. Kelly, M. A., Buonchristiani, J.-F. and Schlüchter, C. (2004). A reconstruction of the last glacial maximum (LGM) ice-surface geometry in the western Swiss Alps and contiguous alpine regions in Italy and France. *Eclogae Geologicae Helvetiae*, 97, 57-75.
127. Keshri, A. K., Shukla, A. and Gupta, R. P. (2009). ASTER ratio indices for supraglacial terrain mapping. *International Journal of Remote Sensing*, 30, 519-524.
128. Khromova, T. E., Osipova, G. B., Tsvetkov, D. G., Dyurgerov, M. B. and Barry, R. G. (2006). Changes in glacier extent in the eastern Pamir, Central Asia, determined from historical data and ASTER imagery. *Remote Sensing of Environment*, 102, 24–32.
129. Kieffer, H. H., Kargel, J. S., Barry, R., Bindschadler, R., Bishop, M. and Mackinnon, D. (2000). New eyes in the sky measure glaciers and ice sheets. *EOS, Transactions of the American Geophysical Union*, 81, 265–271.
130. Kulkarni, A. V. (1992). Mass balance of Himalayan glaciers using AAR and ELA methods. *Journal of Glaciology*, 38, 101– 104.
131. Kulkarni, A. V. and Alex, S. (2003). Estimation of recent glacial variations in Baspa basin using remote sensing technique. *Journal of the Indian Society of Remote Sensing*, 31, 81-90.
132. Kulkarni, A. V., Bahuguna, I. M., Rathore, B. P., Singh, S. K., Randhawa, S. S., Sood, R. K. and Dhar, S. (2007). Glacial retreat in Himalaya using Indian remote sensing satellite data. *Current Science*, 92, 69–74.
133. Kulkarni, A. V., Dhar, S., Rathore, B. P., Raj, B. G. and Kalia, R. (2006). Recession of samundra tapu glacier, Chandra river basin, Himachal Pradesh. *Journal of the Indian Society of Remote Sensing*, 34, 39–46.
134. Kulkarni, A. V., Rathore, B. P., and Alex, S. (2004). Monitoring of glacial mass balance in the Baspa basin using accumulation area ratio method. *Current Science*, 86, 185-190.

135. Kumar, S. and Dhobal, D. P. (1994). Snout fluctuation study of Chhota Shigri glacier, Lahaul and Spiti district, Himachal Pradesh. *Journal of Geological Society of India*, 4, 581-585.
136. Kumar, S. and Dhobal, D. P. (1997). Climatic effects and bedrock control on rapid fluctuations of Chhota Shigri glacier, northwest Himalaya, India. *Journal of Glaciology*, 43, 467-472.
137. Kumar, S., Rai, H., Purohit K. K., Rawat, B. R. S. and Mundepi, A. K. (1987). *Chhota Shigri Glacier*, Technical report on Multi disciplinary glacier expedition to Chhota Shigri Glacier, Department of Science and Technology, 1, 1-29.
138. Kumar, S.V., Peters-Lidard, C.D., Tian, Y., Houser, P.R., Geiger, J., Olden, S., Lighty, L., Eastman, J.L., Doty, B., Dirmeyer, P., Adams, J., Mitchell, K., Wood, E.F. and Sheffield, J. (2006). Land information system —an interoperable framework for high resolution land surface modeling. *Environmental Modelling and Software*, 21, 1402–1415.
139. Kumar, V., Venkataraman, G., and Rao, Y. S. (2009). SAR interferometry and speckle tracking approach for glacier velocity estimation using ERS-1/2 and TerraSAR-X spotlight high resolution data. *IEEE International Geoscience and Remote Sensing Symposium, IGARSS'09,* 12-17 July, Capetown, South Africa, 5, V-332-V-335.
140. Kurtz, N. T. and Markus, T. (2012). Satellite observations of Antarctic sea ice thickness and volume. *Journal of Geophysical Research: Oceans*, 117, C08025, pp. 1-9.
141. Kwok, R. and Fahnestock, M. (1996): Ice sheet motion and topography from radar interferometry. *IEEE Transactions on Geosciences and Remote Sensing*, 34, 189-200.
142. Kwok, R., Cunningham, G. F., Wensnahan, M., Rigor, I., Zwally, H. J. and Yi, D. (2009). Thinning and volume loss of the Arctic Ocean sea ice cover: 2003–2008. *Journal of Geophysical Research: Oceans*, 114, C07005, pp. 1-16.
143. Lefauconnier, B., Hagen, J. O. and Rudant, J. P. (1994). Flow speed and calving rate of Kronebreen glacier, Svalbard, using SPOT images. *Polar Research*, 13, 59–65.

144. Lemke, P., Ren, J., Alley, R. B., Allison, I., Carrasco, J., Flato, G., Fujii, Y., Kaser, G., Mote, P., Thomas, R. H. and Zhang, T. (2007). Observations: changes in snow, ice and frozen ground. In: Solomon, S., Qin, D., Manning, M., Chen, Z., Marquis, M., Averyt, K. B., Tignor, M. and Miller, H. L. (Eds.), *Climate Change 2007: The physical science basis. Contribution of Working Group I to the Fourth Assessment Report of the Intergovernmental Panel on Climate Change*. Cambridge University Press, Cambridge, 4, 987 p.

145. Leprince, S., Barbot, S., Ayoub, F. and Avouac, J. P. (2007). Automatic and precise ortho-rectification, coregistration,andsubpixel correlation of satellite images, application to ground deformation measurements. *IEEE Transactions on Geoscience and Remote Sensing*, 45, 1529-1558.

146. Leprince, S., Berthier, E., Ayoub, F., Delacourt, C. and Avouac, J. (2008). Monitoring Earth surface dynamics with optical imagery. *EOS Transactions American Geophysical Union*, 89, 1–2.

147. Lougeay, R. (1974). Detection of buried glacial and ground ice with thermal infrared remote sensing. In: Santeford, H. S. and Smith, J. L. (Eds.), *Advanced concepts and techniques in the study of snow and ice resources.* National Academy of Sciences, Washington, DC, 800 p.

148. Lucchitta, B. K. and Ferguson, H. M. (1986). Antarctica—measuring glacier velocity from satellite images. *Science*, 234, 1105–1108.

149. Lucchitta, B. K., Mullins, K. F., Allison, A. L. and Ferrigno, J. G. (1993). Antarctic glacier-tongue velocities from Landsat images: first results. *Annals of Glaciology*, 17, 356-366.

150. Luckman, A., Quincey, D. and Bevan, S. (2007). The potential of satellite radar interferometry and feature tracking for monitoring flow rates of Himalayan glaciers. *Remote Sensing of Environment*, 111, 172–181.

151. Malenovsky, Z., Rott, H., Cihlar, J., Schaepman, M. E., García-Santos, G., Fernandes, R. and Berger, M. (2012). Sentinels for science: Potential of Sentinel-1, -2, and -3 missions for scientific observations of ocean, cryosphere, and land. *Remote Sensing of Environment*, 120, 91–101.

152. Marzeion, B., Jarosch, A. H. and Hofer, M. (2012). Past and future sea-level change from the surface mass balance of glaciers. *The Cryosphere*, 6, 1295–1322.

153. Mayo, L. R., Meier, M. and Tangborn, W. A. (1962). System to combine stratigraphic and annual mass balance systems: A contribution to the International Hydrological decade. *Journal of Glaciology*, 11, 3–14.
154. McDermid, G. J. and Franklin, S. E. (1994). Spectral, spatial, and geomorphometric variables for the remote sensing of slope processes. *Remote Sensing of Environment,* 49, 57-71.
155. McNabb, R.W., Hock, R., O'Neel, S., Rasmussen, L.A., Ahn, Y., Braun, M., Conway, H., Herreid, S., Joughin, I., Pfeffer, W.T., Smith, B.E. and Truffer, M. (2012). Using surface velocities to calculate ice thickness and bed topography: A case study at Columbia Glacier, Alaska. *Journal of Glaciology,* 58, 1151-1164.
156. Meier, W. N., Stroeve, J. Barrett, A. and Fetterer, F. (2012). A simple approach to providing a more consistent Arctic sea ice extent time series from the 1950s to present. *The Cryosphere*, 6, 1359–1368.
157. Mellor, M. (1977). Engineering properties of snow. *Journal of Glaciology*, 19, 15-66.
158. Mihalcea, C., Mayer, C., Diolaiuti, G., Lambrecht, A., Smiraglia, C. and Tartari, G. (2006). Ice ablation and meteorological conditions on the Debris covered areas of Baltoro glacier, Karakoram, Pakistan. *Annals of Glaciology,* 43, 292-300.
159. Moll, A. and Braun, M. (2006). Determination of Glacier Velocities on King George Island (Antarctica) by DInSAR. *IEEE International Conference on Geoscience and Remote Sensing Symposium IGARSS'06*, 31 July - 4 Aug, Denver, Colorado, 1236 – 1239.
160. Mori, N., Yasuda, T., Mase, H., Tom, T. and Oku, Y. (2010). Projection of extreme wave climate change under global warming. *Hydrolological Research Letters*, 4, 15–19.
161. Mundepi, A. K., Kumar, S. and Purohit, K. K. (1994). Fluctuation in the thickness, velocity and ice discharge of monsoon arid zone glaciers: An example from Chhota-Shigri glacier, Himachal Himalaya, India. *Geoscience Journal*, 15, 163-169.
162. Nagar, V. K. and Bahuguna, V. B. (1989). A study of Chhota-Shigri glacier dynamics and its monitoring. In: *Proceedings of National Meet on Himalayan*

Glaciology, 5-6 June, 1989, Department of Science and Technology, Government of India, New Delhi, 99-111.

163. Nagler, T. and Rott, H. (1997). The application of ERS-1 SAR for snowmelt runoff modelling. In: Baumgartner, M. F., Schultz, G. A. and Johnson, I. A. (Eds.), *Proceedings of IAHS Symposium,* S3, Publication no. 242., 260 p.
164. Nijampurkar, V. N. and Rao, D. K. (1992). Accumulation and flow rates of ice on Chhota Shigri Glacier, 30 central Himalaya, using radio-active and stable isotopes. *Journal of Glaciology*, 38, 43–50.
165. Oerlemans, J. (2005). Extracting climate signals from 169 glacier records. *Science,* 308, 675−677.
166. Osmanglu, B., Braun, M., Hock, R., Navarro, F.J. (2013). Surface velocity and ice discharge of glaciers on King George Island, Antarctica. *Annals of Glaciology,* 54, 111–119.
167. Østrem, G. (1975). ERTS-1 data in glaciology - An effort to monitor glacier mass balance from satellite imagery. *Journal of Glaciology*, 15, 403–415
168. Østrem, G. and Brugman, M. (1991). *Glacier-mass balance measurements : A manual for field and office work.* National Hydrology Research Institute Science Report: Saskatoon, Sask, 224 p.
169. Pandey, P., Kulkarni, A. V. and Venkataraman, G. (2012). Remote sensing study of snowline altitude at the end of melting season, Chandra-Bhaga basin, Himachal Pradesh, 1980–2007. *Geocarto International*, 28, 311-322.
170. Parrot, M., Achache, J., Berthelier, J. J., Blanc, E., De-schamps, A., LeFeuvre, F., Menvielle, M., Plantet, J. L., Tarits, P. and Villain, J. P. (1993). High frequency seismo-electromagnetic effects. *Physics of the Earth and Planetary Interiors,* 77, 65-83.
171. Paterson, W. (1994). *The Physics of Glaciers*, 3rd Edn., Elsevier, Oxford, UK, 704 p.
172. Paul, F. (2000). Evaluation of different methods for glacier mapping using Landsat TM, Workshop on Land Ice and Snow, EARSEL eProceedings, 1, 239-244.
173. Paul, F. (2002a). Changes in glacier area in Tyrol, Austria, between 1969 and 1992 derived from Landsat 5 TM and Austrian Glacier Inventory data. *International Journal of Remote Sensing,* 23, 787–799.

174. Paul, F. (2002b). Combined technologies allow rapid analysis of glacier change. *EOS Transactions American Geophysical Union,* 83, 253-261.

175. Paul, F., Bolch, T., Kääb, A., Nagler, T., Nuth, C., Scharrer, K., Shepherd, A., Strozzi, T., Ticconi, F., Bhambri, R., Berthier, E., Bevan, S., Gourmelen, N., Heid, T., Jeong, S., Kunz, M., Lauknes, T. R., Luckmann, A., Merryman, J., Moholdt, G., Muir, A., Neelmeijer, J., Rankl, M., Van Looy, J., and Van Niel, T. (2013). The Glaciers Climate Change Initiative: Methods for creating glacier area, elevation change and velocity products. *Remote Sensing of Environment,* In press, (doi:10.1016/j.rse.2013.07.043).

176. Paul, F., Huggel, C. and Kaab, A. (2004). Combining satellite multispectral image data and a digital elevation model for mapping debris-covered glaciers. *Remote Sensing of Environment*, 89, 510-518.

177. Paul, F., Kaab, A. and Haeberli, W. (2007). Recent glacier changes in the Alps observed by satellite: consequences for future monitoring strategies. *Global and Planetary Change*, 56, 111–122.

178. Philip, G. and Mathew, J. (2005). Climato-tectonic impression on Trans Himalayan lakes: A case study of Kyun Tso basin of the Indus Suture Zone in NW Himalaya using remote sensing techniques. *Current Science*, 89, 1941-1947.

179. Philip, G. and Mazari, R. K. (2003). Remote sensing applications in glaciers: a review and case study of Himalayan glaciers. In P.S. Roy (Ed.), *Geoinformatics for Tropical Ecosystem*, Working Group on Tropical Ecosystem Management, Asian Association of Remote Sensing, Japan, 638 p.

180. Philip, G. and Ravindran, K. V. (1998). Glacial mapping using Landsat TM data: A case study in parts of Gangotri glacier NW Himalaya. *Journal of the Indian Society of Remote Sensing*, 26, 29-34.

181. Philip, G. and Sah, M. P. (2004). Mapping repeated surges and retread of glaciers using IRS-1C/1D Data: A case study of Shaune Garang glacier, northwestern Himalaya. *International Journal for Applied Earth Observation and Geoinformation,* 6, 127-141.

182. Pithan, F. (2011). A model study of the energy and mass balance of Chhota Shigri glacier in the Western Himalaya, India. *The Cryosphere Discussion*, 5, 95–129.

183. Prest, V. K., Grant, D. R. and Rampton, V. N. (1968). Glacial Map of Canada. *Geological Survey of Canada Map*, 1253A, Scale 1:5,000,000.
184. Pritchard, H. D., Murray, T., Luckman, A., Strozzi, T., and Barr, S. (2005). Glacier surge dynamics of Sortebræ, East Greenland, from synthetic aperture radar feature tracking. *Journal of Geophysical Research: Earth Surface*, 110, F03005.
185. Punkari, M. (1982). Glacial geomorphology and dynamics in the eastern parts of the Baltic Shield interpreted using Landsat imagery. *Photogrammetric Journal of Finland*, 9, 77-93.
186. Quincey, D. J. and Glasser, N. F. (2009). Morphological and ice-dynamical changes on the Tasman Glacier, New Zealand, 1990–2007. *Global and Planetary Change*, 68,185–197.
187. Quincey, D.J., Braun, M., Glasser, N. F., Bishop, M. P., Hewitt, K. and Luckman, A. (2011). Karakoram glacier surge dynamics. *Geophysical Research Letters*, 38 (L18504).
188. Quincey, D., Lucas, R. M., Richardson, S. D., Glasser, N. F., Hambrey, M. J. and Reynolds, J. M. (2005). Optical remote sensing techniques in high-mountain environments: application to glacial hazards. *Progress in Physical Geography*, 29, 475-505.
189. Rabatel, A., Francou, B., Jomelli, V., Naveau, P. and Grancher, D. (2008). A chronology of the Little Ice Age in the tropical Andes of Bolivia (16 degrees S) and its implications for climate reconstruction. *Quaternary Research*, 70, 198–212.
190. Rack, W., Rott, H., Siegel, A. and Skvarca, P. (1999). The motion field of northern Larsen Ice Shelf, Antarctic Peninsula, derived from satellite imagery. *Annals of Glaciology*, 29, 261–266.
191. Racoviteanu, A. E., Manley, W. F., Arnaud, Y. and Williams, M. W. (2007). Evaluating digital elevation models for glaciologic applications: an example from Nevado Coropuna, Peruvian Andes. *Global and Planetary Change*, 59, 110–125.
192. Racoviteanu, A. E., Paul, F., Raup, B., Siri, J. S. and Armstrong, R. (2010). Challenges and recommendations in mapping of glacier parameters from space space. *Annals of Glaciology*, 50, 53-69.

193. Racoviteanu, A. E., Williams, M. W. and Barry, R. G. (2008). Optical Remote Sensing of Glacier Characteristics: A Review with Focus on the Himalaya. *Sensors*, 8, 3355-3383.

194. Radić, V., and Hock, R. (2010). Regional and global volumes of glaciers derived from statistical upscaling of glacier inventory data. *Journal of Geophysical Research: Earth Surface*, 115, F01010, pp. 1-10.

195. Radić, V., Bliss, A., Beedlow, A. C., Hock, R., Miles, E. and J. G. Cogley, (2013). Regional and global projections of the 21st century glacier mass changes in response to climate scenarios from GCMs. *Climate Dynamics*, 1-22.

196. Ramanathan, A. L. (2011). *Status Report on Chhota Shigri Glacier (Himachal Pradesh)*, Department of Science and Technology, Ministry of Science and Technology, New Delhi. Himalayan Glaciology Technical Report No.1, 88 p.

197. Rankl, M., Vijay, S. and Kienholz, S. (2013). Glacier changes in the Karakoram region mapped by multi-mission satellite imagery. *The Cryosphere Discussion*, 7, 4065-4099.

198. Ranzi, R., Grossi, G., Iacovelli, L. and Taschner, S. (2004). Use of multispectral ASTER images for mapping debris-covered glaciers within the GLIMS project. *IEEE Transactions on Geoscience and Remote Sensing Symposium*, 20-24 Sept, Anchorage, Alaska, 1144-1147,

199. Raup, B, A. Kääb, Kargel, J. S., Bishop, M. P., Hamilton, G., Lee, E., Paul, F., Rau, F., Soltesz, D., Khalsa, S. J. S., Beedle, M. and Helm, C. (2007). Remote Sensing and GIS Technology in the Global Land Ice Measurements from Space (GLIMS) Project. *Computers and Geosciences*, 33, 104-125.

200. Rawat, B. R. S., Mundepi, A. K. and Kumar, S. (1989). Mass balance, surface lowering, velocity pattern and variation in Chhota Shigri glacier, Lahaul and Spiti Distt. (H.P.). In: *Proceedings of National Meet on Himalayan Glaciology*, 5 – 6 June 1989, New Delhi, 113 – 120.

201. Reynolds, J.M., Dolecki, A. and Portocarrero, C. (1998). Construction of a drainage tunnel as part of glacial lake hazard mitigation at Hualcán, Cordillera Blanca, Peru. In: Maund, J. G. and Eddleston, M. (Eds.), *Geohazards in Engineering Geology*. Engineering Geology Special Publications, Geological Society, London, 15, 41–48.

202. Ritchie, J., C. Lingle, M. Truffer, R. Motyka, A. Arendt, A. Prakash, K. Echelmeyer, and S. Zirnheld (2006). Seasonal and spatial variations in the advance of Hubbard Glacier, south-central Alaska, U.S.A. *Geophysical Research Abstract*, 8, Abstract 06345.

203. Rolstad, C., Amlien, J., Hagen, J. O. and Lunden, B. (1997). Visible and near-infrared digital images for determination of ice velocities and surface elevation during a surge on Osbornebreen, a tidewater glacier in Svalbard. *Annals of Glaciology*, 24, 255–261.

204. Rose, J. and Letzer, J. M. (1975). Drumlin measurements: a test of the reliability of data derived from 1:25,000 scale topographic maps. *Geological Magazine*, 112, 361–371.

205. Rose, J. and Letzer, J. M. (1977). Superimposed Drumlins. *Journal of Glaciology*, 18, 471–480.

206. Rosenthal, W., and Dozier, J. (1996). Automated mapping of montane snow-cover at sub-pixel resolution from the Landsat Thematic Mapper. *Water Resources Research*, 100, 115-130.

207. Rott, H. (1976). Analyse der Schneeflächen auf Gletschern der Tiroler Zentralalpen aus Landsat Bildern. *Zeitschrift für Gletscherkunde und Glazialgeologie*, 12, 1–28.

208. Rott, H. (1994). Thematic studies in alpine areas bymeans of polarimetric SAR and optical imagery. *Advances in Space Research*, 14, 217–226.

209. Rott, H., and Markl, G. (1989). Improved snow and glacier monitoring by the Landsat Thematic Mapper. In: *Proceedings of a workshop on Landsat Thematic Mapper applications*, December 1987, Frascati, Italy, ESA SP-1102, 3–12.

210. Sangewar, C. V. and Shukla, S. P. (2009). *Inventory of the Himalayan Glaciers: A Contribution to the International Hydrological Programme.* Special Publication, Geological Survey of India, 34: An Updated Edition, 594 p.

211. Scambos, T. A., Dutkiewicz, M. J., Wilson, J. C., and Bindschadler, R. A. (1992). Application of image cross-correlation to the measurement of glacier velocity using satellite image data. *Remote Sensing of Environment*, 42, 177–186.

212. Scherler, D., Bookhagen, B., and Strecker, M. R. (2011a). Hillslope-glacier coupling: The interplay of topography and glacial dynamics in High Asia. *Journal of Geophysical Research*, 116, 1-21.

213. Scherler, D., Bookhagen, B., and Strecker, M. R. (2011b). Spatially variable response of Himalayan glaciers to climate change affected by debris cover. *Nature Geoscience*, 4, 156-159.

214. Scherler, D., Leprince, S. and Strecker, M. R. (2008). Glacier-surface velocities in alpine terrain from optical satellite imagery - Accuracy improvement and quality assessment. *Remote Sensing of Environmen*t, 112, 3806–3819.

215. Semedo, A., Weisse, R., Beherens, A., Sterl, A., Bengtson, L. and Gunther, H. (2013). Projection of global wave climate change towards the end of the 21st century. *Journal of Climate*, 26, 8269-8288.

216. Shapiro, L G. and Stockman, G. C. (2002). *Computer Vision*. Prentice Hall, USA, 608 p.

217. Sharma, M. L. and Owen, L. A. (1996). Quaternary glacial history of NW Garhwal, Central Himalayas. *Quaternary Science Reviews*, 15, 335-365.

218. Sharma, P., Ramanathan, A. L. and Pottakkal, J. (2013). Study of solute sources and evolution of hydrogeochemical processes of the Chhota Shigri Glacier meltwaters, Himachal Himalaya, India. *Hydrological Sciences Journal*, 58, 1128-1143.

219. Sharp, R. P. (1988). *Living Ice: Understanding Glaciers and Glaciation*. Cambridge University Press, Cambridge, UK, 248 p.

220. Shi, J., Dozier, J. and Davis, R. E. (1990). Simulation Of Snow-depth Estimation From Multi-frequency Radar. *IEEE International Geoscience and Remote Sensing Symposium, IGARSS'90*, 20-24 May, Washington, DC, 1129-1132.

221. Shimamura, Y., Izumi, T. and Matsumaya, H. (2006). Evaluation of a useful method to identify snow-covered areas under vegetation- comparisons among a newly proposed snow index, normalized difference snow index and visible reflectance. *International Journal of Remote Sensing*, 27, 4867-4884.

222. Shruti (2008). Study of Glacio – morphological features and deglaciation pattern using field observation data, GIS and remote sensing techniques in the Himachal Himalaya. *Ph.D. Thesis*, Jawaharlal Nehru University, New Delhi, 128 p.

223. Shukla, A., Arora, M. K. and Gupta, R. P. (2010). Synergistic approach for mapping debris-covered glaciers using optical–thermal remote sensing data with

inputs from geomorphometric parameters. *Remote Sensing of Environment,* 114, 1378-1387.

224. Shukla, A., Gupta, R. P. and Arora, M. K. (2010). Delineation of debris-covered glacier boundaries using optical and thermal remote sensing data. *Remote Sensing Letters*, 1, 11−17.
225. Sidjak, R. W. and Wheate, R. D. (1999). Glacier mapping of the Illecillewaet icefield, British Columbia, Canada, using Landsat TM and digital elevation data. *International Journal of Remote Sensing*, 20, 273-284.
226. Silverio, W. and Jaquet, Jean-Michel (2005). Glacial cover mapping (1987-1996) of the Cordillera Blanca (Peru) using satellite imagery. *Remote Sensing of Environment*, 95, 342-350.
227. Singh, S. (1998). *Geomorphology*. Prayag Pustak Bhavan, Allahabad, India, 652 p.
228. Singh, P., Spitzbart, G., Hübl, H. and Weinmeister, H. W. (1997). Hydrological response of snowpack under rain-on-snow events: a field study. *Journal of Hydrology*, 202, 1–20.
229. Singh, S. K., Rathore, B. P., Bahuguna, I. M. and Ramnathan, A. L. (2012). Estimation of glacier ice thickness using Ground Penetrating Radar in the Himalayan region. *Current Science*, 103, 68-73.
230. Singh, V. B., Ramanathan, A. L., Pottakkal, J. G., Linda, A. and Sharma, P. (2013a). Temporal Variation in the Major Ion Chemistry of Chhota Shigri Glacier Meltwater, Lahaul–Spiti Valley, Himachal Pradesh, India. *National Academy Science Letters*, 36, 335-342.
231. Singh, V. B., Ramanathan, A. L., Sharma, P. and Pottakkal, J. G. (2013b). Dissolved ion chemistry and suspended sediment characteristics of meltwater draining from Chhota Shigri Glacier, Western Himalaya, India. *Arabian Journal of Geosciences*, 6, 1-13.
232. Singh, V., Singh, P. and Haritashya, U. (Eds.) (2011). *Encyclopedia of Snow, Ice and Glaciers.* Springer, Berlin, 1253 p.
233. Sinha, R. and Rasik, R. (Eds.) (2013). *Earth system processes and disaster management.* (Vol. 1), Springer-Verlag, Berlin-Heidelberg, 244 p.

234. Skvarca, P., Raup, B. and De Angelis, H. (2003). Recent behaviour of Glacier Upsala, a fast-flowing calving glacier in Lago Argentino, southern Patagonia. *Annals of Glaciology*, 36, 184–188.

235. Slater, M. T., Slogett, D. R., Rees, W. G. and Steel, A. (1999). Potential operational multi-satellite sensor mapping of snow cover in maritime sub-polar regions. *International Journal of Remote Sensing*, 20, 3019-3030.

236. Slater, P. N. (1980). *Remote Sensing – Optics and Optical Systems*. Addison-Wesley, Reading, UK, 575 p.

237. Smith, G. C., Saucier, F. J. and Straub, D. (2006). Response of the lower St. Lawrence estuary to external forcing in winter. *Journal of Physical Oceanography*, 36, 1485–1501.

238. Stokes, C. R., Popovnin, V., Aleynikov, A., Gurney, S. D. and Shahgedanova, M. (2007). Recent glacier retreat in Caucasus Mountains, Russia and associated increase in supraglacial debris cover and supra-/proglacial lake development. *Annals of Glaciology*, 46, 95-213.

239. Strozzi, T., Luckman, A., Murray, T., Wegmüller, U., and Werner, C. (2002). Glacier motion estimation using SAR offset-tracking procedures. *IEEE Transactions on Geoscience and Remote Sensing*, 40, 2384–2391.

240. Strozzi, T., Wegmüller, U., Werner, C., Wiesmann, A., Santoro, M., Delaloye, R., Raetzo, H. and Ambrosi, C. (2008). Survey of landslide activity in the Swiss Alps with ALOS PALSAR. In: *Proceedings of the 2008 Joint PI Symposium of the ALOS Data Nodes*, 3-7 Nov 2008, Rhodes, Greece, ESA SP-664.

241. Taschner, S. and Ranzi, R. (2002). Comparing opportunities of Landsat-TM and ASTER data for monitoring a debris covered glacier in the Italian Alps within the GLIMS project. *IEEE Transactions on Geoscience and Remote Sensing Symposium*, 2, 1044-1046.

242. Tiwari, R. K., Gupta, R. P. and Arora, M. K. (2014). Estimation of surface ice velocity of Chhota-Shigri glacier using sub-pixel ASTER image correlation. *Current Science*, 106, 853-859.

243. Trouvé, E., Vasile, G., Gay, M., Bombrun, L., Grussenmeyer, P., Landes, T., Nicolas, J-M, Bolon, P., Petillot, I., Julea, A., Valet, L., Chanussot, J. and Koehl, M. (2007). Combining airborne photographs and spaceborne SAR data to monitor

temperate glaciers: Potentials and limits. *IEEE Transactions on Geoscience and Remote Sensing*, 45, 905−924.

244. UNEP Report (2008). Global glacier changes: Facts and figures. 88 p. (Available online: *http://www.grid.unep.ch/glaciers/pdfs/glaciers.pdf*. Accessed June 2011).
245. Vikhamar, D. and Solberg, R. (2003). Snow-cover mapping in forests by constrained linear spectral unmixing of MODIS data. *Remote Sensing of Environment*, 88, 309-323
246. Vincent, C., Ramanathan, Al., Wagnon, P., Dobhal, D. P., Linda, A.,Berthier, E., Sharma, P., Arnaud, Y., Azam, M. F., Jose, P. G., and Gardelle, J. (2013). Balanced conditions or slight mass gain of glaciers in the Lahaul and Spiti region (northern India, Himalaya) during the nineties preceded recent mass loss. *The Cryosphere*, 7, 569–582.
247. Vitek, J. D., Giardino, T. R. and Fitzgerald, J. W. (1996). Mapping geomorphology: a journey from paper maps, through computer mapping to GIS and virtual reality. *Geomorphology*, 16, 233-249.
248. Wadhams, P., and Comiso, J. C. (1992). The ice thickness distribution inferred using remote sensing techniques. In: Carsey, F. (Ed.), *Microware Remote Sensing of Sea Ice*. American Geophysical Union, Washington, DC, 462 p.
249. Wagnon, P., Linda, A., Arnaud, Y., Kumar, R., Sharma P., Vincent, C., Pottakkal, J. G., Berthier, E., Ramanathan, A. L., Hasnain, S. I. and Chevallier, P. (2007). Four years of mass balance on Chhota Shigri glacier, Himachal Pradesh, India, A new benchmark glacier in the western Himalaya. *Journal of Glaciology*, 53, 603-611.
250. Walsh, S. J., Butler, D. R. and Malanson, G. P. (1998). An overview of scale, pattern, process relationships in geomorphology: A remote sensing and GIS perspective. *Geomorphology*, 21, 183-205.
251. Wang, X. L. and Swail, V. R. (2006). Climate change signal and uncertainty in projections of ocean wave heights. *Climate Dynamics*, 26, 109–126.
252. WGMS, (1989). *World glacier inventory—Status 1988*. Haeberli, W., H. Bösch, K. Scherler, G. Østrem and C. C. Wallén (Eds.) IAHS (ICSI)/UNEP/ UNESCO, World Glacier Monitoring Service, Zurich, Switzerland, 458 p.

253. Williams, R. S., Jr., and Hall, D. K. (1993). Glaciers. In: Gurey, R. J., Foster, J. L., and Parkinson, C. L. (Eds.), *Atlas of Satellite Observations Related to Global Change.* Cambridge University Press, Cambridge, UK, 484 p.

254. Williams, R. S., Jr., Hall, D. K. and Benson, C. S. (1991). Analysis of glacier facies using satellite techniques. *Journal of Glaciology*, 37, 120–127.

255. Williams, R. S., Jr., Hall, D. K., Sigurdsson, O., & Chien, J. Y. L. (1997). Comparison of satellite-derived with ground-basedmeasurements of the fluctuations of themargins of Vatnajökull, Iceland, 1973–1992. *Annals of Glaciology*, 24, 72–80.

256. Winther, J. G. and Hall, D . K. (1999). Satellite derived- snow coverage related to hydropower production in Norway: Present and future. *International Journal of Remote Sensing*, 20, 2991−3008.

257. Xiao, X., Shen, Z. and Qin, X. (2001). Assessing the potential of VEGETATION sensor data for mapping snow and ice cover: A normalized difference snow and ice index. *International Journal of Remote Sensing*, 22, 2479-2487.

258. Yao, T., Thompson, L., Yang, W., Yu, W., Gao, Y., Guo, X., Yang, X., Duan, K., Zhao, H., Xu, B., Pu, J., Lu, A., Xiang, Y., Kattel, D. B., and Joswiak, D. (2012). Different glacier status with atmospheric circulations in Tibetan Plateau and surroundings. *Nature Climate Change*, 2, 663–667.

259. Zhang, T., Barry, R. G., Knowles, K., Heginbottom, J. A. and Brown, J. (1999). Statistics and characteristics of permafrost and ground ice distribution in the Northern Hemisphere. *Polar Geography*, 23, 147–169.

260. Zhang, T., R. G. Barry, K. Knowles, F. Ling, and R. L. Armstrong, 2003: Distribution of seasonally and perennially frozen ground in the Northern Hemisphere. In: Phillips, M., Springman, S. M. and Arenson, L.U. (Eds)., In*: Proceedings of the 8th International Conference on Permafrost,* A. A. Balkema, Lisse, The Netherlands, 1289–1294.

261. Zwally, H. J., Comiso, J. C., Parkinson, C. L., Cavalieri, D. J., Gloersen, P. (2002). Variability of Antarctic sea ice 1979–1998. *Journal of Geophysical Research: Oceans*, 107, 9-1: 9-19.